PROBABILISTIC REASONING FOR DYNAMIC SPECTRUM ACCESS

by

Todd W Martin
A Dissertation
Submitted to the
Graduate Faculty
of
George Mason University
In Partial fulfillment of
The Requirements for the Degree
of
Doctor of Philosophy
Systems Engineering and Operations Research

Committee:

________________ Dr. Kuo-Chu Chang, Dissertation Director

________________ Dr. Paulo Costa, Committee Member

________________ Dr. Kathryn B. Laskey, Committee Member

________________ Dr. Brian Mark, Committee Member

________________ Dr. Ariela Sofer, Department Chair

________________ Dr. Kenneth Ball, Dean, The Volgenau School of Information Technology and Engineering

Date: ________________ Fall Semester 2016
George Mason University
Fairfax, VA

Probabilistic Reasoning for Dynamic Spectrum Access

A dissertation submitted in partial fulfillment of the requirements for the degree of Doctor of Philosophy at George Mason University

By

Todd W Martin
Master of Science
George Mason University, 2006
Bachelor of Science
The Pennsylvania State University, 1991

Director: Dr. Kuo-Chu Chang, Professor
Department of Systems Engineering and Operations Research

Fall Semester 2016
George Mason University
Fairfax, VA

Dedication

To my wife Helen and children Rachel, Andrew, and Jacob; and to my parents William and Phoebe Martin. Soli Deo Gloria.

Acknowledgments

I would like to thank those who have contributed to my success in this endeavor: My committee—Drs. KC Chang, Kathryn Laskey, Paulo Costa, and Brian Mark—for their time and help in making this a better, more coherent work; Drs. Paul Kolodzy, Larry Stotts, Dick Ridgway, and Keith Gremban for your encouragement (and harassment) along the way; Mr. Jim Meni at Science and Technology Associates for your generosity in many ways... affording me the flexibility at work to pursue my degree, providing tuition assistance, and always offering encouragement; Colleagues Karen Martin and Adam Landry for picking up the slack when I needed to defer some tasks at work to make progress on my research and writing; Dr. Mark McHenry at Shared Spectrum Company and Dr. Paul Kolodzy for providing spectrum measurement data; And again Dr. Paul Kolodzy and Karen Martin, for helping me find places to go and concentrate on research and writing when I needed it most.

I would especially like to thank Dr. KC Chang, who has been my advisor through my Masters and Doctorate studies. Who would have guessed that a simple question after class many years ago would lead to many years of collaboration and two degrees?

And finally, I offer my deepest gratitude to my wife Helen and children Rachel, Andrew, and Jacob. Thank you for your encouragement and patience over these many years.

Table of Contents

List of Tables

List of Figures

Abstract

PROBABILISTIC REASONING FOR DYNAMIC SPECTRUM ACCESS

Todd W Martin, PhD

George Mason University, 2016

Dissertation Director: Dr. Kuo-Chu Chang

Dynamic Spectrum Access (DSA) systems combine situational awareness development, decision assessment, and spectrum adaptation to provide greater spectrum access to wireless systems. While significant progress has been made in system dynamics and policy conformance reasoning, concern still exists regarding a DSA systems ability to reliably determine the operating conditions for policy compliance in situ. Current methods in literature and recent FCC policies generally develop global operating constraints based on a priori modeling and analysis, which potentially reduces DSA system performance in all cases in order to mitigate risks that occur only in a few cases. Furthermore, the a priori determination of in situ operating constraints is inconsistent with the premise of a “smart” or “cognitive” wireless system.

The primary hurdle to in situ compliance is situational awareness uncertainty, which results from the inherently stochastic nature of wireless communications and dynamics of spectrum user activity. Lacking trusted mechanisms for handing in situ uncertainty in DSA systems, regulators manage uncertainty and associated risk through policy specifications that impose conservative operating constraints in order to maintain high degrees of interference prevention. In managing risk via specifying inflexible a priori rules, the process

is necessarily and provably inefficient in the majority of operating conditions.

The thesis proposed and tested here is that improved spectrum sharing is possible via in situ probabilistic reasoning coupled with rule specifications that enable DSA spectrum access flexibility. The observation is made that current spectrum management processes are based in part on mitigating and managing risk. The concept of risk management is extended as a means to manage DSA spectrum access behaviors such as transmit power and standoff distance. The result is a risk-constrained spectrum access model, in which DSA systems govern their behaviors based on situational uncertainty subject to operating below a specified level of risk.

The research provides logical, mathematical, analytical, and quantitative evidence to support the thesis. Logically, it is shown that the reasoning process leading to lower levels of uncertainty provides lower levels of risk or increased performance at the same level of risk. A probabilistic reasoning model is constructed based on the assertion that DSA processes are inherently causal, which motivates a causal inference approach to DSA situational awareness using Functional Causal Models. The approach provides a formal and systematic means for probabilistic reasoning that is built upon well-established engineering models for wireless communications and the theoretical foundation of causal networks while incorporating uncertainty inherent in wireless communications and DSA operations. The model is used to demonstrate the link between path loss uncertainty and permitted DSA behaviors in a risk-constrained construct. Theoretical relationships are developed and analyzed. A simulation model is developed and results from several notional scenarios are presented. All results support the thesis.

Chapter 1: Introduction

Dynamic spectrum sharing concepts are being developed to enable continued growth in wireless broadband services [1, 2]. By allowing spectrum users to dynamically access spectrum subject to real-time conditions, spectrum access efficiency increases can be achieved and enable greater wireless user capacity and/or density. Dynamic Spectrum Access (DSA) technologies have progressed in many areas but methods for providing trusted and reliable interference avoidance remains a challenge. Regulatory processes and implementation approaches are subsequently limited in their effectiveness.

The following sections provide an overview of spectrum management and DSA, associated implementation challenges, and a proposed concept for enabling greater spectrum sharing. Section 1.1 describes the basic spectrum management process as it exists today, proposed approaches for enabling dynamic spectrum sharing, and key issues affecting spectrum sharing gains. Section 1.2 presents an example showing the impact that uncertainty inherent in mobile wireless operations has on spectrum sharing potential. Sections 1.3 and 1.4 then propose the thesis that probabilistic reasoning can increase spectrum access efficiency and provide an overview of the research and evaluation approach.

1.1 Spectrum Management and Dynamic Spectrum Access

Dynamic Spectrum Access (DSA) systems are wireless devices that adapt their transmission characteristics to opportunistically use available spectrum rather than rely on static spectrum assignments. They employ various technologies and algorithms to make more effective and efficient use of available spectrum by real-time adjustment of spectrum utilization in response to changing environmental conditions and user objectives. Ultimately, DSA systems are envisioned to have the authority and responsibility for managing their spectrum access "behaviors"—the means by which they adapt their operating characteristics such as frequency, power, and bandwidth—in a manner that enables spectrum sharing with other spectrum users [3,4]. They take advantage of spectrum access opportunities resulting from temporal and geographical variations caused by wireless user activity dynamics, signal propagation phenomenology, and mobility.

The DSA concept is very different than the current mode of spectrum access and management, which uses a centralized man-in-the-loop process of granting spectrum access to users [1,2,5]. Under the current approach, access is granted to enable a range of wireless services such as mobile communications, television (TV) broadcasts, and various radar applications in a manner that minimizes interference among users. Spectrum is allocated to service types and assigned to specific users based upon service needs and constraints derived from extensive modeling and analyses. In this manner, current spectrum management practices specify spectrum access behaviors *a priori*; that is, system operating behaviors such as maximum transmit power and bandwidth are specified at the time of regulation using some set of prior assumptions about possible operating conditions. Those regulations apply for long time periods (typically years) and generally large geographic extents (regional or national) and must be suitable for a diverse range of possible operating environments (e.g., urban and rural, flat and mountainous terrain). DSA systems, however, are ultimately envisioned to determine their own spectrum access behaviors *in situ* for comparatively shorter periods of time. They observe local environmental conditions, to which they apply sets of regulatory policies defining operating principles in order to derive permitted spectrum usage behaviors. This real-time adaptation provides the potential to dramatically increase spectrum access for wireless services relative to what can be accomplished with the current spectrum management process.

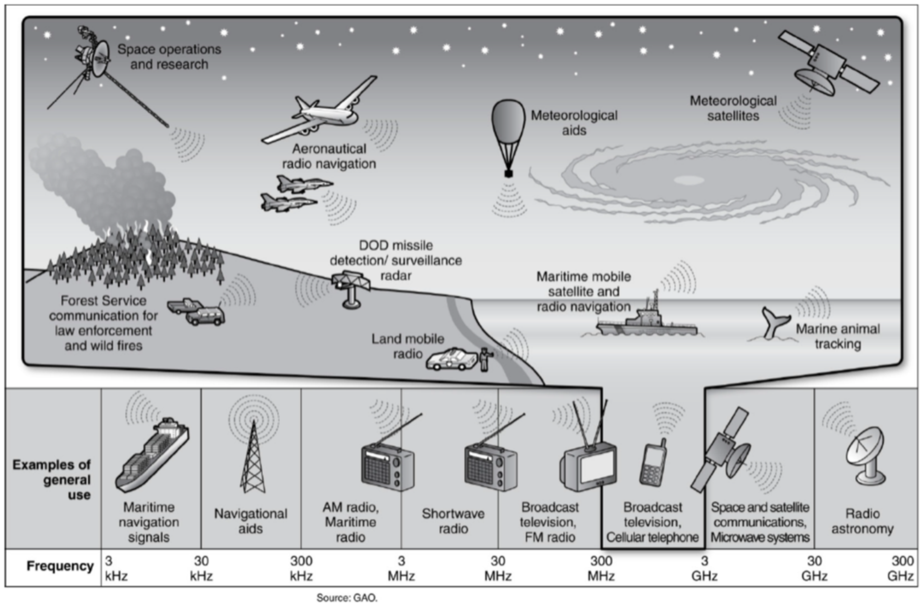

Figure 1.1: High-level depiction of applications associated with various spectrum bands

1.1.1 Spectrum Management

Spectrum management is fundamentally concerned with the allocation and assignment of wireless spectrum to wireless services and users in a manner that meets service needs and minimizes interference among services and users. Electromagnetic waves generated at different frequencies propagate differently and dictate system characteristics such as link range, channel capacity, and equipment size and power requirements [6–8]. Different service types are therefore allocated to different portions of the spectrum based upon the suitability of a spectrum band's physical characteristics, the services' requirements (e.g., mobility), and characteristics of the corresponding equipment (e.g., size and power). Figure 1.1 provides an example of how some common wireless services and applications are allocated across various spectrum bands [9]. [1]

Within those service classes, current spectrum regulatory and management practices grant long-term, exclusive spectrum assignments to specific users. The exclusivity of the assignments along with their long duration and broad geographic scope, however, is at odds

[1] See [10] for a complete allocation of US Federal services.

with how spectrum is actually used for many services. Actual usage for many applications, service types, and users varies on a much shorter timescale (sub-seconds to minutes) and smaller geographic scale (meters to tens of kilometers) than the assignment scope due to intermittent usage and user mobility. The mismatch between static assignments and dynamic usage produces inefficient spectrum usage. Measurements of spectrum usage indicate that significant amounts of spectrum—as much as 90% in some cases—are unused at any given time and location [5, 11–13]. This high inefficiency occurs despite the fact that nearly all the spectrum in the measured bands is assigned to users. Studies determined that the underlying issue limiting increased spectrum use is one of spectrum *access* (i.e., the ability to access available spectrum) rather than *scarcity* of spectrum availability [5].

The dichotomy between assignment and usage rates results from the characteristics of users' spectrum access and geographic considerations for signal propagation and spectrum assignment. Many spectrum devices do not constantly emit energy; they only emit when information is to be exchanged with other devices. This on/off nature creates temporally-varying usage that results in "unused" spectrum. If the wireless service includes mobile users, then the movement of users away from a particular area creates additional unused spectrum. Similarly, the assignments for a given frequency are done in a way that ensures sufficient geographic separation among users to avoid the possibility of interference among them. Conservative assumptions regarding signal propagation are commonly used, resulting in large separations among re-used frequencies. This large separation produces locations where neither user's signal can be detected and the spectrum goes unused.

Examples of geographic and temporal variations in spectrum use are shown in Figures 1.2 through 1.4. Figure 1.2 shows the approximate coverage area for all broadcast TV stations operating on channel 7 (174-180 MHz) as reported by Spectrum Bridge[2]. In general, broadcast TV stations operating on the same frequency are assigned with significant geographic spacing between them, causing spectrum to remain unused in much of the US. Figure 1.3 shows a map of broadcast TV channel availability—essentially the inverse of

[2]See whitespaces.spectrumbridge.com

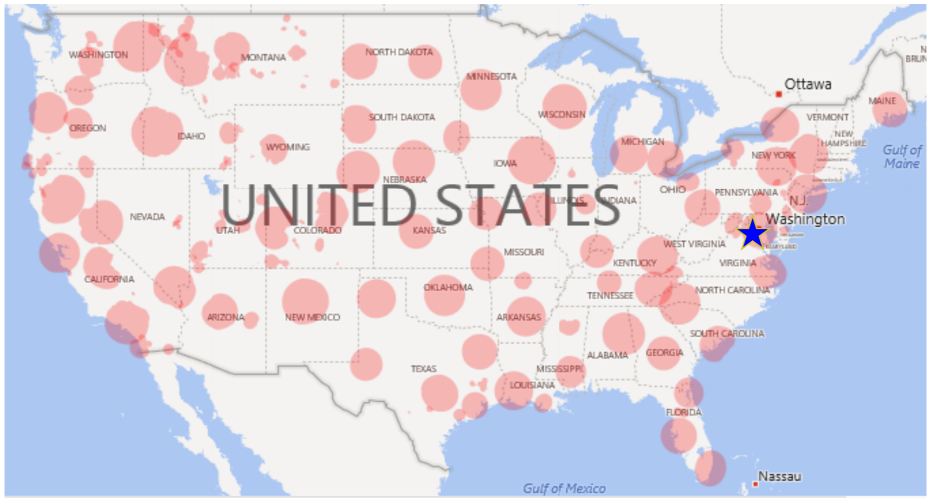

Figure 1.2: TV Band channel 7 spectrum coverage areas (red) for the Continental US (from the Spectrum Bridge TV Spectrum Exclusion Zone Database)

broadcast TV channel use density—throughout the United States (US) as reported by the Google Spectrum Database[3]. It is easily seen that heavy TV channel use occurs around metropolitan areas, while few channels are used in lightly populated areas.

Figure 1.4 provides a waterfall plot of spectrum usage variation in time and frequency from an NTIA spectrum study [14]. The data show detections of transmitted signals within the 763–800 MHz band (horizontal axis) for a period of approximately 58 hours (vertical axis). Some frequencies are used almost continuously in time (appearing as vertical lines) while others show different degrees of usage variation over the measurement time period. Some of the dynamics may be attributed to differences in the service characteristics while others may be attributed to user behaviors (e.g., mobility or daily life patterns). Regardless, the data demonstrate how the dynamics of spectrum use create significant spectrum availability that varies significantly in time and frequency.

[3] www.google.com/get/spectrumdatabase

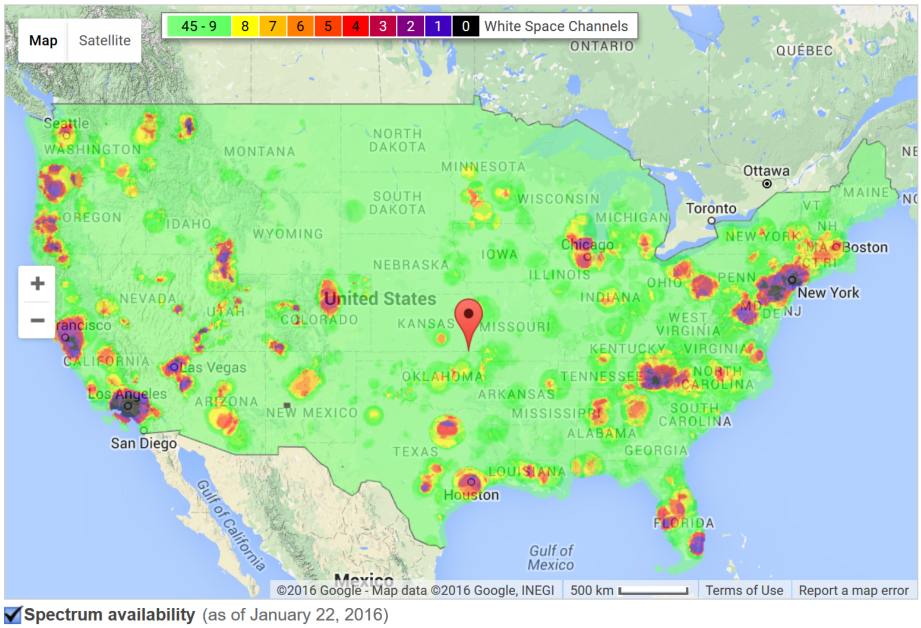

Figure 1.3: TV Band spectrum availability map for the Continental United States (from the Google Spectrum Database)

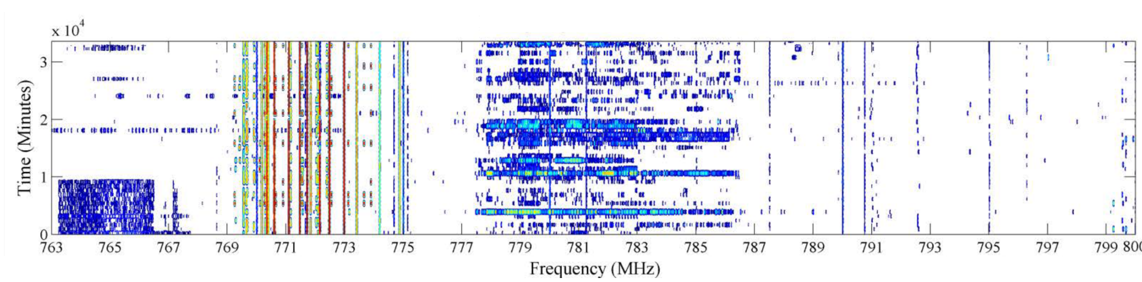

Figure 1.4: NTIA Spectrum Measurement Example - Denver

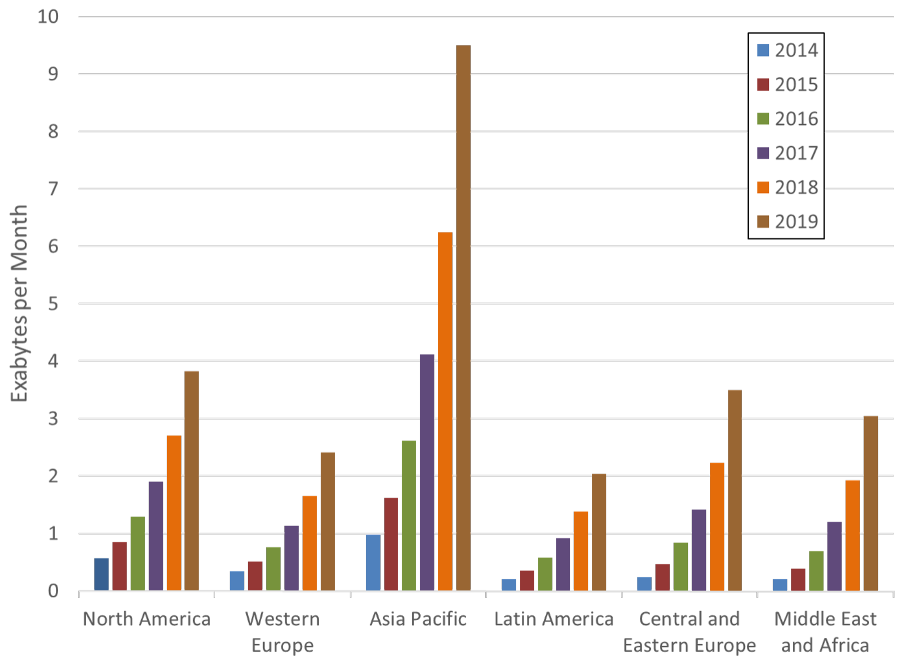

Figure 1.5: Cisco mobile data forecast 2014-2019.

1.1.2 Dynamic Spectrum Access

The motivation for DSA stems from the need to increase spectrum access to meet increasing demands for wireless services. While individual studies vary on the amount of historical and projected mobile data demand growth, they all indicate an accelerated rate of growth such as that shown in Figure 1.5 [15] and Figure 1.6 [16]. The continued growth is driven by increased demand for existing services such as mobile broadband as well as by emerging applications such as the Internet of Things (IoT). By contrast, the amount of spectrum available to support the increased demand cannot grow at a comparable rate; spectrum suitable for most wireless services—particularly mobile wireless services—is limited by a combination of physical properties of wireless signal propagation and technology constraints as discussed in Section 1.1.1. That spectrum is already allocated and assigned to other services and users and only modest increases in spectrum access are possible with traditional technologies and spectrum management practices.

Thus providing spectrum to meet increased demand requires the ability to increase the

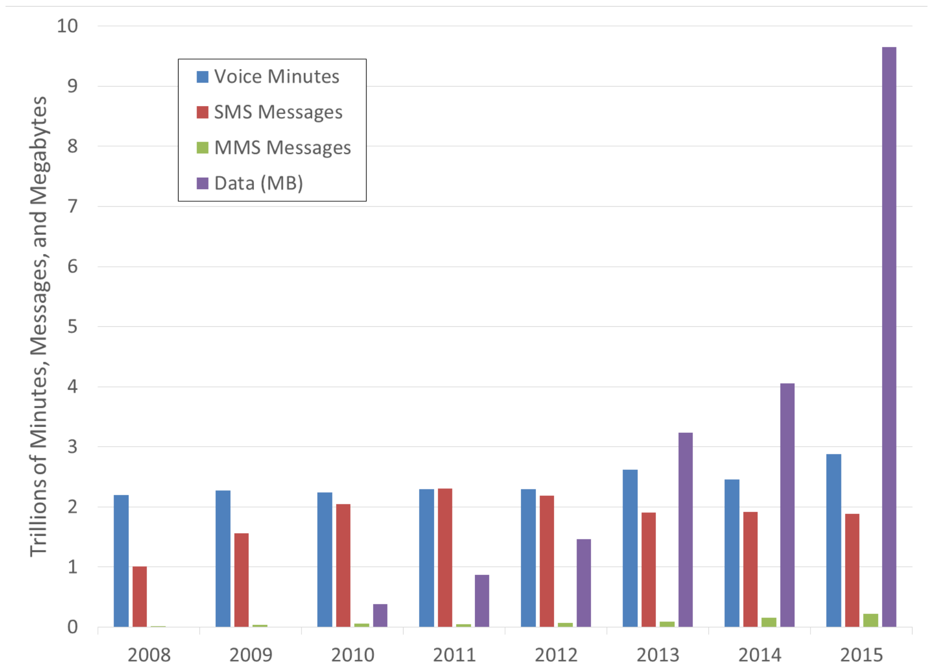

Figure 1.6: US mobile service usage statistics from the CTIA 2015 Annual Summary Report.

density of users. Various mechanisms such as smaller, denser cells or opportunistically offloading data demand to WiFi provide some mitigation for individual service providers, but do not enable sharing among different services [17]. Enabling spectrum sharing requires operational and technical solutions coupled with new regulatory processes. Users sharing a common portion of the spectrum in a given area must be able to coexist without causing harmful interference to each other.

Numerous operating concepts and system technologies have been investigated to enable spectrum sharing (see e.g., [1,18,19]). Sharing approaches use varying degrees of interaction among spectrum users, ranging from cooperative to non-cooperative sharing. Cooperative sharing entails that all spectrum users seeking a shared portion of the spectrum implement a common spectrum access protocol that affords each user access to spectrum resources without causing harmful interference to other users. While conceptually attractive, cooperative sharing imposes standardization and potential information sharing requirements on users that may be unattractive in terms of economics (e.g., equipment and infrastructure costs), security in the information exchange channel, or limited flexibility to quickly adopt new technologies as they emerge over time [20]. By contrast, non-cooperative sharing allows users to "opportunistically" access available spectrum. These opportunistic users must employ potentially more complex mechanisms for inferring when to access spectrum, with what transmit powers, and for how long in order to avoid causing harmful interference to other spectrum users. In between these two sharing types are variations that employ differing degrees of coordination. The ability to implement any DSA approach requires complimentary development of technologies and new regulatory processes.

Technology and regulatory developments to date demonstrate that significant potential and interest exists for increasing spectrum access through various DSA mechanisms (see e.g., [1, 21]). Concerted research efforts from the Defense Advanced Research Projects Agency (DARPA) and the National Science Foundation (NSF) beginning circa 2001 established significant momentum in DSA-related research, including the development of algorithms, sensing technologies, policy-based reasoning capabilities, and hardware prototypes within the DoD, industry, and commercial sectors [22–26].[4] The progress has enabled new policy and regulatory efforts that pursue implementations of DSA technologies. In 2010, a Presidential Memorandum was issued to reallocate 500 MHz of spectrum to support the rapidly growing demand for wireless broadband [27]. The initiative was further defined in the United States (US) Federal Communications Commission (FCC) and US Department of Commerce National Telecommunication and Information Administration (NTIA) *Ten Year Plan* [28, 29]. Included in the plans were considerations for the development and eventual deployment of dynamic spectrum sharing technologies. The FCC sought to apply some of the DSA principles for increased spectrum utilization by enabling access to unused television (TV) spectrum [30]. Meanwhile, the President's Council of Advisors on Science and Technology (PCAST) released a report in 2012 advocating for DSA on a larger scale for increasing wireless broadband access to consumers [1]. The continued desire by commercial

[4]See also `http://www.nsf.gov/cise/cns/prowin.jsp` and solicitations NSF 04-540, NSF 05-505, NSF 06-516, and NSF 07-507

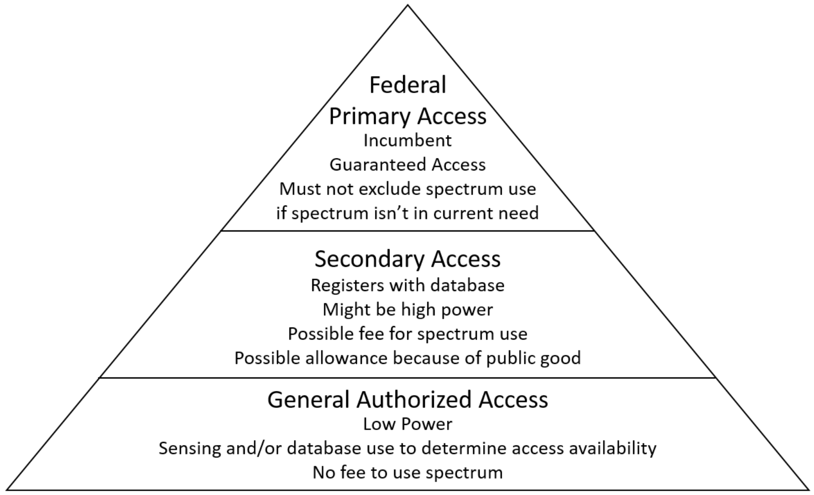

Figure 1.7: Three-tiered spectrum access framework proposed in the PCAST report and implemented by the FCC policies governing spectrum sharing in the 3.5 GHz band.

broadband providers for more spectrum access and the US Government's need to maintain sufficient public services resulted in a spectrum sharing approach to be implemented in the 3.5 GHz band (covering 3.55-3.655 GHz) that uses exclusion zones to protect incumbent users and provide spectrum access on a tiered basis [31].[5]

The FCC policies governing the 3.5 GHz sharing approach follows a three-tiered approach proposed in the PCAST report [1, 2]. As depicted in Figure 1.7, the highest level is Federal Primary Access, which provides unencumbered access for existing Federal services such as radar and satellite downlink. Those services were found to be geographically and/or temporally sparse and provide significant potential for spectrum sharing. Secondary Access provides dynamic spectrum sharing through coordination with other secondary access users via spectrum access managers, which may provide guaranteed secondary access conditions (e.g., bandwidth, duration) in exchange for payment. General Authorized Access provides for opportunistic access, which enables spectrum users access on a non-guarantee basis—possibly without coordination among users—provided they do not impose harmful interference on other users belonging to the other two tiers.

[5]The discussion here focuses on developments in the US, but it should be noted that significant research and regulatory activity is also occurring in Europe and Asia.

The PCAST and FCC tiered access approach reflects concerns regarding the extent to which DSA systems can sufficiently understand their environment and operate without causing harmful interference to other spectrum users. DSA devices were originally envisioned to be highly-autonomous and adaptive, operating in a largely decentralized manner. They would understand the relevant spectrum rules governing spectrum access, understand their operating environment, and adapt their spectrum access behaviors (e.g., frequency, transmit power, and bandwidth) accordingly. Thus DSA systems would be able to understand constraints; characterize their environment to evaluate an action's compliance with policies (e.g., interference power limits); and develop spectrum access strategies that meet DSA user goals (e.g., data rates). Approaches for codifying operating rules and constraints as machine-readable policies have been developed and undergone varying degrees of testing [32–34]. Methods for situational understanding have been pursued, including real-time spectrum sensing and the use of database information. Ultimately, however, the ability to attain a sufficient real-time understanding of the operating environment and ensure that spectrum access behaviors can meet user goals (e.g., capacity) and policy constraints (e.g., non-interference) remains a challenge. Regulators are therefore pursuing spectrum sharing architectures having centralized access control mechanisms to minimize the likelihood of interference among users.

1.2 The Impact of Uncertainty on Spectrum Access

A fundamental hurdle for reliably determining the implications of a DSA system's actions is uncertainty stemming from practical limits on situational awareness, the inherent probabilistic nature of wireless communications, and limited knowledge about the world state. Perhaps the most significant compliance concern is the risk of causing harmful interference to other spectrum users due to decisions made by DSA systems with imperfect and incomplete awareness. Interference avoidance depends on the DSA system's ability to assess the impact of its desired operations on other spectrum users while meeting user needs. Lacking an accepted method for operating with imperfect and incomplete knowledge, policy-makers and spectrum regulators must use conservative mechanisms and assumptions to mitigate interference risks when developing spectrum sharing policies. Similarly, broadband service providers hesitate to adopt spectrum sharing technologies and business models due to the risks associated with providing reliable service to a customer base in an uncertain environment.

The TV whitespace implementation illustrates some of the key issues associated with spectrum management, DSA implementation, and the impact of uncertainty on policy on efficient spectrum access [30]. While not universally considered to be DSA, the TV White Space operating concept was a notable step in that direction.[6] The proximate cause for the limited flexibility afforded to devices operating under the TV White Space policy is the a priori process by which spectrum access behaviors were specified. Two ultimate causes are the uncertainty inherent in wireless spectrum usage and the inability for existing DSA technologies to enable trusted operations in an uncertain environment. Without solutions to the latter two issues, regulators have limited ability to afford users with significant degrees of freedom.

These issues and their impact are discussed in the following sections. A summary of the TV White Space policy is presented in the following section. The connection between uncertainty, spectrum access regulation, and spectrum access efficiency limitations are then discussed in Section 1.2.2. Further, it is concluded that gains in spectrum access will *necessarily* be limited unless a process is established that incorporates and manages uncertainties associated with spectrum access.

1.2.1 A Summary of the TV White Space Policy

White Space refers to spectrum that is unused at any given time or location. The term stems from spectrum measurements (see e.g., [11]) associated with early DSA research.

[6] A distinction is sometimes made between DSA systems and "opportunistic white space radios" such as TVBDs (see e.g., [1, pg. 31]). For the purposes of this thesis, TVBDs are treated as a DSA device having a subset of possible DSA characteristics.

Plots of spectrum occupancy as a function of time depicted unoccupied spectrum as empty or "white" spaces on the graphs (see e.g., Figure 1.4); thus the term "white space" emerged as a term to describe unused spectrum. TV White Space refers specifically to VHF and UHF television broadcast bands that are either unassigned or unused in a given area. US television broadcast services are allocated spectrum in the 54-72 MHz, 76-88 MHz, 174-216 MHz, 470-608 MHz, and 614-692 MHz bands, with 6 MHz allocated to each TV channel. Assignments vary by location, and not all TV channels are used for broadcast in any given area for reasons that include broadcast TV market demand and spectrum management practices for interference avoidance among broadcasters as described in Section 1.1.1. While some other wireless services such as low-power wireless microphones were authorized to use unused TV spectrum, opportunistic use of the unused spectrum was not permitted prior to the FCC TV White Space regulations [30].

The primary challenge faced by a practical DSA implementation in the TV bands centered around the ability to protect broadcast TV receivers and low-power wireless microphone systems operating in the TV bands from harmful interference. Both systems use a broadcast mode of operation, which includes one set of devices that actively transmit but do not receive signals, and another set of devices that are receive-only. In the case of TV, one broadcast tower transmits to many TV receivers spread throughout a designated service area. Conversely, wireless microphone systems use a centralized receiver to process signals from one or more microphones equipped with low-power transmitters. In both cases, the TV and microphone receivers are passive spectrum users. While sensing-based DSA systems can detect the presence of the transmitters given a sufficiently-strong signal, they cannot readily determine the presence of the passive receivers. The receivers, however, are the devices that would incur interference. Regulators determined that protection of the passive receivers may not be done reliably by sensing techniques, which could result in potential interference by DSA users due to missed detections. Thus without other information regarding the presence of active receivers, DSA systems would need to rely on other mechanisms to determine if they could operate at a given location and time.

To overcome the sensing challenge, the FCC implemented the use of exclusion zones, which are geographic regions in which a TV band device (TVBD) cannot transmit. The FCC rules specify that portable TVBDs can transmit at 100 mW (20 dBm) if they a) are able to determine their own location to within ± 50 meters, b) are in a permitted geographic location, and c) are not within 400 meters of a registered, low-power wireless microphone [30]. The policy essentially creates two types of exclusion zones. The first exclusion zone provides interference protection to TV broadcast receivers within reception range of a given TV transmitter (see Figure 1.2), while the second creates a similar (but geographically smaller) exclusion zone around locations using wireless microphone devices. These locations are specified in a controlled database, which must be accessed by the TVBD before it can operate [30].

In determining the size of the exclusion zones and associated minimum standoff distance, the policy-makers specified a range of signal propagation conditions that could exist. By modeling those environments, they estimated the probability that a TVBD signal power imposed on a TV or wireless microphone receiver would cause harmful interference. Thus they were able to evaluate the risk of causing harmful interference to the receivers given various standoff distances, TVBD transmit powers, and signal propagation assumptions. To be acceptable, the specified transmit power and standoff distance limits needed to produce a low probability of interference across *all possible* operating conditions (e.g., rural and urban, flat and mountainous). Thus the operating limits are necessarily determined by generally low probability "worst case" operating conditions to achieve an acceptably low risk of interference.

While the TVWS policy provided for greater geographical sharing than previously existed, achievable spectrum access gains are still limited by the use of a priori spectrum access behavior determinations. TVBDs are afforded the ability to access unused spectrum based on their location, but the decision relies on an a priori process that pre-defines their behavior (e.g., transmit power) for all time and all locations regardless of actual in situ spectrum usage and environmental conditions. This practice of creating a single transmit power and standoff distance limit to be applied universally to all situations is shown to be highly inefficient in the following sections. Specifically, it is shown that this a priori process of establishing universal operating conditions to achieve an acceptable level of risk *necessarily* leads to very inefficient spectrum access.

1.2.2 An Analysis of Spectrum Access Limitations

Of fundamental concern to the regulators and operators is avoiding harmful interference, which is caused by insufficient Signal to Interference plus Noise Ratio (SINR) or Carrier to Interference plus Noise Ratio (CINR) at the receiver. SINR is given as

$$SINR = \frac{P^*_{rx}}{P^*_{rx,int} + N^*} \tag{1.1}$$

where P^*_{rx} is the received power of the wanted signal, $P^*_{rx,int}$ is the received power of the interfering signal, and N^* is broadband environmental noise.[7],[8] To establish a threshold condition, the lowest acceptable SINR or CINR for interference-free TV or wireless microphone operation is established. Similarly, a minimum received signal power P^*_{rx} is determined, which establishes a maximum acceptable interfering signal level $P^*_{rx,Int}$ from a TVBD at the TV or wireless microphone receiver.

The maximum transmit power of the TVBD and minimum standoff distance is then determined by a combination of TVBD service goals and signal propagation. Many of the performance goals—such as link range and data rate—are functions of the TVBD transmit power. TVBD transmit power also translates into interference power at the protected user by

$$P_{rx,TVBD} = P_{tx,TVBD} - L_p, \tag{1.2}$$

[7]Note that variables annotated with "*" use a power scale; all others are expressed in decibel (dB) scale.

[8]For CINR, P^*_{Rx} and $P^*_{Rx,Int}$ are the received power of the wanted and interfering carrier signal, respectively.

where L_p is the signal power loss from the TVBD transmitter to the TV or wireless microphone receiver [7]. Thus for a given interference power limit $P_{rx,int}$ of a protected receiver, trades can be made between TVBD maximum transmit power and minimum standoff distance subject to a specified path loss model L_p such that $P_{rx,TVBD} < P_{rx,int}$.

Path loss, however, depends on signal propagation, which is a random process and must be treated statistically. The mean path loss is affected by factors including terrain, foliage, man-made structures, weather (e.g., humidity, rain), and antenna heights of the transmitter and receiver. In conducting predictive studies, statistical path loss models such as the Irregular Terrain Model (ITM) are used to account for environmental variations and uncertainties [6, 35–38] and can produce path loss predictions based on confidence levels (see Figure 1.8) The general path loss models are augmented with other models for evaluating specific situations (e.g., cosite interference) along with data from propagation and interference experiments. Given the results of path loss and interference studies, one can assess the statistical characteristics of the operating conditions relative to interference probability, which can be use as a measure of risk (e.g., the 99% confidence in interference-free operation).

To illustrate, let the probability of interference Φ_{Int} be defined as the probability q_{int} that the received interfering TVBD signal power $P_{rx,TVBD}$ exceeds the interference power threshold $P_{rx,int}$:

$$\Phi_{Int} = \Phi(P_{rx,TVBD} \geq P_{rx,int}) = q_{int}. \tag{1.3}$$

For a given TVBD transmit power $P_{tx,TVBD}$, (1.2) and (1.3) become

$$\Phi_{Int} = \Phi(P_{tx,TVBD} - L_p \geq P_{tx,TVBD} - L_{p,int}) = \Phi(L_p \leq L_{p,int}) \tag{1.4}$$

where $L_{p,int}$ is the minimum path loss such that $P_{rx,int} > P_{tx,TVBD} - L_{p,int}$. The result in (1.4) therefore states that interference probability can be defined as the probability that the actual path loss L_p is less than the minimum path loss required to ensure that the

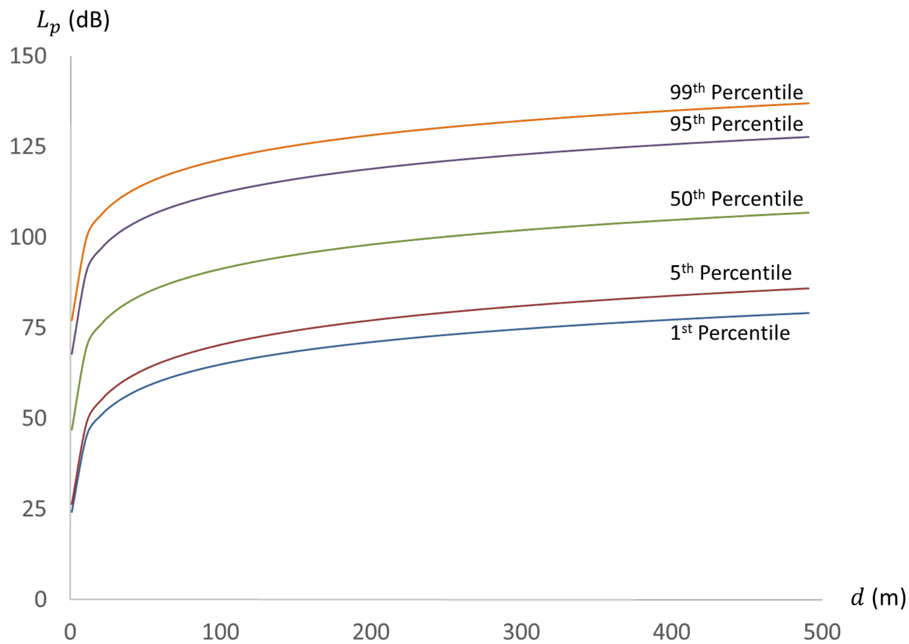

Figure 1.8: Example path loss as a function of distance for various percentile levels. Produced from the Irregular Terrain Model.

interfering signal power is less than $P_{rx,int}$ at the protected receiver. Referring to Figure 1.9, it is shown that

$$\Phi_{Int} = \Phi(L_p \leq L_{p,int}) = q_{int}, \tag{1.5}$$

where the probability q_{int} can be interpreted as a measure of interference risk. Thus given some uncertainty about the propagation environment (as well as other factors that will be addressed in later chapters), one can evaluate the probability (i.e. risk) of interference for some set of candidate spectrum access behaviors.

Applying these concepts to the TV Whitespace rules provides insights into the issues and limitations associated with traditional spectrum management. Recall that the TV Whitespace rules specified a minimum standoff distance and maximum transmit power based on *a priori* analyses. To assess the appropriateness of those specifications, Erpek et. al. [39] conducted a study of the TV White Space standoff distance specification.

The study compared the requisite standoff distance specified by the FCC with sets of

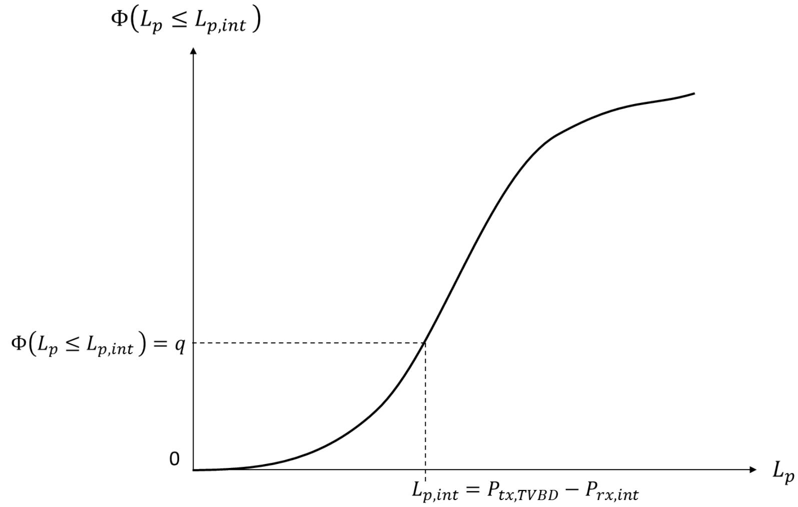

Figure 1.9: Percentile mapping from an interference path loss threshold value $L_{p,int}$ to the exceedance probability $P(L_p \geq L_{p,int}) = q$, where q represents interference risk.

measured data. Path loss data was determined from received signal power measurements from a transmitter with known power and location. Data was collected from a total of 4094 measurement locations associated with three indoor public venues. The resulting path loss results are shown in Figure 1.10 with each location indicated by a different color marker in the graph [39]. The study concluded that the standoff distance could be significantly reduced to 131 m—compared with the policy-specified 400 m distance—with zero probability of interference given the measurement conditions. Thus the model used by the FCC produced results that were much more conservative than the measured conditions and resulted in much stricter standoff distances than what could be supported under the measured conditions. Other studies further illustrate the difficulty in applying a priori signal propagation predictions without knowledge of the specific propagation environment (see e.g., [40, 41]).

The disconnects between model predictions and actual results anecdotally point to potential performance limitations imposed by a priori specification of spectrum access behaviors. In specifying behaviors under the current regulatory process, limitations must account for a range of operating conditions and associated uncertainties. Modeled results reflect *generalized* conditions and are not necessarily representative of any specific condition. Their

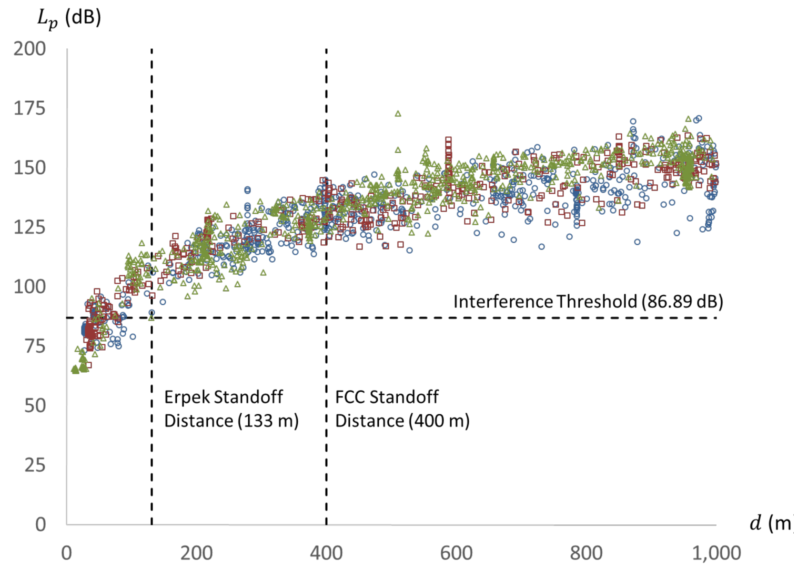

Figure 1.10: TV Whitespace path loss data from three wireless microphone venues (provided courtesy of Shared Spectrum Company.

formulations are based largely upon statistical characterizations of signal attenuation phenomenology [36]. Relying on a priori rather than in situ behavior determination, significant spectrum access opportunities and efficiencies may be lost. Increasing predictive accuracy can only occur by an increased understanding (i.e., reduced uncertainty) regarding the in situ conditions and applying the corresponding inputs to the model.

1.3 Thesis: Probabilistic Reasoning for DSA Systems

The discussions presented here anecdotally demonstrate the inherent reliance of spectrum access policies and behaviors on risk mitigation. In managing risk, spectrum access efficiency is necessarily reduced. The extent of that reduction depends upon the amount of uncertainty present at the time the spectrum access behaviors are determined. The key to increased spectrum access, therefore, is to establish DSA mechanisms that are able to a) characterize and assess the levels of uncertainty in the decision-making process, and 2) make those determinations in situ.

Regulators must have confidence that the such processes and the systems that use them are able to reliably operate under uncertainty. Primarily, regulators will need assurance that the DSA systems can evaluate the interference risks of candidate actions and select those that are below some specified threshold. Additionally, potential DSA network users must have confidence that the DSA systems can maintain reliable access to sufficient spectrum that meets their Quality of Service or Quality of Experience needs.

It is proposed here that DSA systems must be able to characterize and sufficiently manage uncertainty and associated risks. Situational awareness must incorporate uncertainty assessments derived from sets of qualified algorithms and in situ observations to enable DSA behaviors to be managed according to risk conditions. Polices must also be written to ensure interference prevention without being overly restrictive. They should govern the resulting effects that are desired while permitting DSA systems to determine the means by which those conditions are met. This concept is perhaps best described as risk-constrained spectrum access, in which spectrum policies specify the minimum interference risk threshold and DSA systems employ qualified algorithms for assessing risk. Proving that in situ probabilistic reasoning in DSA systems enables greater spectrum access potential than existing methods is a first step towards such an approach.

The research conducted and presented in this dissertation addresses the hypothesis that *in situ probabilistic reasoning in DSA systems enables greater spectrum access potential than existing methods*. The thesis is based upon the observation that uncertainty characterizations in DSA knowledge represent useful information for situational awareness and decision-making but are not exploited by any known DSA model. As a result, current approaches must rely on conservative assumptions and heuristics—generally applied *a priori* during policy development—to account for risks associated with uncertainty. As demonstrated in the TV whitespace example, the result is a loss in spectrum access in the majority of cases to protect against risks associated with a very small percentage of outcomes. It is proposed that applying probabilistic reasoning to locally-collected observations regarding the operating environment can reduce situational awareness uncertainty, thus enabling better spectrum sharing assessments and greater spectrum sharing efficiency.

1.4 Research Approach Summary

The thesis is evaluated in two ways. A general argument is made in Chapter 2 that probabilistic reasoning with in situ information provides greater spectrum access efficiency than current methods that specify operating behaviors from a priori assessments. The line of reasoning is built upon the characterization of spectrum management in terms of risk management. It then argues that a priori behavior specifications lead to worst-case spectrum access efficiency, which can be improved without increasing risk through in situ assessments of environmental conditions and the application of probabilistic reasoning.

Specifically, they analysis shows that the current process of specifying spectrum access behaviors (e.g., DSA transmit powers and exclusion zones) during the policy formulation process limits system performance and spectrum efficiency due to the risk of rare events. Since regulators and users desire low levels of interference risk (e.g., $\approx$ 5%), spectrum sharing policies are driven by low probability events that occur in the tails of a probability distribution. The operating limits are only efficient when actual conditions correspond with those associated with the risk threshold, and are by definition inefficient under more favorable conditions. If risk is set to a low probability such as 5%, then more favorable conditions exist 95% of the time.

The magnitude of the inefficiency lies with the combination of the low risk threshold and uncertainty associated with the assessment of spectrum access behaviors. Currently, spectrum sharing policies specify transmit powers and exclusion zones based on a priori analysis—that is, analysis conducted at the time of policy specification using generalized information rather than within the specific context of a specific situation. Because of the uncertain nature of signal propagation and user behaviors, the analysis contain significant amounts of uncertainty that are shown in this thesis to increase the magnitude of spectrum sharing inefficiencies.

The key to minimizing the inefficiency therefore requires a reduction in uncertainty regarding the spectrum sharing environment. Specifically, gaining a better estimate of the path loss between the spectrum users provides the ability to increase spectrum sharing. Reducing uncertainty therefore requires the ability to establish spectrum access behaviors using information focused on the specific operating context.

Given the general argument, an inference model that defines logical and mathematical relationships among information types, information sources, and decision attributes for DSA communication systems is developed and characterized in Chapter 3. The inference model builds on well-established communication theory relationship and enables assessments of performance differences as functions of situational uncertainty and risk.

The inference model uses a form of Bayesian Network called a Functional Causal Model. It leverages theoretically-based, analytical formulations for awareness and decision processing, which are implemented in a computer-based model for conducting analyses. The core inference model was derived from a causal interpretation of mathematical models that define relevant phenomena (e.g., signal propagation). The probabilistic model enables situation-specific uncertainty characterizations and governs spectrum access according to established risk thresholds. Specifically, spectrum sharing behaviors are shown to be functions of how well a DSA system can assess path loss to neighboring spectrum users. Increased levels of uncertainty lead to decreased transmit power and increased standoff distances between the DSA and protected users (PUs). Conversely, if a DSA system can improve its estimate of the path loss (e.g., through spectrum sensing), then it has greater spectrum access potential without increasing interference risk.

The probabilistic reasoning model is developed into a computer-based simulation that is used to analyze multiple scenarios in Chapter 4. The analysis addresses eight different spectrum access conditions categorized into two scenario types. The first category represents mobile PU conditions, in which significant uncertainty exists regarding the DSA$\rightarrow$PU distance and associated path loss. The second category represents conditions in which the DSA$\rightarrow$PU distance is known with small uncertainty (similar to the TV Whitespace and 3.5 GHz band situations). The results show that the probabilistic reasoning model produced increased capabilities when permitted by the updated findings, but also further restricted them when required. Specifically, capacity, link range, and spectrum access efficiency potential were increased with corresponding increases path loss between the DSA and PU. The converse held true as well; the metrics indicated lower performance levels under less favorable operating conditions.

The concepts developed in this thesis enable additional capabilities in spectrum sharing. Appendix A develops a decision model for DSA based on the probabilistic reasoning approach in this thesis. Probabilistic decision-making is a natural extension of the probabilistic reasoning model. The decision model uses utility theory—specifically multi-attribute utility theory—to enable evaluation and choice among alternative DSA actions. Utility theory provides an axiomatic system of choice evaluation that captures the relationships among goals, constraints, and uncertainty in a decision-making process. The decision model incorporates DSA channel capacity, interference, and monetary cost for spectrum access as decision attributes into a joint utility function.

The utility function is simulated and analyzed to assess DSA decision behaviors and trades under a range of spectrum sharing options and degrees of situational uncertainty. The analyses demonstrate the impact of spectrum usage volatility on preferences between emerging usage options under the tiered access model. Formulations are developed that identify the impact of cost and spectrum access uncertainty on decision trades between General Authorized Access (access without guarantees) and fee-based Secondary Access (access with guarantees). Analysis also characterizes decision trades between fee-based and auction-based spectrum pricing, leading to the insight that auction-based pricing incurs a distinct disadvantage relative to fee-based pricing due to the inherent uncertainty and pricing volatility.

The underlying probabilistic reasoning model for spectrum access is also applied to a satellite communications (SATCOM) system in Appendix B. SATCOM systems and networks require reliable management decisions for efficient and effective use of SATCOM resources. High demand on a SATCOM payload increases resource allocation challenges and amplifies the impacts of service shortfalls from unforeseen changes in user demand or service capabilities due to issues such as weather. By applying the probabilistic reasoning with risk-based assessments, SATCOM operators can assess the impacts of uncertainty on SATCOM system performance. The probabilistic reasoning method enables the quantitative representation of SA uncertainties and probabilistic reasoning for prediction, planning, and diagnosis of SATCOM payload performance. Furthermore, it provides the ability to conduct risk-based decision-making.

Thus the research presented in the following chapters and appendices presents a concept that has application to many aspects of spectrum usage and sharing. Chapter 2 provides the foundational argument that current spectrum sharing practices are necessarily and systemically limited in their ability to provide for effective spectrum sharing. Given the framework of that assessment, Chapter 3 develops the probabilistic reasoning model, mathematical basis for risk-constrained spectrum access, and theoretical foundation for assessing spectrum sharing potential as a function of situational awareness uncertainty. Chapter 4 presents and analyses simulation results of the concepts developed in Chapter 3, providing insight and demonstrating the viability of the probabilistic reasoning concept. Appendix A extends the probabilistic reasoning model with a multi-attribute decision model, enabling DSA systems to make spectrum access decisions based on multiple decision factors. Finally, Appendix B demonstrates the application of the probabilistic reasoning model to SATCOM resource management.

Chapter 2: A Logical and Mathematical Argument

This chapter provides a generalized logical and mathematical argument[1] that in situ probabilistic reasoning can improve spectrum access potential under situational uncertainty. The argument first establishes the premise that risk mitigation is an essential element in spectrum management. It summarizes the principles of the spectrum management process discussed in Chapter 1. It then formulates the basis for uncertainty as the means by which spectrum access risks can be assessed and defines the relationships among uncertainty, risk, and spectrum access efficiency. Finally, it shows that context-specific probabilistic reasoning for DSA systems provides the potential to reduce the assessment of situational uncertainties relative to a priori processes, therefore reducing risks associated with spectrum access decision-making and providing a corresponding improvement in spectrum access.

2.1 Risk Management Foundations of Spectrum Management

A central function of spectrum management is enabling access to spectrum while mitigating harmful interference among spectrum users [42]. When a new spectrum user requests access to spectrum, the spectrum user submits the desired characteristics of its equipment operating parameters (e.g., frequency band, signal bandwidth, operating locations/areas, and transmit power) to the spectrum regulators. Those system characteristics are tied to the goals (e.g., coverage area and data capacity) of the proposed wireless service. Regulators evaluate the potential impact that the new user and associated service could have on other spectrum users. To be granted a license to operate, the proposed system characteristics and associated operations must maintain an acceptable risk level with respect to interference to

[1]While the argument in this chapter acts as a type of general proof for the thesis, the term "proof" is withheld because the argument is not structured as a formal proof.

other users.[2]

In the assessment process described in Chapter 1, spectrum users and regulators utilize various analysis tools to conduct interference and performance assessments. Among them are signal propagation models that predict signal power levels across a geographic area as they propagate from the transmitter. Propagation models typically include random processes to characterize the complex interaction between an electromagnetic signal and its environment [6]. In using these models, regulators are able to assess the likelihood that the proposed spectrum use will cause harmful interference to other spectrum users. Similarly, the new spectrum user can determine the likelihood that the proposed spectrum access rules will provide sufficient coverage area and data capacity.

One prominent propagation model is the Irregular Terrain Model (ITM) [36, 37]. The ITM is a computer model for RF signal propagation at frequencies between 20 MHz and 20 GHz [36, 37]. It implements the Longley-Rice propagation model [38] and statistical analyses that incorporate terrain features affecting signal propagation and attenuation. The computer model was developed by the National Telecommunications and Information Administration (NTIA) Institute for Telecommunication Sciences (ITS) and is often used in developing and evaluating spectrum regulations and policies in the U.S. (see e.g., [35]). The treatment of uncertainty in the ITM provides a convenient framework for understanding the main aspects of signal propagation uncertainty.

The ITM groups uncertainty in three categories, which are incorporated into the mathematical propagation model [36]. The first category is time variability, which reflects long-term variations (days to years) in signal propagation due primarily to environmental changes (e.g., foliage). The second category is location variability, which accounts for differences in signal propagation among communications links having identical characteristics (e.g., link range and transmitter power) and operating in a similar propagation environment (e.g., terrain features), but with a variation in geographic location. The third and final uncertainty type is situation variability, which attempts to capture the less tangible aspects of signal

[2]Other factors–including economic and social benefits and risks–also enter the decision process but are not addressed here. The primary focus of this effort is on technical aspects related to spectrum access.

propagation uncertainty and is sometimes referred to as "prediction error".

The ITM model produces statistical prediction of signal strength loss (i.e., path loss) as a function of distance using the three variability categories. The probability assessments are expressed as quantiles, with a given result represented as a joint function $A(q_T, q_L, q_S)$. This function is interpreted as, "In q_S of like situations there will be <u>at least</u> q_L of the locations where the attenuation does not exceed $A(q_T, q_L, q_S)$ for <u>at least</u> q_T of the time" [36]. If the exact locations of transmitter and receiver are known, digitized terrain data are used to more accurately characterize the path loss rather than use location variability. The joint function $A(q_T, \ell, q_S)$ is then produced where ℓ represents the specified link conditions using terrain profile data associated with the specific locations. As potential variations of the three uncertainty factors are reduced or eliminated, the resulting uncertainty produced by the model is similarly reduced.

Other scenario-based uncertainty factors may also enter the assessment that are assumed to be known values used as inputs to the propagation models. For example, path loss is specified as a function of link range. While the ITM calculates path loss uncertainty for a specified link range, a DSA system may not know the distances between itself, or it may only be known only with a significant degree of uncertainty. Similarly, receiver performance characteristics (e.g., interference rejection) for protected users can vary among equipment types, manufacturers, and model variants. A probability-based assessment of spectrum access would need to add these factors into the distribution. Characterizing them as random variables and allowing them to be grouped into a common fourth category E for the purposes of this assessment would result in a joint probability function of $A(q_T, q_L, q_S, q_E)$.

The methodology for establishing exclusion zones in the 3.5 GHz spectrum sharing rules provides an example of how spectrum management processes address uncertainty factors [2, 31]. The 3.5 GHz band built in part on the existing TVWS approach discussed in Section 1.2.1 and followed from the PCAST report recommendations [1]. The rules enable low-powered small cell deployments in frequency bands already in use for other services and

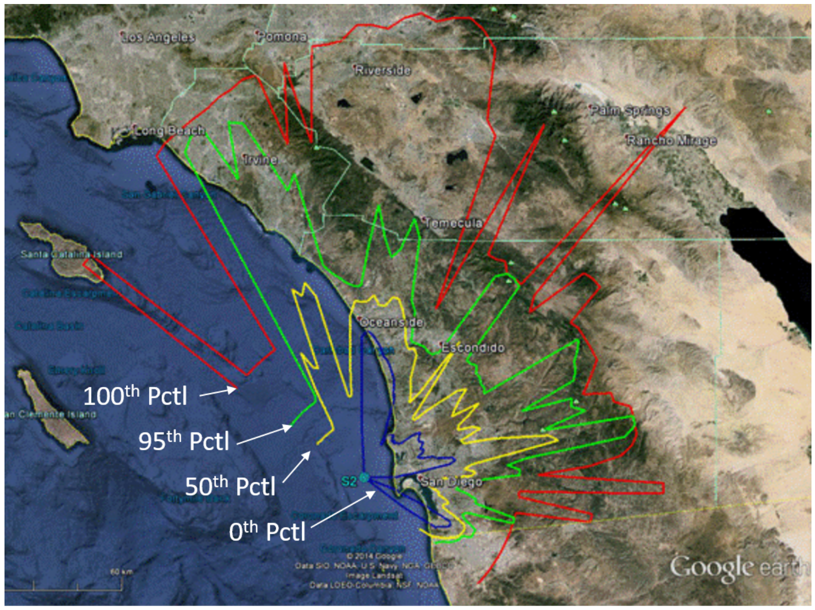

Figure 2.1: Example 3.5 GHz study exclusion zone confidence contours.

establish exclusion zones to protect radar systems. The NTIA, which manages Federal Government spectrum usage, undertook a study to determine the extent of the exclusion zones [31]. The model developed for the study involved probabilistic factors associated with the locations of the small cell user equipment, quantities of users (referred to as "market penetration"), and building characteristics in urban areas. A Monte Carlo simulation process was used to evaluate signal propagation, resulting in confidence intervals for quantifying the uncertainty associated with interference potential to the radar. Figure 2.1 presents an example of the exclusion zone confidence interval contours for a shipborne radar in a particular location and orientation produced in [31]. Exclusion zones were established at the 95 percent confidence level based on the composite results of all possible shipborne radar locations and orientations.

As the example shows, spectrum regulators and users assess the risks of the proposed spectrum usage with respect to the range of uncertainty factors associated with spectrum sharing. They evaluate spectrum access rules in terms of interference to other spectrum users as well as the technical and economic viability of the proposed spectrum service. Risk can be formally treated by determining the probability of meeting, exceeding, or falling short of some threshold. In the case of interference, risks can be assessed in the context of creating unwanted signal power that exceeds some received power level at a given location. Alternatively, an applicant can assess the probability that the proposed regulations enable the new spectrum user to achieve some threshold usage capability (e.g., link range, channel capacity, or populations served). In both cases, risks are used as a basis for making spectrum access decisions.

2.2 Defining Uncertainty, Risk, and Spectrum Access Efficiency

Before establishing an argument in support of the proposed thesis, a few key concepts need to be more formally and clearly defined. These concepts—namely uncertainty, risk, and spectrum access efficiency—are essential in the argument. While they have been treated anecdotally thus far, they require more formal definitions to ensure clarity in the arguments made in the following section.

Uncertainty can be defined or quantified using various measures such as entropy or variance [43, 44]. Information entropy as proposed by Shannon [45] has applications in machine learning [46], which relates to the DSA process of information discovery and classification. The focus here, however, is on parameter estimation. Thus uncertainty will be characterized in this study by the variance associated with a probability distribution. The relationship between uncertainty and variance is a commonly accepted one and is readily connected to the Bayesian probability and utility theory concepts presented later.

Risk is defined here as the exceedance probability for some uncertain event. As asserted in the previous section, spectrum management involves risk management. Spectrum access behaviors such as maximum transmit powers and standoff distances are determined in part by establishing acceptable probabilities of interference under a range of operating conditions. As presented in Figure 1.9 of Section 1.2.2, interference risk can be defined as the probability

q that the power imposed by a DSA system P_{rx} on a protected user will exceed some specified interference power threshold $P_{rx,int}$ and is defined by

$$\Phi_{Int} = \Phi(P_{rx} \geq P_{rx,int}) = \int_{P_{rx,int}}^{\infty} \phi\left(P_{rx}\right) = q. \tag{2.1}$$

It is similarly shown that interference risk can be expressed in terms of path loss. In this case, however, interference risk is defined as the probability q that the encountered path loss L_p is *less* than a threshold path loss $L_{p,int}$ and is defined by

$$\Phi_{Int} = \Phi(L_p \leq L_{p,int}) = \int_{0}^{P_{rx,int}} \phi\left(L_p\right) = q. \tag{2.2}$$

The risk concept can easily be extended to other attributes such as capacity and cost. To ensure clarity and generality in subsequent discussions, risk will be defined as the probability q associated some action $do(\cdot)$ produces a result x that violates (i.e, exceeds or falls short of) some threshold condition x_q. The existence of an upper or lower threshold will be made apparent by the particular attribute x under discussion.

Note that risk as used here differs somewhat from the approach of assessing Value at Risk (VaR) [47]. VaR is the amount of the parameter at risk, typically within some specified time period or frame of reference. In the context of interference from spectrum sharing, VaR would be the magnitude of $P_{rx,int}$ associated with some risk level q. While current approaches of interference specifications typically use a single threshold value, regulators could potentially specify degrees of harm associated with a graduated scale of $P_{rx,int}$ thresholds and associated risks q. To maintain consistency with current approaches, the approach selected here specifies a single interference threshold and associated risk level q.

The final term to be defined is spectrum access efficiency. Qualitatively, spectrum access efficiency is used here to refer to the difference between the optimal and selected spectrum access behaviors. The comparison is made relative to the specific situation in which the spectrum user operates and in the context of one or more quantifiable dimensions. Individual measures include link capacity, monetary cost associated with sharing, interference risk, and link range or coverage area. Aggregate measures are those that assess the overall effects with respect to group of spectrum users. That category includes network or user density, which is the number of networks (or users) per unit area. Those metrics will be presented in Chapter 3 and expressed either in a differential context (i.e., Δx) or relative context (i.e., $\frac{x_2}{x_1}$) to understand general insights across a range of scenarios.

2.3 A Logical Argument

As discussed in Chapter 1, current spectrum access processes produce policies that specify fixed sets of spectrum access behaviors. The adjective "fixed" refers to the universal nature of the specifications—such as the standoff distance or maximum transmit power in the TVWS and 3.5 GHz policy—that are unchanging even if a radio could exceed them without causing harmful interference to other users. The process of establishing fixed or universally-applied spectrum access behaviors in order to maintain acceptable levels of risk in uncertain environments *necessarily* leads to inefficient spectrum access. It can be illustrated by a simple reasoning exercise:

1. In establish operating limits, a spectrum access policy must consider all possible conditions χ for which the policy applies (i.e., all times, locations, and situations);

2. Policies establish limits on spectrum access behaviors (e.g., transmitter power, bandwidth, and standoff distances) associated with a specified probability of interference, which can be characterized by a probability threshold q;

3. These operating limits are only efficient when actual conditions χ_i correspond with those associated with q, i.e., $\chi_i = \chi_q$ and are necessarily inefficient under more favorable conditions $\chi_i \neq \chi_q$ such that $\chi_i \prec \chi_q$;

4. Policies *necessarily* lead to inefficient spectrum access in $1 - q$ percent of conditions.

That is, by establishing an operating behavior such that some resulting condition x meets a threshold condition x_q subject to some risk q, more favorable conditions occur with a probability $\approx 1-q$;

5. Since in general $q \ll 0.5$ to attain low interference risk, this process is *necessarily* inefficient in the majority of scenarios. That is, more favorable conditions $\chi_i \prec \chi_q$ exist in $1-q$ percent of situations;

Reducing the magnitude of this inefficiency requires a reduction in the range between the expected value $\mathrm{E}[\chi] = \bar{v}$ and threshold percentile value v_q. That is, reducing the uncertainty decreases the variance, which results in a smaller differential between the expected value and risk quantile and a corresponding increase in spectrum access efficiency. This assertion depends on the assumption that variance necessarily decreases with decreased uncertainty. While no universal proof is known to exist to support this claim, Chen et. al. [48], have developed the sufficient and necessary conditions under which the relationship holds. Specifically, the following theorem is presented:

> "Let X be a random variable with cumulative distribution function $F(x)$. If $F(x)$ is log-concave on any interval C, then $\textsc{Var}\{X|X \in A\} \leq \textsc{Var}\{X|X \in B\}$ for any intervals $A \subset B \subset C$." [48]

The log-concavity condition for many common continuous distributions is assessed by Bergstrom and Bagnoli [49], showing that many commonly-used distributions fulfill the criteria. Chen [48] further demonstrates that the sufficient conditions similarly apply to discrete distributions including unimodal, geometric, and Poisson functions. Therefore, the arguments made here will be subject to those conditions.

Given those conditions, consider two alternative spectrum access decision processes.[3] The first uses only a priori information and analyses to establish acceptable spectrum access behaviors. The second process augments the a priori information with in situ observations and assessments to determine acceptable spectrum access behaviors. Suppose the

[3]Note that the argument is developed here in the context of DSA systems, but is applicable to any system with similar processes.

two decision processes are equivalent in the sense that both will produce the same result given the same information. Also let both processes be able to sufficiently characterize their respective state spaces, accounting for all possible states and associated probabilities of occurrence. Thus the in situ assessments revise the probability assessments of the a priori process rather than the expansion of the state spaces.[4]

To construct the general argument, let the decision processes characterize any future state χ_i in which a wireless system may operate by a set of attributes. Without loss of generality, suppose the relevant attributes are time $T \equiv \{t_0, t_1, \ldots t_J\}$, location $L \equiv \{l_0, l_1, \ldots l_K\}$, situation $S \equiv \{s_0, s_1, \ldots s_M\}$, and environment $E \equiv \{e_0, e_1, \ldots e_N\}$ as presented in Section 2.1. Suppose further that each attribute's values are mutually exclusive such that only one value for each attribute can exist for any given state χ_i. Thus each state can be uniquely defined as:

$$\chi_i = \{T = t_j, L = l_k, S = s_m, E = e_n\}. \tag{2.3}$$

Also let each attribute have some non-zero probability of occurring. The probability of each state χ_i in the state space χ is therefore a function of the attribute probabilities:

$$P(\chi_i) = P(T = t_j, L = l_k, S = s_m, E = e_n). \tag{2.4}$$

The probability characteristics of the state space χ is then dependent upon the probability characteristics of the attributes T, L, S, E. The set of all possible relevant operating conditions can be defined as the power set of the attributes, namely $\chi \equiv \{T \times L \times S \times E\}$. Applying this construct to the two decision processes, let the first state space χ_1 represent the range of possible future states to be considered under the existing a priori regulatory scheme, and χ_2 represent the range of possible states under the in situ reasoning scheme.

[4]Note that this argument does not apply to learning processes that include the discovery and introduction of state spaces not included in the original set [50]. Such learning processes may (although perhaps not necessarily) lead to better decisions relative to those made with the original (incomplete) state space but are beyond the scope of this effort.

As previously discussed, the a priori regulatory model generally must establish risk thresholds that apply for longer periods of time as well as greater range of locations, situations, and environments than a system enabled to make in situ assessments. Thus it can be shown that $T_1 \supseteq T_2, L_1 \supseteq L_2$, and $S_1 \supseteq S_2$, which in turn necessarily leads to $\chi_1 \supseteq \chi_2$. Therefore any possible state considered by the in situ process will be also considered by the a priori process. Further, the in situ process may eliminate (i.e., apply zero probability to) one or more states in χ_1 based on new information. Given those conditions, it follows that $\chi_2 \subseteq \chi_1$ and $\textsc{Var}\{\chi_1\} \geq \textsc{Var}\{\chi_2\}$ by Chen's theorem [48]. *Thus in situ probabilistic reasoning in DSA systems enables greater spectrum access potential than existing methods, which establish operating limits using a priori information.*

While a complete accounting of all elements in $\{T, L, S, E\}$ may be impractical (perhaps even impossible), it is practical to account for their *effects* with respect to χ. Consider the case where χ represents path loss $L_P(\chi)$. It is infeasible to enumerate all the possible conditions $\{T, L, S, E\}$ that belong to χ, but it is quite easy to establish the relevant range of values for $L_P(\chi)$ a priori. That is, the uncountably large state space associated with χ maps to a reasonably small range of relevant values for $L_P(\chi)$, which can be determined a priori and in situ. It will be shown later that the same reasoning applies to other relevant parameters in the DSA reasoning model such as distance and transmit power.

What may be lost with incomplete enumeration of the state space, however, is the accuracy of probability valuations associated with the values of $L_P(\chi)$. By not fully accounting for the elements of χ, it may not be possible to properly characterize $\phi(\chi)$. This limitation, however, provides further support to the proposed hypothesis. A priori assessments generally must incorporate a larger set of possible state spaces than in situ processes, making accurate a priori probability assessments more difficult than in situ assessments that consider much smaller state spaces. By beginning with the a priori probability assessment, a DSA system can refine it with information acquired in situ—eliminating some states and accounting for a greater percentage of relevant states and thus reduce uncertainty.

This process of improving estimates by gaining information through observations is well-studied in estimation theory and in applications such as signal processing and tracking. The Fisher Information provides a metric for assessing the amount of information that an observation provides regarding some other parameter [51]. Given some observation x, the variance of a related (but unobserved) variable θ is given by

$$\textsc{Var}\left(\theta\right) = -\mathrm{E}\left[\frac{\partial^2 \ln \phi(x;\theta)}{\partial \theta^2}\right]^{-1}. \tag{2.5}$$

As the observation x noise (i.e., the variance) decreases, the Fisher Information is increased and the variance of the estimate of θ is decreased.

In a similar manner, the Kalman Filter provides a means for updating an estimate given the information associated with an observation [51, 52]. The Kalman Filter algorithm contains a factor often referred to as the "filter gain", which determines the rate at which the estimate is updated in response to the measurement. The filter gain is a function of the measurement and prior estimate error variances. As the measurement error variance approaches zero, the measurement contains more information and the filter gain increases. Thus we see another example of how increased information attained through an observation leads to decreased uncertainty regarding an estimation.

2.4 Summary

The discussion here provides an argument supporting the thesis that *in situ probabilistic reasoning in DSA systems enables greater spectrum access potential than existing methods.* Section 2.1 asserted that risk management is a core element in spectrum management. Spectrum access behaviors are constrained in large part by acceptable levels of risk, which can be represented as probabilities that establish confidence levels associated with factors such as interference. Together with the anecdotes provided in Chapter 1, it is shown that uncertainty becomes a limiting factor in spectrum access potential. It is demonstrated that behaviors established a priori that are associated with a probability q (i.e., risk level of q) are *necessarily* lead to inefficient access in $1 - q$ percent of situations. Given that $q \ll 0.5$, inefficient behaviors are established in the majority ($\gg 0.5$ percent) of cases.

To increase spectrum access, the uncertainty associated with spectrum behavior determination must be reduced. Current spectrum practices make a priori determinations, which entail significant levels of uncertainty due to their application to a broad scope (time duration, geographic extent, and operating environments). DSA systems, however, have the potential to characterize their particular operating environment and make in situ uncertainty assessments, resulting in potentially reduced levels of uncertainty relative to those of the a priori process. A logical argument of the thesis is supported by the mathematical basis and conditions under which the argument holds.

To expound on the argument, the following chapters develop a model that incorporates probability assessments in the DSA situational awareness and decision process. Chapter 3 establishes a probabilistic situational awareness and reasoning model. It establishes the theoretical basis for the model and identifies the formal relationships between uncertainty and DSA performance. Chapter 4 analyzes the simulation results of the probabilistic reasoning model in a range of scenarios.

Chapter 3: A Probabilistic Reasoning Model for Dynamic Spectrum Access

A DSA probabilistic reasoning model enables a DSA system to characterize risks (e.g., probability of causing harmful interference or achieving a user-specified need) derived from a set of qualified algorithms and imperfect information. The characterization must be such that—despite the uncertainty—a DSA system can make a valid decision relative to the specified goals and constraints and adapt its behavior accordingly. That decision may be to access a particular wireless channel with some set of transmission characteristics or to withhold a transmission in favor of continued information gathering. Ultimately, the model must allow a DSA system to evaluate the cause-effect relationships of observable phenomena and its own actions.

Causality is not only a fundamental characteristic of DSA systems, but is the principle problem that DSA systems attempt to solve. Specifically, DSA systems attempt to identify actions that lead to (i.e., *cause*) the provisioning of sufficient communications capacity while not creating (i.e., not *causing*) harmful interference to other spectrum users. Therefore they need to make assessments about their operating environment based on acquired awareness, and then use that information to project the potential consequences of alternative actions. In causal terms, the DSA system is inferring the cause of its observations and then inferring the effects of prospective interventions (e.g., transmissions) in the operating environment. Thus the notion of DSA is not possible without the basic assumption of cause and effect—both in terms of deriving situational awareness from observations and assessing the effects of prospective actions. Evaluating causes and effects, however, is laden with uncertainty due partly to limitations on situational awareness and partly due to the inherent stochastic nature of wireless communications processes. Thus awareness may be characterized by imperfect and incomplete information.

One approach for capturing the causal and probabilistic nature of the DSA inference problem is to use probabilistic Functional Causal Models (FCMs) [53,54] for DSA situational awareness. FCMs can provide a logical and ontological rigor consistent with accepted policy-based reasoning methods [32–34] while enabling the ability to reason about cause-effect relationships and risks associated with potential DSA actions. FCMs can be developed naturally from well-known functional relationships used in communications theory (e.g., signal propagation and detection) to quantify variables and associated uncertainties.

The following section provides an overview of Functional Causal Models, including the underlying theory and rationale for application to the DSA domain. Section 3.2 then develops a DSA situational awareness FCM, which is used in Section 3.3 to characterize the theoretical uncertainty relationships among model parameters applied to a computer simulation model in Chapter 4.

3.1 Causal inference for DSA systems

Causality among a set of entities or observations implies the existence of an ontological or structural relationship rather than a mere associative one [53, 54]. Associative relationships can be fully characterized by joint probability distributions and related concepts such as correlation, likelihood, and conditional independence. Causal relationships, however, require more than statistical characteristics in defining their interrelationships; they require concepts such as influence, effect, and explanation that involve an ordering or temporal relationship such that effect follows cause.

Functional causal inference models indicate the functional cause-effect relationships among a set of variables. The definition of a (deterministic) causal model C_d is formally defined [53] as a triple $C_d = \langle U, V, F \rangle$ where

1. U is a set $\{U_1, U_2, \ldots, U_n\}$ of *background variables* that are determined by factors outside the model;

2. V is a set $\{V_1, V_2, \ldots, V_n\}$ of *endogenous variables* that are determined by background and other endogenous variables. V_i is therefore determined by the set of all other variables, i.e., $U \cup V \setminus V_i$;

3. F is a set $\{f_1, f_2, \ldots, f_n\}$ of functions such that each f_i is a mapping from the respective domains of $U_i \cup PA_i$ to V_i:

$$v_i = f_i\left(pa_i, u_i\right), i = 1, \ldots, n, \tag{3.1}$$

where pa_i are the parents $PA_i \subseteq V \setminus V_i$ of v_i. Each f_i in $v_i = f_i(pa_i, u_i), i = 1, \ldots, n$ assigns a value to V_i that depends on the values of a select set of variables in $V \cup U$, and the entire set F has a unique solution $V(u)$.

A *probabilistic* causal model C_p follows from the definition of C_d as a pair $C_p = \langle C_d, P(u)\rangle$ where $P(u)$ is a probability function defined over the domain of U. The functions f_i comprising C (either C_d or C_p) in their general form are sets of equations, which represent a structural equation model (SEM). The relationships defined by the functions can represent physical or other well-codified relationships from various domains (e.g., economic). Due to the causal nature of the functions, queries representing specific actions or conditions can be applied to a SEM by fixing the value of one or more variables $X = x$. In applying such changes, a submodel is created from the original SEM, which is itself a valid SEM. Formally, a submodel $C(x)$ is defined in C as $C(x) = \langle U, V, F_x\rangle$ such that $X \subseteq V$, x is a particular realization of X, and $F_x = \{f_i : V_i \notin X\} \cup \{X = x\}$. Thus the transformation between C and $C(x)$ is a modification of F.

As a consequence, a causal model C can be queried to determine the effects of (potential) actions and explore the characteristics of alternative world states. Pearl [53] defines a causal calculus around an action "$do(X = x)$", which applies a set of alterations to F and produces F_x. The result is a transformation of C into $C(x)$ via some (minimal) set of alterations. The calculus of $do(\cdot)$ thus enables queries regarding interventions—"What is the expected response of Y due to action $do(X = x)$?"—and counterfactuals—"Would $Y = y$ in situation $U = u$ had X been x?" Those types of queries along with predictive capabilities of the causal network are essential for decision-making.

A Functional Causal Model (FCM) combines the functional relationships of SEMs, the potential outcome framework, and graphical models for probabilistic reasoning [54]. Consequently, every causal model C_d and probabilistic causal model C_p can be represented as a directed graph $G(C_d)$ and $G(C_p)$, respectively. Variables of $v_i = f_i(pa_i, u_i)$ are represented as nodes, with edges connecting parent and background variables (pa_i, u_i) to endogenous variables v_i. The direction of edges naturally follows the direction of influence, that is from (pa_i, u_i) to v_i. A probabilistic causal model can be represented as a Bayesian Network. The $do(\cdot)$ operator acts upon the nodes of the graph, affecting the value of the represented variables and therefore generating sub-graphs to answer queries regarding interventions and counterfactuals. Note that the edges are *not* altered (but may be made irrelevant) by the $do(\cdot)$ operator, thus ensuring that the resulting model is consistent with (i.e., is a submodel of) the original model.

The modeling and inferential characteristics of causal modeling as presented here support the awareness and decision-making functions of DSA systems. Key characteristics that are fundamentally enabling to DSA systems include the following:

1. Formal mechanisms to support DSA decision-making through assessing cause-effect relationships of candidate actions
2. Formal mechanisms for learning through counterfactual queries and observations following interventions
3. Potentially lower data acquisition requirements
4. Support for spectrum regulatory processes through the use of ontology-based models with provable logic structures and SEMs built upon accepted engineering methods.

A cause-effect determination is essential for the action-based DSA process, which seeks to achieve the desired goals through some action. The causal calculus is unique in its ability to differentiate between causes and effects; associative (i.e., non-causal) logics can only indicate degrees of correlation among conditions and symptoms. For example, associative methods can only determine that the magnitudes of a transmit power P_{tx} and received power P_{rx} are correlated; they cannot specify whether P_{tx} influences P_{rx} or vice versa. Causal methods, however, encode cause-effect information into the ontological structure derived from the physical meaning of the SEM, thus allowing the determination of actions and conditions preceding some event. That is, the logic $P_{tx} \rightarrow P_{rx}$ derived from physical principles is encoded along with the functional relationship $P_{rx} = f\left(P_{tx}, L_p\right)$.

Additionally, the interventional nature of DSA operations requires a formal mechanism for reasoning about changing environmental conditions. A DSA system is a participant in the environment that it observes; acting within that environment potentially has a causal effect on other users and thus changes the nature of the environment. Associative methods can only establish validity under static environmental conditions or make assumptions of conditional independence between past and present states [55]. Similarly, DSA systems must make decisions in dynamic, partially-observable conditions; observations are taken over time and used to support decisions involving anticipated conditions in some future time frame. Underlying conditions—spectrum occupancy, propagation conditions, transmitter/receiver positions—within those two frames can change significantly. Furthermore, a causal approach is needed to support the function of interacting (e.g., transmitting, collecting evidential data for greater awareness) with entities in the observed environment and in some cases seeking to determine the effect of those actions on others (e.g. interference) [56].

Functional causal modeling may also help with DSA learning potential. While learning is not a necessary function of DSA systems[1], performance can theoretically be improved through better prediction based on learned concepts. Learning may happen through various DSA methods including passive observations, statistical analysis, observations regarding responses to interventions, and counterfactual queries. As previously stated, interventional queries seek to predict the results of actions based on existing (perceived) conditions, where

[1] A differentiate here between DSA as an adaptive process and learning new concepts as a supplement to that process.

counterfactual queries seek to predict the results of actions using hypothetical conditions. Thus a causal model allows a DSA system to explore the combined effects of conditions, acquired knowledge, and actions on performance and policy compliance in a manner analogous to the discovery of policy constraints in proposed policy control mechanisms [32–34].

FCMs may also have generally lower observational data requirements relative to associative models that result from knowledge inherent in causal relationships [57]. Causal models tend to be sparser as they are often formed by natural processes with well-defined variables [56]. Lower data acquisition requirements translates to reduced data collection demand and reduced information processing needs. The timeframe for making decisions in a DSA system is dictated by the operating environment; quickly-changing environments require more rapid decisions to maintain sufficient link capacity and avoid causing harmful interference to other users. Reduced data collection and processing requirements provide better support for those conditions than a process with higher data collection and processing burdens.

Support for regulatory compliance is essential for technology implementation in DSA systems. As discussed in Chapter 1, existing DSA policy reasoning efforts were established due to the need to ensure regulatory compliance and have generally been viewed favorably by the regulatory community [32–34]. While policy controls deduce the constraints and permissions specified by the established rules governing spectrum access, they require a compatible quantitative computing approach for developing strategies. Causal models representing relevant operational conditions and causal phenomenology provide the ability to make risk assessments based on acquired awareness that characterize possible in situ conditions. An FCM approach provides logical inference chains that leverage mathematical expressions of physical phenomena, ontological information regarding cause-effect relationships, and the inference methods of Bayesian Networks. Chains of probabilistic reasoning can be built around (and thus gain credibility from) commonly-accepted mathematical relationships among observational and consequential variables of the model. The causal nature of the encoded information along with the $do(\cdot)$ calculus enables prediction, intervention, and counterfactual queries for awareness development.

The following section presents a conceptual architecture and examples of a causal reasoning approach to DSA situational awareness. They are then used for characterizing the theoretical uncertainty relationships among model parameters in Section 3.3 and to develop a computer simulation model in Chapter 4.

3.2 Functional causal models for DSA

As previously stated, DSA systems assess the cause of observed phenomena and the effects of any possible action they wish to take. The effects primarily fall into two categories: the potential impact to other spectrum users (i.e., interference) relative to established policy constraints; and the impact to its own performance relative to user goals (e.g., link capacity). The basis for establishing those assessment models can be built from established principles and mathematical representations of wireless signal propagation and communication systems that are widely used by engineers, system designers, and spectrum managers (see e.g., [6, 7]). Leveraging the probabilistic foundation of communications theory, these same sets of principles and associated mathematical models can be developed into situational awareness and reasoning models for DSA systems that are represented as Functional Causal Models.

Consider first the signal power P_{rx} at some receiver, which (in decibel scale) is the transmitted power P_{tx} less the magnitude of the path loss L_p:

$$P_{rx} = P_{tx} - L_p. \tag{3.2}$$

Letting P_{tx} and L_p be independent random variables, the received power probability distribution conditioned on P_{tx} and L_p can be defined as

$$\phi\left(P_{rx}|P_{tx}, L_p\right) = \phi\left(P_{tx} - L_p\right). \tag{3.3}$$

The graphical representation of the resulting received power FCM is given in Figure 3.1a,

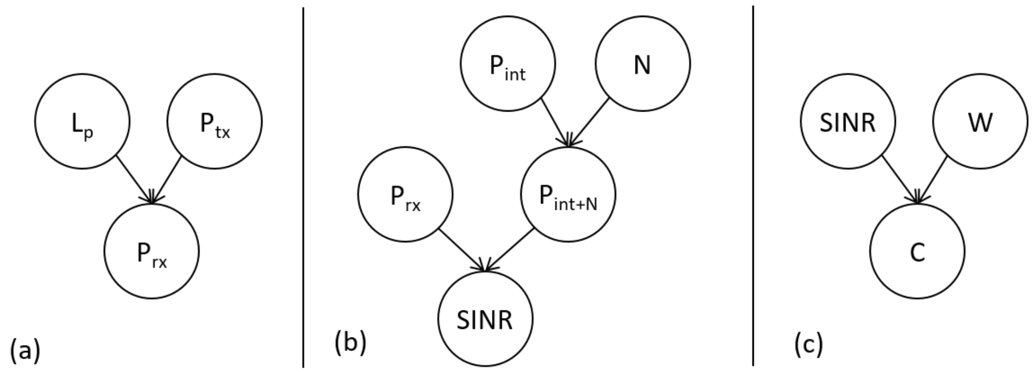

Figure 3.1: Graphical depictions of functional causal models for a) received power, b) SINR, and c) capacity.

which is formally defined as

$$G\left(P_{rx} = \langle U, V, F \rangle\right) \text{ for } \begin{cases} U \equiv \{L_p, P_{tx}\} \\ V \equiv \{P_{rx}\} \\ F \equiv \{P_{rx} = P_{tx} - L_p\} \end{cases} \tag{3.4}$$

Similar FCMs can be developed for other key parameters such as link capacity, which is a function of the signal-to-interference-plus-noise ratio (SINR). SINR indicates the relative proportion of wanted signal power P_{rx} to the total of unwanted signal power P_{int} (interference) and environmental noise N_0 integrated over the channel bandwidth W. Interference arises from other intentional transmitters on the same frequency band and unintentional signals (e.g., harmonics) generated by RF and electromagnetic devices. SINR is given in linear scale by

$$SINR^* = \frac{P_{rx}^*}{P_{int}^* + N^*}, \tag{3.5}$$

where the superscript "*" used here indicates linear scale variables (i.e., power in Watts or milliWatts and SINR as a ratio). Using the conversion to decibel scale,

$$X = 10\log_{10}(X^*), \tag{3.6}$$

SINR is also given as

$$SINR = P_{rx} - P_{I+N} \tag{3.7}$$

where P_{I+N} is the total noise power from the interference and noise given by

$$P_{I+N} = 10\log_{10}\left(P^*_{int} + N^*\right). \tag{3.8}$$

Note that P^*_{int} and N^* are in linear scale and converted from decibel scale using the inverse of (3.6). The SINR FCM is given in Figure 3.1b and is formally defined as

$$G\left(SINR = \langle U, V, F\rangle\right) \text{ for } \begin{cases} U \equiv \{P_{rx}, P_{int}, N\} \\ V \equiv \{SINR, P_{I+N}\} \\ F \equiv \begin{Bmatrix} P_{I+N} = 10\log_{10}\left(P^*_{int} + N^*\right) \\ SINR = P_{rx} - P_{I+N} \end{Bmatrix} \end{cases} . \tag{3.9}$$

Link capacity C is then found as a function of $SINR$ by

$$C = W\log_{10}\left(1 + SINR^*\right) \text{ bits/s} \tag{3.10}$$

where W is the bandwidth of the channel and $SINR^*$ is a ratio in linear scale. The associated FCM is given in Figure 3.1c, which is formally defined as

$$G\left(C = \langle U, V, F \rangle\right) \text{ for } \begin{cases} U \equiv \{SINR, W\} \\ V \equiv \{C\} \\ F \equiv \{C = W \log_{10}\left(1 + SINR^{*}\right)\} \end{cases} . \tag{3.11}$$

The equations presented above are regularly combined to present various communications link analyses. The resulting system of equations is by definition a Structural Equation Model (SEM) as described in Section 3.1. The FCMs from Figure 3.1 can similarly be combined into a larger FCM, such as the one in Figure 3.2 representing a communications link. The graph definition becomes

$$G\left(Link = \langle U, V, F \rangle\right) = G(P_{rx}) \cup G(SINR) \cup G(C)$$

$$\text{for } \begin{cases} U \equiv \{L_p, P_{tx}, P_{int}, N, W\} \\ V \equiv \{P_{rx}, SINR, C\} \\ F \equiv \begin{Bmatrix} P_{rx} = P_{tx} - L_p, \\ P_{I+N} = 10 \log_{10}\left(P^{*}_{int} + N^{*}\right) \\ SINR = P_{rx} - P_{I+N} \\ C = W \log_{10}\left(1 + SINR^{*}\right) \end{Bmatrix} \end{cases} \tag{3.12}$$

The model in Figure 3.2 can be appended with additional elements to extend the model and include additional concepts. For example, path loss L_p as depicted in the model is defined as a background variable U and is characterized by factors and an associated model that are external to the FCM. Alternatively, a path loss model can be included in the FCM if those variables can be estimated and are important for the DSA reasoning process. Thus path loss would become an endogenous variable (i.e.,$L_p \in V$), with the defining parameters

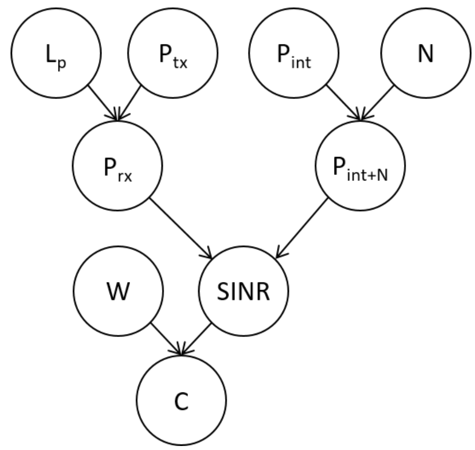

Figure 3.2: Communications link functional causal model.

added as background variables U.

The model can also be expanded to encompass a larger reasoning process or situational model. Note that P_{int} is a received power and can be represented using (3.2) and the FCM in Figure 3.1. Similarly, the effect of multiple interfering emitters could be modeled and aggregated into the $SINR$ calculation. The FCM shown in Figure 3.3 illustrates a case with two interference sources, each using the received power FCM to represent the corresponding link.

Models can also be combined to represent the cause-effect awareness needed by a DSA system. A DSA causal model contains three basic components. The first is the impact that the DSA system would have on a protected user (PU), for which some maximum interference power threshold may be established. This can be modeled as a propagation path from the DSA transmitter to the PU receiver $G(P_{rx,D\to P})$ using (3.2) and the FCM in Figure 3.1a. The same received power model can also be used for the second component, which is the impact that the PU signal would have on the DSA receiver in terms of interference power $G(P_{rx,P\to D})$. The third component is the resulting link performance, which can be modeled using the $G(Link_{D\to D})$ FCM shown in Figure 3.2. These three components can be combined

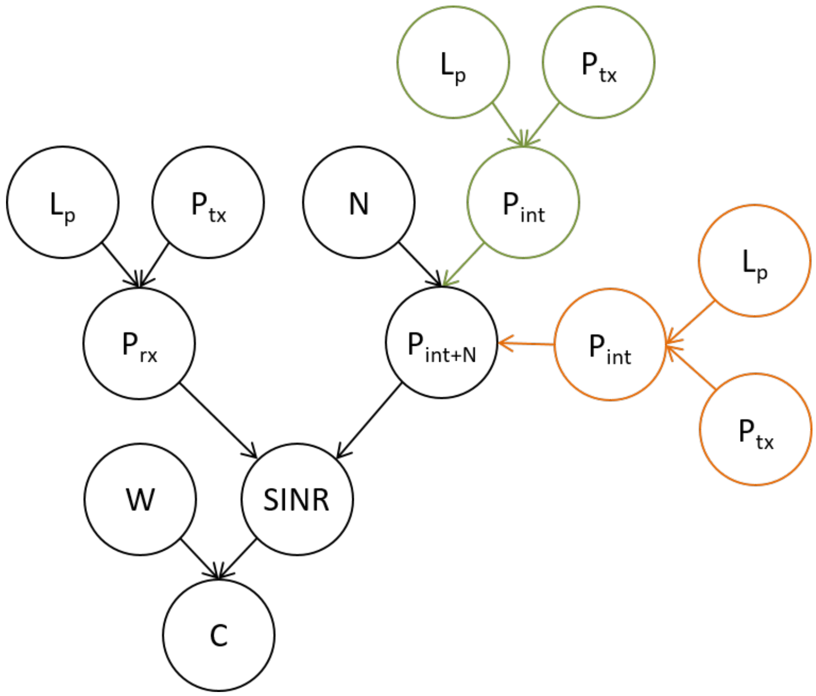

Figure 3.3: Communications link functional causal model with multiple interference sources.

to create the DSA situational awareness model shown in Figure 3.4, and are defined by

$$G\left(DSA = \langle U, V, F\rangle\right) = G(P_{rx,D\rightarrow P}) \cup G(P_{rx,P\rightarrow D}) \cup G(Link_{D\rightarrow D})$$

$$\text{for} \begin{cases} U \equiv \{L_{p,D\rightarrow P}, P_{tx,D}, L_{p,P\rightarrow D}, P_{tx,P}, N, W\} \\ V \equiv \{P_{rx,D\rightarrow P}, P_{rx,P\rightarrow D}, P_{rx,D\rightarrow D}, P_{I+N}, SINR, C\} \\ F \equiv \begin{Bmatrix} P_{rx,D\rightarrow P} = P_{tx,D} - L_{p,D\rightarrow P}, \\ P_{rx,P\rightarrow D} = P_{tx,P} - L_{p,P\rightarrow D}, \\ P_{rx,D\rightarrow D} = P_{tx,D} - L_{p,D\rightarrow D}, \\ P_{I+N} = 10\log_{10}\left(P^{*}_{rx,P\rightarrow D} + N^{*}\right), \\ SINR = P_{rx,D\rightarrow D} - P_{I+N}, \\ C = W\log_2\left(1 + SINR^{*}\right) \end{Bmatrix} \end{cases} \tag{3.13}$$

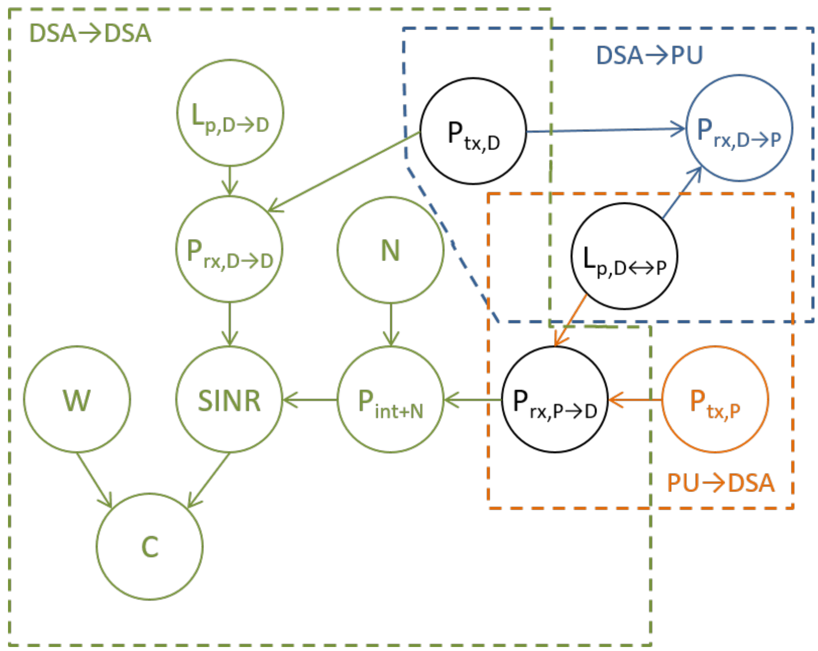

Figure 3.4: DSA situational awareness functional causal model.

.

The FCM in Figure 3.4 can be directly applied to DSA systems that incorporate sensing. When a DSA system senses the spectrum, it observes sum of the noise N and any signal that is present on the channel, which corresponds with P_{I+N}. This sensed power is equivalent to the signal plus interference term in the SINR equation (3.8).

To illustrate how a DSA system would use the sensing model to gather information about its local environment, let the DSA system establish its prior beliefs regarding channel characteristics and the potential users. The prior data may come from a combination of location awareness via onboard GPS sensors, propagation models of the local environment as described in Chapter 2, and protected user data derived from regulatory policies and databases [32–34]. Let spectrum policies provide the users with a specified degree of protection from interference, as discussed in Chapter 2. Thus the DSA system wishes to use the prior beliefs and knowledge of regulatory constraints and user goals to determine if it is able to access the channel at a given capacity level without causing harmful interference to any protected user (PU) that may be present.

To evaluate a given communications channel, the DSA system needs to determine its maximum permitted transmit power $P_{tx,D,max}$, which in part establishes the maximum channel capacity. The maximum transmit power is set by the maximum interference power P_{int} at the PU by $\Phi\left(P_{rx} < P_{int}\right) \geq q$ as defined in Chapter 2. Thus, $P_{rx,D\to P}$ is set to P_{int} and the maximum transmit power is determined by the uncertainty associated with the path loss $L_{p,D\to P}$:

$$P_{int} = P_{tx,D,max} - L_{p,D\to P,q} \tag{3.14}$$

where $L_{p,D\to P,q}$ is the path loss associated with the corresponding risk level q and is defined as

$$\Phi\left(P_{rx,D\to P} \geq P_{int}\right) = \int_{P_{int}}^{\infty} \phi\left(P_{rx,D\to P}\right) = \int_{0}^{L_{p,D\to P,q}} \phi\left(L_{p,D\to P}\right) = q. \tag{3.15}$$

With $P_{tx,D,max}$ defined, the DSA can now refine the channel capacity estimate on the DSA link. Thus the DSA determines $\Phi\left(C|U, P_{rx,D\to P} \leq P_{int}\right)$ where U is the set of background variables. From a causal perspective, this equates to $G\left(DSA|do(P_{tx,D} \leq P_{tx,D,max}\right))$.

When sensing the RF environment to gain a better estimate of the path loss to the PU, $L_{p,D\to P}$, it observes P_{I+N} and infers the path loss posterior probability $\left(L_{p,D\to P}|P_{I+N}\right)$ using Bayes' theorem

$$\phi\left(L_{p,D\to P}|P_{I+N}\right) = \frac{\phi\left(P_{I+N}|L_{p,D\to P}\right)\phi\left(L_{p,D\to P}\right)}{\phi\left(P_{I+N}\right)}, \tag{3.16}$$

where

- $\phi\left(L_{p,D\to P}|P_{I+N}\right)$ is the updated (posterior) path loss probability given the measurement;
- $\phi\left(P_{I+N}|L_{p,D\to P}\right)$ is the likelihood distribution of observed power given the prior path loss probability;

- $\phi(L_{p,D\rightarrow P})$ is the prior path loss probability distribution; and

- $\phi(P_{I+N})$ is the measured received power probability.

The FCM would then be updated to $G(DSA|P_{I+N})$. The DSA system can then use the updated graph in determining $P_{tx,D,max}$ and C as before, giving

$$G\left(DSA|do\left(P_{tx,D} \leq P_{tx,D,max}|L_{p,D\rightarrow P|P_{I+N}}\right)\right). \tag{3.17}$$

Note that DSA systems would generate the SA FCM from Figure 3.4 for each channel it wished to evaluate. A scalable means for creating and managing the FCM is therefore necessary given that the DSA would want to evaluate potentially hundreds of channels, each possibly having multiple PUs. To find a solution, first consider that each channel can be represented independently. Thus the FCM for a given channel such as the one in Figure 3.4 becomes the largest FCM (modulo the number of PUs on the channel). Next, observe that each FCM contains some repeated subnets, each of which was built from smaller building blocks—one for each equation in the FCM as depicted in Figure 3.1. It can be seen that the DSA system can compose large SA models from a relatively small number of subnets. Multi-Entity Bayesian Networking (MEBN) theory provides a means for composing those larger models in a way that is ontologically consistent and provably sound with respect to first order logic and BN theory [58]. With the MEBN approach, the FCMs of Figure 3.1 become MEBN Fragments (MFrags), which are the basic building blocks for the FCM. The process is analogous to object oriented programming's use of classes to generate complex computer models having many objects derived from a small set of class definitions. This approach will be demonstrated in the simulation model development in Chapter 4 as well as the satellite communication (SATCOM) model in Appendix B.3.

The following sections analyze a DSA FCM based on the one developed here. Section 3.3 conducts an assessment of the theoretical relationships among the model's elements with respect to uncertainty. Chapter 4 implements the FCM in a simulation model and assesses the ability to reduce situational uncertainty through sensing and thereby improve spectrum access performance as argued in Chapter 2.

3.3 Theoretical Characterization and Analysis of DSA Situational Awareness Uncertainty

The DSA FCM provides the basis for characterizing DSA situational awareness uncertainty. Specifically, uncertainty associated with the background variables U propagate through the model and determine the uncertainty associated with key operating conditions such as interference and capacity. Of particular importance is understanding the impact that path loss uncertainty between the DSA transmitter and PU receiver $L_{p,D\to P}$ has on DSA SA and predicted performance.

As shown in (3.14), the path loss $L_{p,D\to P,q}$ determines the maximum transmit power $P_{tx,D,max}$ which in turn affects DSA link capacity C. It will also be shown that $L_{p,D\to P,q}$ also affects the requisite standoff distance and spectrum access density, defined as the number of wireless networks per unit area.

The following sections develop the theoretical relationships between path loss uncertainty, DSA system behavior and performance bounds, and spectrum access efficiency. Section 3.3.1 establishes the theoretical characterization for each variable in terms of its relation to path loss mean $\mu_{L_{p,D\to P,q}}$, standard deviation $\sigma_{L_{p,D\to P,q}}$, and risk q. Section 3.3.2 uses those equations to establish DSA behavior and performance bounds as well as spectrum access efficiency impacts as functions of changes path loss mean $\Delta\mu_{L_{p,D\to P,q}}$ and standard deviation $\Delta\sigma_{L_{p,D\to P,q}}$, which enable assessments in term of uncertainty $\sigma^2_{L_{p,D\to P,q}}$.

3.3.1 Theoretical Characterization of DSA SA Uncertainty

Beginning with the DSA→PU subgraph in Figure 3.4, the signal power that the DSA transmitter imposes on the PU receiver is given by (3.2). The received power at the PU from the DSA $P_{rx,D\to P}$ represents unwanted power (i.e., interference) and must meet interference limits specified by spectrum policies. The mean and variance of $P_{rx,D\to P}$ are

$$\mu_{P_{rx,D\to P}} = \mu_{P_{tx,D}} - \mu_{L_{p,D\to P}}, \tag{3.18a}$$

$$\sigma^2_{P_{rx,D\to P}} = \sigma^2_{P_{tx,D}} + \sigma^2_{L_{p,D\to P}}. \tag{3.18b}$$

Using the risk-constrained spectrum access concept presented in Chapter 2 and further developed in Section 3.2, a specified risk threshold can be defined in terms of a percentile q associated with the received DSA power at the PU. The DSA must transmit such that the received power $P_{rx,D\to P}$ at the PU is less than the interference threshold $P_{rx,int}$ with probability of at least q; that is $\Phi(P_{rx,D\to P} < P_{rx,int}) \geq q$. With $L_p = P_{tx} - P_{rx}$, and setting the DSA transmit power to some maximum permitted value $P_{tx,D,q}$, the interference power constraint (3.15) can be rewritten as

$$\Phi(L_{p,D\to P} \geq P_{tx,D,q} - P_{rx,D\to P}) = \Phi(L_{p,D\to P} \geq L_{p,D\to P,q}) \geq q. \tag{3.19}$$

For a fixed transmit power $P_{tx,D,q}$, the probability distribution of the path loss $\phi\left(L_{p,D\to P}\right)$ defines the received power distribution $\phi\left(P_{rx,D\to P}\right)$ as

$$\phi\left(P_{rx,D\to P}\right) = \phi\left(L_{p,D\to P,q}\right) + P_{tx,D,q}. \tag{3.20}$$

Thus $\phi\left(P_{rx,D\to P}\right)$ is $\phi\left(L_{p,D\to P,q}\right)$ shifted by an amount equal to $P_{tx,D,q}$.

The percentile (i.e., risk) q can therefore be associated with some path loss value $L_{p,D\to P,q}$ on the probability distribution $\phi\left(L_{p,D\to P}\right)$ as specified in (3.14) and (3.15). Specifically, $L_{p,D\to P,q}$ can be expressed in terms of the path loss mean $\mu_{L_{p,D\to P}}$ and some multiple a_q of $\sigma_{L_{p,D\to P}}$ by

$$L_{p,D\to P,q} = \mu_{L_{p,D\to P}} - a_q \sigma_{L_{p,D\to P}} \tag{3.21}$$

as illustrated in Figure 3.5.

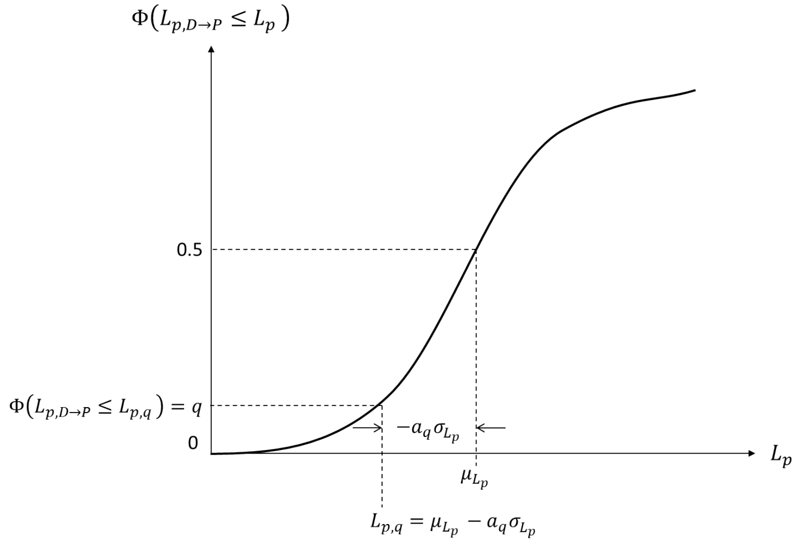

Figure 3.5: The relationship between path loss mean μ_{L_p}, standard deviation σ_{L_p}, and interference risk percentile q.

Given (3.14) and (3.21), the maximum DSA transmit power associated with the risk level q and PU interference threshold $P_{rx,int}$ is then defined as a function of $\mu_{L_{p,D\to P}}$ and $\sigma^2_{L_{p,D\to P}}$ by

$$P_{tx,D,q} = P_{rx,int} + \mu_{L_{p,D\to P}} - a_q\sigma_{L_{p,D\to P}}. \tag{3.22}$$

Note that this expression directly links the risk-constrained DSA transmit power $P_{tx,D,q}$ to the PU interference threshold $P_{rx,int}$, risk level q, and SA uncertainty associated with the operating environment. Specifically, $P_{tx,D,q}$ increases linearly with mean DSA→PU path loss increases, and is reduced as DSA→PU uncertainty $\sigma_{L_{p,D\to P}}$ increases.

With $P_{tx,D,q}$ defined, the DSA system can assess the potential DSA link capacity C using the functional relationships defined in (3.13). Capacity is defined as

$$C = W\log_2\left(1 + SINR^*\right). \tag{3.23}$$

Defining a closed-form solution for μ_C requires an approximation for the logarithm term.

The first-order Taylor Series approximation for mean is given as [59, 60]:

$$\mathrm{E}\left[f(X)\right] \approx f(\mu_X) \tag{3.24}$$

The mean of (3.23) can be found as

$$\mu_C \approx W \log_2\left(1 + \mu_{SINR^*}\right) \tag{3.25}$$

A similar approximation of the variance, however, is not guaranteed to be valid for large variances [61, 62]. A characterization of the impacts of uncertainty will be made empirically in Section 3.3.2 as well as in the simulation results of Chapter 4.

The $SINR^*$ mean can similarly be approximated by applying the first order Taylor Series to (3.13):

$$\mu_{SINR^*} \approx 10^{0.1\mu_{SINR}} \tag{3.26}$$

Defining useful expressions for the SINR mean requires several steps. First, let SINR be defined in terms of $L_{p,D\to P,q}$ by the following derivation:

$$\begin{aligned} SINR &= P_{rx,D\to D} - P_{I+N} \\ &= P_{rx,D\to D} - 10\log_{10}\left(P^*_{rx,P\to D} + N^*\right) \\ &= P_{tx,D} - L_{p,D\to D} - 10\log_{10}\left(P^*_{rx,P\to D} + N^*\right). \end{aligned} \tag{3.27}$$

Applying the risk constrained transmit power limit given in (3.22) then gives the SINR function

$$\begin{aligned} SINR = P_{rx,D\to P,int} + \mu_{L_{p,D\to P}} - a_q\sigma_{Lp,D\to P} - L_{p,D\to D} - \\ 10\log_{10}\left(P^*_{rx,P\to D} + N^*\right). \end{aligned} \tag{3.28}$$

The approximation for $\mu_{P_{I+N}}$ using the first-order Taylor Series approximation (3.24) is then given as follows:

$$\mu_{P_{I+N}} \approx 10\log_{10}\left(\mu_{P^*_{rx,P\to D}} + \mu_{N^*}\right). \tag{3.29}$$

The function can be further developed by considering the corresponding means of $P^*_{rx,P\to D}$ and N^*. For $P^*_{rx,P\to D}$:

$$\mu_{P^*_{rx,P\to D}} \approx 10^{0.1\mu_{P_{rx,P\to D}}}, \tag{3.30}$$

The noise term is similarly found:

$$\mu_{N^*} \approx 10^{0.1\mu_N}, \tag{3.31}$$

Folding (3.29), (3.30), and (3.31) back into (3.28) provides the SINR mean:

$$\begin{aligned}\mu_{SINR} \approx\, & P_{rx,D\to P,int} + \mu_{L_{p,D\to P}} - a_q\sigma_{Lp,D\to P} - \mu_{L_{p,D\to D}} \\ & - 10\log_{10}\left(10^{0.1\mu_{P_{rx,P\to D}}} + 10^{0.1\mu_N}\right)\end{aligned} \tag{3.32}$$

The expression for μ_{SINR} in (3.32) can be combined with (3.26) and (3.25) for defining capacity C as a function of $\mu_{L_{p,D\to P}}$ and $\sigma_{L_{p,D\to P}}$.

The mathematical relations in (3.18) through (3.32) provide a theoretical basis for characterizing and evaluating the impact of uncertainty in the DSA probabilistic reasoning model proposed in Section 3.2. It is easily shown by inspection of the equations that increases in path loss uncertainty $\sigma^2_{L_{p,D\to P}}$ reduce the transmit power (3.32) and consequently the potential capacity available to a DSA system. The following section builds on this theoretical basis to quantitatively analyze the impacts and further assess capacity, standoff distance, and network density impacts.

3.3.2 Theoretical Analysis of Uncertainty Impacts on DSA

The thesis proposed in Chapter 1 and formulated in Chapter 2 from a theoretical perspective relies upon the assertion that reduced levels of uncertainty lead to improved levels of performance (e.g., spectrum access efficiency or user utility) at equivalent levels of risk. This section provides mathematical support to the thesis by deriving theoretical formulas that enable quantitative comparisons of relative performance as functions of situational uncertainty. The formulations enable quantitative comparisons of a priori and in situ processes, or comparisons of imperfect assessments relative to the actual state (i.e., perception vs. truth). The assessments are specifically conducted as functions of DSA→PU path loss parameters $\mu_{L_{p,D\to P}}$ and $\sigma_{L_{p,D\to P}}$, which reflects the primary importance of $L_{p,D\to P}$ characterizations on DSA spectrum access performance. As uncertainty is characterized by the variance (see Section 2.2), analyses regarding DSA awareness and behavior limits are further provided as functions of DSA→PU path loss varaince $\sigma^2_{L_{p,D\to P}}$.

The first assessment is the variation of the DSA→PU path loss interference risk limit $L_{p,D\to P,q}$ as a function of risk q and $\sigma_{L_{p,D\to P}}$. The variation between two conditions or beliefs can be defined from (3.21) as the difference

$$\begin{aligned}\Delta L_{p,D\to P,q} &= L_{p,D\to P,q,2} - L_{p,D\to P,q,1} \\ &= \Delta\mu_{L_{p,D\to P}} - \left(a_{q,2}\sigma_{L_{p,D\to P},2} - a_{q,1}\sigma_{L_{p,D\to P},1}\right).\end{aligned} \tag{3.33}$$

In this formulation, the change $\Delta L_{p,D\to P,q}$ is linear with any difference in the means of the two conditions. If the means are equivalent, then the change $\Delta L_{p,D\to P,q}$ is a function of the risk q (a_q is a function of q) and uncertainties as quantified by σ. Further, if the risk level remains constant between the two cases, then (3.33) becomes

$$\Delta L_{p,D\to P,q} = a_q\left(\sigma_{L_{p,D\to P},1} - \sigma_{L_{p,D\to P},2}\right). \tag{3.34}$$

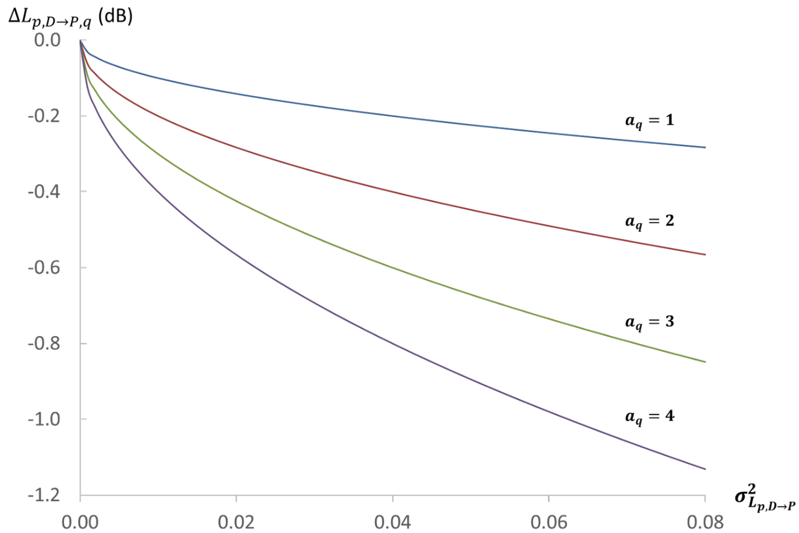

Figure 3.6: Relative path loss $\Delta L_{p,D\to P,q}$ change as a function of uncertainty $\sigma^2_{L_{p,D\to P}}$ and a_q.

Thus increased uncertainty $\sigma^2_{L_{p,D\to P}}$ reduces the path loss limit $L_{p,D\to P,q}$ non-linearly and in proportion to a_q, which is has a multiplying effect as shown in Figure 3.6.[2]

An assessment of $\Delta L_{p,D\to P,q}$ as a function of risk q needs to be made in the context of the probability distribution. The context-specific variations occur because the mapping from some path loss value L_p to a risk level q depends upon the probability distribution characteristics (i.e., distribution type and defining parameters). For the purposes of this assessment, consider the range of Beta probability distributions shown in Figure 3.7. The distributions present variations in skewness and dispersion for a set of distribution means normalized on the range (0,1).

First consider path loss variation as a function of distribution mean and variance. Figure 3.8 illustrates the relative path loss limit $L_{p,D\to P,q}$ as a function of risk q for various $\sigma^2_{L_{p,D\to P,q}}$ calculated across the normalized range $0 \le L_{p,D\to P} \le 1$. Note that each series corresponds to a distribution in Figure 3.7 (left). Figure 3.8 shows that greater uncertainty $\sigma^2_{L_{p,D\to P,q}}$

[2]Note that the use of a common a_q in the two cases assumes similarity in the probability distributions for the two cases. Otherwise $a_{q,1} \neq a_{q,2}$

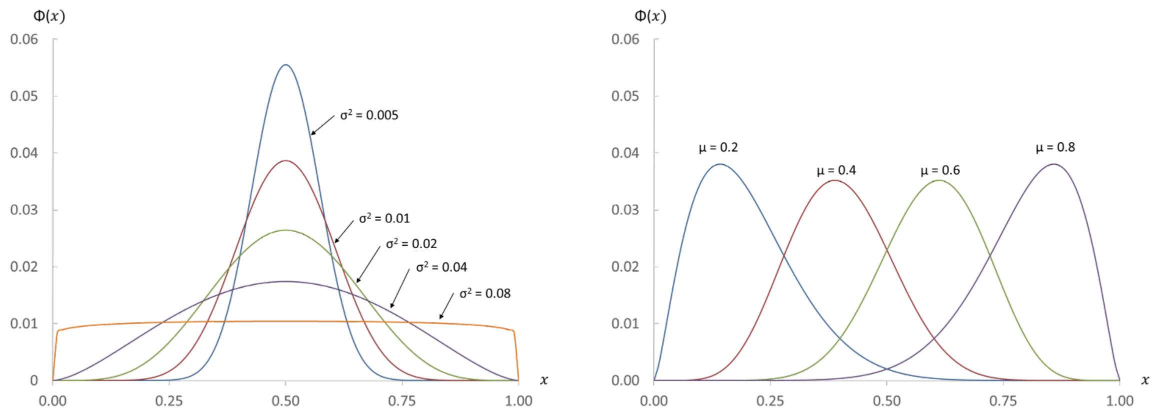

Figure 3.7: Beta pdfs for a range of variances (left) and means (right).

leads to lower estimated path loss threshold $L_{p,D\to P,q}$ for a given percentile q. Thus as uncertainty increases, the DSA must base its behaviors on increasingly conservative (i.e., low) DSA→PU path loss estimates. It also shows the accelerating rate of decrease as $q \to 0\%$. Figure 3.9 depicts path loss variation as a function of uncertainty $\sigma^2_{L_{p,D\to P,q}}$ at a risk level $q = 0.99$ for various distribution means associated with Figure 3.7 (right). The data show how skewness imposes a non-linear rate of path loss change.

As defined in (3.22) , the risk-derived path loss $L_{p,D\to P,q}$ determines the risk-constrained DSA transmit power $P_{tx,D,q}$. Thus the variation in maximum transmit power $\Delta P_{tx,D,q}$ can be derived from (3.22) and (3.33) as:

$$\begin{aligned}\Delta P_{tx,D,q} &= P_{tx,D,q,2} - P_{tx,D,q,1} \\ &= \Delta\mu_{L_{p,D\to P}} - \left(a_{q,2}\sigma_{L_{p,D\to P},2} - a_{q,1}\sigma_{L_{p,D\to P},1}\right), \qquad (3.35)\end{aligned}$$

where the assumption is made that the interference power threshold at the protected user $P_{rx,D\to P,q}$ is identical for the two cases. Note that the result for $\Delta P_{tx,D,q}$ is identical to that of $\Delta L_{p,D\to P,q}$. Thus the variations of $\Delta P_{tx,D,q}$ are identical to those of $\Delta L_{p,D\to P,q}$ presented in Figures 3.6, 3.8, and 3.9. Furthermore, the same characterizations apply to the received

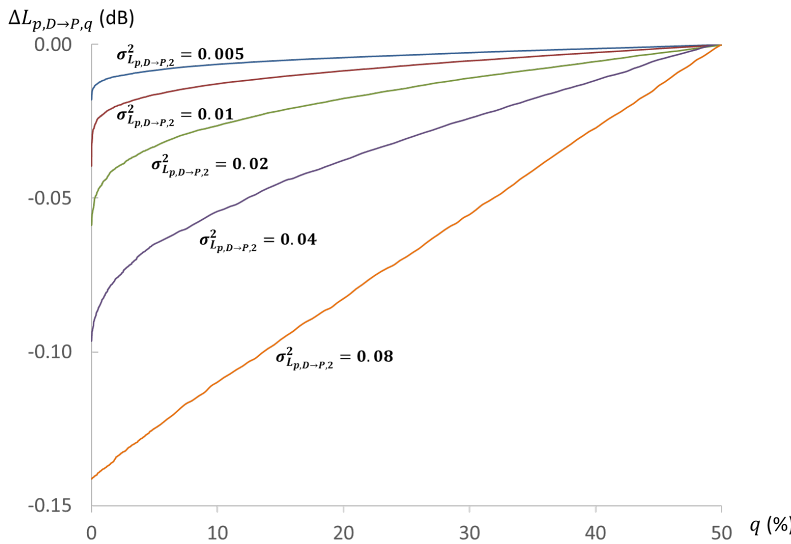

Figure 3.8: Relative path loss $\Delta L_{p,D\to P}$ as a function of interference percentile q for various Beta probability distributions with mean $\mu_{L_{p,D\to P}} = 0.5$ and path loss uncertainty $\sigma^2_{L_{p,D\to P}}$.

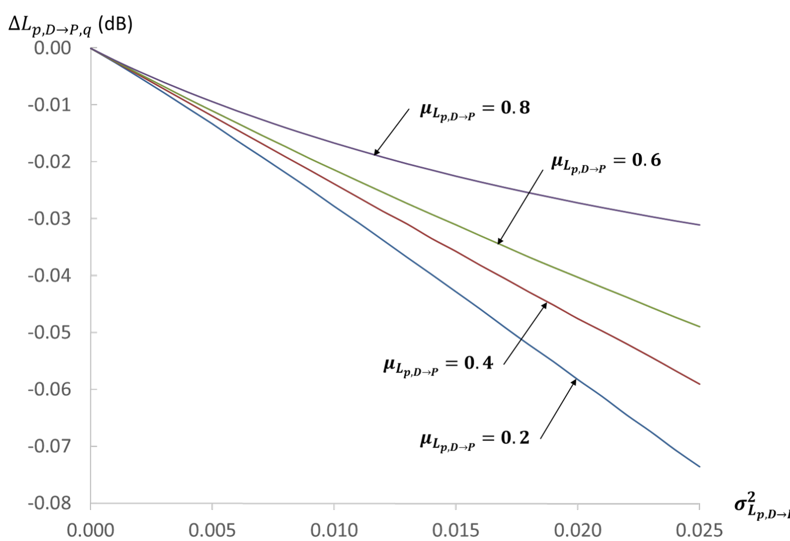

Figure 3.9: Relative path loss $\Delta L_{p,D\to P}$ as a function of path loss uncertainty $\sigma^2_{L_{p,D\to P}}$ for various probability distributions $Beta(\mu_{L_{p,D\to P}}, \sigma_{L_{p,D\to P}})$.

DSA signal power $P_{rx,D\to D}$, which is linearly related to $P_{tx,D}$ by $P_{rx,D\to D} = P_{tx,D} - L_{p,D\to D}$ as given in (3.13).

Uncertainty Impacts on DSA Capacity Assessments

$P_{rx,D\to D}$ in turn affects the DSA link capacity and/or the link distance at which a particular capacity can be attained. Starting with (3.25), the change in expected capacity μ_C can be found as:

$$\begin{aligned}\Delta\mu_C &\approx W\left[\log_2\left(1+\mu_{SINR_2^*}\right) - \log_2\left(1+\mu_{SINR_2^*}\right)\right] \\ &\approx W\log_2\left(\frac{1+\mu_{SINR_2^*}}{1+\mu_{SINR_1^*}}\right). \end{aligned} \tag{3.36}$$

To achieve sufficient capacity, most radio systems require $SINR \gg 1$ [7, 63–65]. Applying this condition yields

$$\Delta\mu_C \approx W\log_2\left(\frac{\mu_{SINR_2^*}}{\mu_{SINR_1^*}}\right). \tag{3.37}$$

Applying the equation for μ_{SINR^*} from (3.26):

$$\begin{aligned}\Delta\mu_C &\approx W\log_2\left(\frac{10^{0.1\mu_{SINR_2}}}{10^{0.1\mu_{SINR_1}}}\right) \\ &\approx W\log_2\left(10^{0.1\left(\mu_{SINR_2}-\mu_{SINR_1}\right)}\right) \\ &\approx 0.1W\log_2(10)\Delta\mu_{SINR}. \end{aligned} \tag{3.38}$$

The expression for $\Delta\mu_{SINR}$ can be derived from (3.32). Since the analysis here is focused on the impact of DSA→PU path loss estimation changes on performance, let all parameters remain constant across $SINR_1$ and $SINR_2$ except for those related to $L_{p,D\to P}$.

The resulting expected SINR difference expression is then

$$\begin{aligned}
\Delta\mu_{SINR} \approx\ & \mu_{L_{p,D\to P},2} - a_{q,2}\sigma_{L_{p,D\to P,2}} - 10\log_{10}\left(10^{0.1\mu_{P_{rx,P\to D,2}}} + 10^{0.1\mu_N}\right) \\
& - \left[\mu_{L_{p,D\to P},1} - a_{q,1}\sigma_{L_{p,D\to P,1}} - 10\log_{10}\left(10^{0.1\mu_{P_{rx,P\to D,1}}} + 10^{0.1\mu_N}\right)\right] \\
\approx\ & \Delta\mu_{L_{p,D\to P}} - \left(a_{q,2}\sigma_{L_{p,D\to P,2}} - a_{q,1}\sigma_{L_{p,D\to P,1}}\right) \\
& - 10\log_{10}\left(\frac{10^{0.1\mu_{P_{rx,P\to D,2}}} + 10^{0.1\mu_N}}{10^{0.1\mu_{P_{rx,P\to D,1}}} + 10^{0.1\mu_N}}\right)
\end{aligned} \tag{3.39}$$

Under the conditions where a common risk level q is applied, (3.39) further simplifies to

$$\Delta\mu_{SINR} \approx \Delta\mu_{L_{p,D\to P}} - a_q\Delta\sigma_{L_{p,D\to P}} - 10\log_{10}\left(\frac{10^{0.1\mu_{P_{rx,P\to D,2}}} + 10^{0.1\mu_N}}{10^{0.1\mu_{P_{rx,P\to D,1}}} + 10^{0.1\mu_N}}\right) \tag{3.40}$$

Thus the capacity change expression in (3.38) becomes

$$\begin{aligned}
\Delta\mu_C \approx 0.1W\log_2(10)\Bigg[&\Delta\mu_{L_{p,D\to P}} - a_q\Delta\sigma_{L_{p,D\to P}} \\
& - 10\log_{10}\left(\frac{10^{0.1\mu_{P_{rx,P\to D,2}}} + 10^{0.1\mu_N}}{10^{0.1\mu_{P_{rx,P\to D,1}}} + 10^{0.1\mu_N}}\right)\Bigg].
\end{aligned} \tag{3.41}$$

To understand the relevant impact of risk and uncertainty on $\Delta\mu_C$ in (3.41), consider two performance bounding cases. For the first case, let noise be the dominant SINR component; that is $N \gg P_{rx,P\to D}$. Under this condition, the last term in (3.41) is 0, simplifying the equation to:

$$\Delta\mu_C \approx 0.1W\log_2(10)\left(\Delta\mu_{L_{p,D\to P}} - a_q\Delta\sigma_{L_{p,D\to P}}\right). \tag{3.42}$$

For the second case, let $P_{rx,P\to D} \gg N$. The expected capacity change is then

$$\begin{aligned}
\Delta\mu_C &\approx 0.1W\log_2(10)\left[\Delta\mu_{L_{p,D\to P}} - a_q\Delta\sigma_{L_{p,D\to P}} - 10\log_{10}\left(\frac{10^{0.1\mu_{P_{rx,P\to D,2}}}}{10^{0.1\mu_{P_{rx,P\to D,1}}}}\right)\right] \\
&\approx 0.1W\log_2(10)\left[\Delta\mu_{L_{p,D\to P}} - a_q\Delta\sigma_{L_{p,D\to P}} - \left(\mu_{P_{rx,P\to D,2}} - \mu_{P_{rx,P\to D,1}}\right)\right] \qquad (3.43) \\
&\approx 0.1W\log_2(10)\left(\Delta\mu_{L_{p,D\to P}} - a_q\Delta\sigma_{L_{p,D\to P}} - \Delta\mu_{P_{rx,P\to D}}\right)
\end{aligned}$$

The PU power received by the DSA system $P_{rx,P\to D}$ is given in (3.13), and it can easily be shown that $\Delta\mu_{P_{rx,P\to D}} = -\Delta\mu_{L_{p,D\to P}}$ for a given $P_{tx,P}$. Substituting in (3.43) gives

$$\begin{aligned}
\Delta\mu_C &\approx 0.1W\log_2(10)\left(\Delta\mu_{L_{p,D\to P}} - a_q\Delta\sigma_{L_{p,D\to P}} + \Delta\mu_{L_{p,D\to P}}\right) \\
&\approx 0.1W\log_2(10)\left(2\Delta\mu_{L_{p,D\to P}} - a_q\Delta\sigma_{L_{p,D\to P}}\right) \qquad (3.44)
\end{aligned}$$

Thus the change in expected capacity is approximately bounded by the two conditions:

$$\Delta\mu_C \approx \begin{cases} 0.1W\log_2(10)\left(\Delta\mu_{L_{p,D\to P}} - a_q\Delta\sigma_{L_{p,D\to P}}\right) & \text{if } N \gg P_{rx,P\to D} \\ 0.1W\log_2(10)\left(2\Delta\mu_{L_{p,D\to P}} - a_q\Delta\sigma_{L_{p,D\to P}}\right) & \text{if } P_{rx,P\to D} \gg N \end{cases} \qquad (3.45)$$

The two cases in (3.45) indicate that $\Delta\mu_C$ varies (approximately) linearly with changes in path loss mean $\mu_{L_{p,D\to P}}$ and non-linearly with uncertainty $\sigma^2_{L_{p,D\to P}}$. Specifically, $\Delta\mu_C$ varies approximately $0.1\ln(10) = 0.33$ bits/sec/Hz per dB change in the DSA→PU path loss mean in the noise limited case. However, path loss affects the interference limited case twice, resulting in an approximate 0.66 bits/sec/Hz per dB change in the DSA→PU path loss mean. With respect to uncertainty $\sigma^2_{L_{p,D\to P}}$, $\Delta\mu_C$ varies in proportion to $0.33\Delta\sigma^2_{L_{p,D\to P}}$ and $0.66\Delta\sigma^2_{L_{p,D\to P}}$ for the noise limited and interference limited cases, respectively. The approximations for the two cases are presented in Figures 3.10 through 3.13 based on the

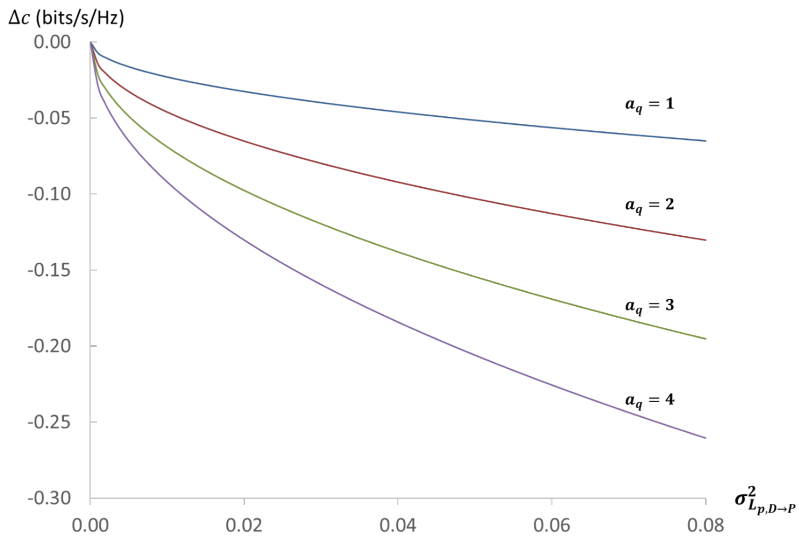

Figure 3.10: Expected capacity variation $\Delta\mu_c$ as a function of DSA→PU path loss uncertainty change $\Delta\sigma^2_{L_{p,D\to P}}$ and a_q.

Beta probability distributions from Figure 3.7.

Uncertainty Impacts on DSA Link Range and Coverage Area

Situational awareness uncertainty can also impact DSA link ranges or coverage areas, which can be converted to other relevant metrics such as populations served for a given area. Link range is a function of transmit power P_{tx} and signal attenuation (3.4). To compare the change in transmit power required to attain equivalent receive power levels (and therefore theoretical capacity) at two different operating conditions, the following relation is established:

$$P_{tx,D,1} - L_{P,D\to D,1} = P_{tx,D,2} - L_{P,D\to D,2}. \tag{3.46}$$

Signal attenuation varies by environment and numerous estimation models exist [6, 66–68]. For analysis here, let the exponential representation be used:

$$L_{p,D\to D} = -10\alpha \log_{10}\left(\frac{c}{4\pi f d}\right), \tag{3.47}$$

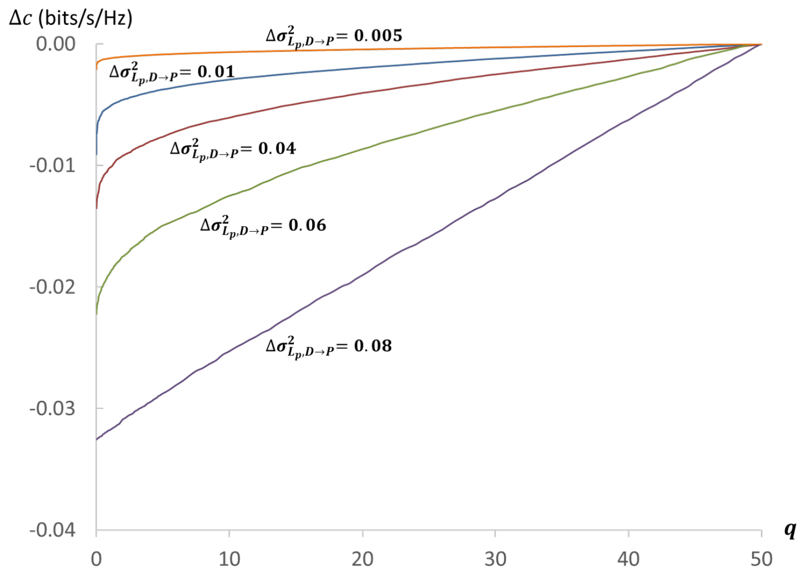

Figure 3.11: Expected capacity variation $\Delta\mu_c$ as a function of DSA$\to$PU path loss risk q and uncertainty $\sigma^2_{L_{p,D\to P}}$.

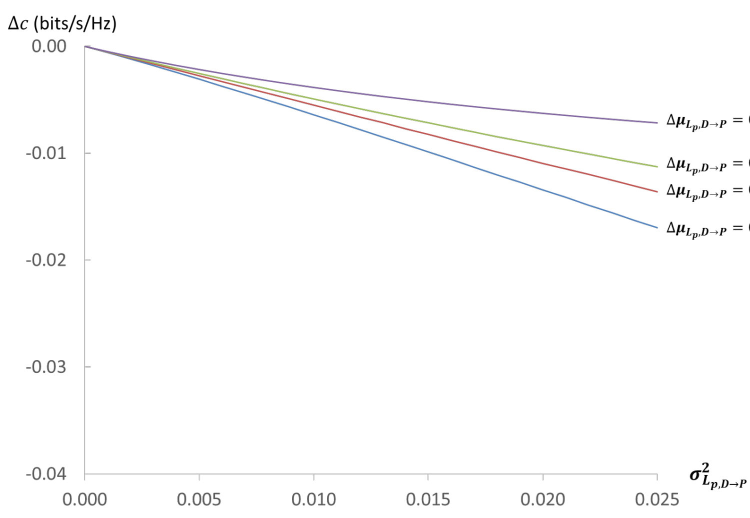

Figure 3.12: Expected capacity variation $\Delta\mu_c$ as a function of DSA$\to$PU path loss uncertainty change $\Delta\sigma^2_{L_{p,D\to P}}$ and $\Delta\mu_{L_{p,D\to P}}$ for $N \gg P_{rx,P\to D}$.

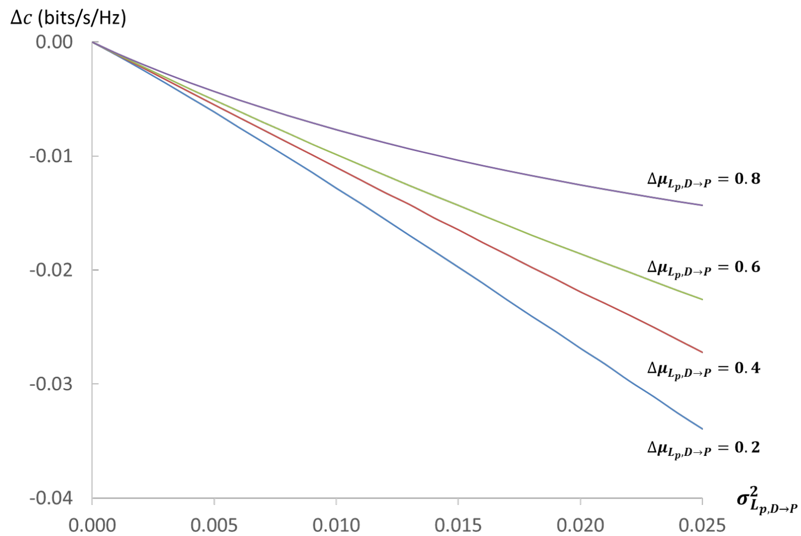

Figure 3.13: Expected capacity variation $\Delta\mu_c$ as a function of DSA→PU path loss uncertainty change $\Delta\sigma^2_{L_{p,D\to P}}$ and $\Delta\mu_{L_{p,D\to P}}$ for $P_{rx,P\to D} \gg N$.

where α is the path loss exponent on the DSA→DSA link, d is the distance from the transmitter, c is the speed of light, and f is the signal carrier frequency. Link distance can be found as a function of path loss as

$$d_{D\to D} = \frac{c}{4\pi f} 10^{\frac{1}{10\alpha} L_{p,D\to D}}. \tag{3.48}$$

The change in link distance as a function of path loss change can be established by considering the distance ratio defined as

$$\begin{aligned}\delta_{D\to D} = \frac{d_2}{d_1} &= 10^{0.1\alpha^{-1}\left(L_{p,D\to D,2} - L_{p,D\to D,1}\right)}, \\ &= 10^{0.1\alpha^{-1}\left(P_{tx,D,2} - P_{tx,D,1}\right)}. \end{aligned} \tag{3.49}$$

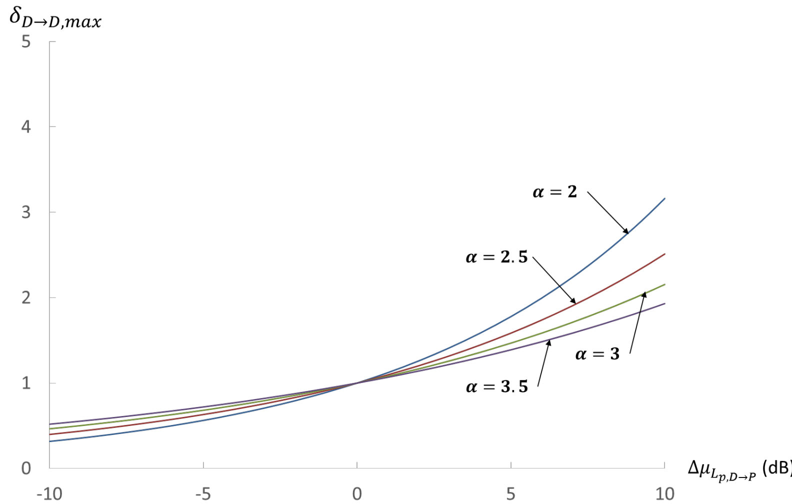

Figure 3.14: DSA link distance ratio as a function of DSA→PU path loss mean change $\Delta\mu_{L_{p,D\rightarrow P}}$ and path loss decay α.

Applying (3.35) gives the ratio of maximum DSA link range ratio of the posterior to prior beliefs:

$$\delta_{D\rightarrow D,max} = 10^{0.1\alpha^{-1}\left(\Delta P_{tx,D,q}\right)} = 10^{0.1\alpha^{-1}\left(\Delta L_{p,D\rightarrow P,q}\right)},$$

$$= 10^{0.1\alpha^{-1}\left(\Delta\mu_{L_{p,D\rightarrow P,q}} - a_q\Delta\sigma_{L_{p,D\rightarrow P,q}}\right)}. \tag{3.50}$$

Note that the formulation assumes a common interference risk q, which allows for a common value of a_q. Figures 3.14 and 3.15 illustrate the change in $\delta_{D\rightarrow D,max}$ as functions of $\Delta\mu_{L_{p,D\rightarrow P,q}}$ and uncertainty $\Delta\sigma^2_{L_{p,D\rightarrow P,q}}$, respectively, for various values of α.

In a similar manner, the relative area $\Pi = \frac{A_2}{A_1}$ enables a similar assessment of spectrum access potential in the context of network area coverage. Given Area $A = \pi d^2_{D\rightarrow D}$ where $d_{D\rightarrow D}$ is link distance and the distance ratio result from (3.50) gives an area ratio of

$$\Pi_{D\rightarrow D,max} = \delta^2_{D\rightarrow D,max} = 10^{0.2\alpha^{-1}\left(\Delta\mu_{L_{p,D\rightarrow P,q}} - a_q\Delta\sigma_{L_{p,D\rightarrow P,q}}\right)} \tag{3.51}$$

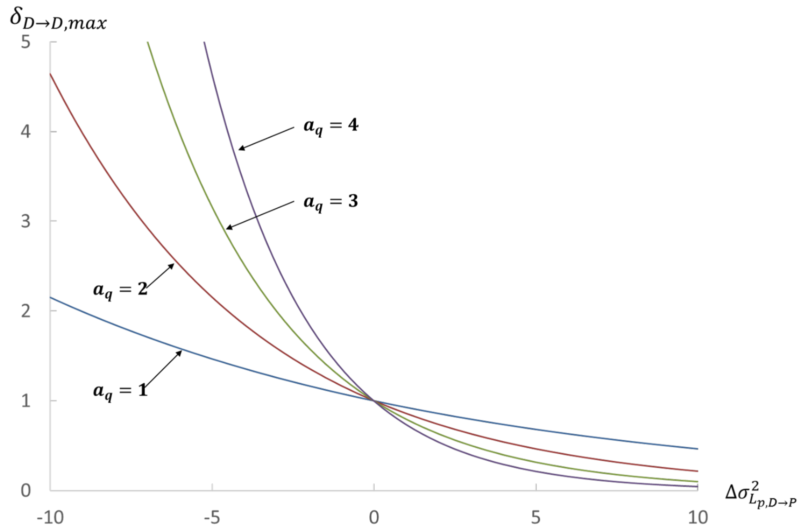

Figure 3.15: DSA link distance ratio as a function of DSA→PU path loss uncertainty change $\Delta\sigma^2_{L_{p,D\to P}}$ and a_q.

Figures 3.16 and 3.17 illustrate the change in $\Pi_{D\to D,max}$ as functions of $\Delta\mu_{L_{p,D\to P,q}}$ and uncertainty $\Delta\sigma^2_{L_{p,D\to P,q}}$, respectively, for various values of α.

While significant capacity, distance, and area coverage gains due to reductions in uncertainty may be theoretically possible, achievable gains will be limited by practical limits on DSA transmit power. Those limits may be imposed by equipment characteristics or by policy fiat. The benefit of increased SA may then come in terms of decreased standoff distances (see e.g., the TVWS example from Section 1.2), which results in increased network density (i.e., more wireless networks per area).

Uncertainty Impacts on Spectrum Access Efficiency

The impact of uncertainty on spectrum access efficiency is somewhat different than the capacity, link range, and coverage area impacts defined in the prior two sections. The system behavior metrics presented in the previous two sections result directly from the allowed (or required) change in transmit power associated with changes in path loss mean and uncertainty. Spectrum access efficiency as will be defined here, however, is characterized

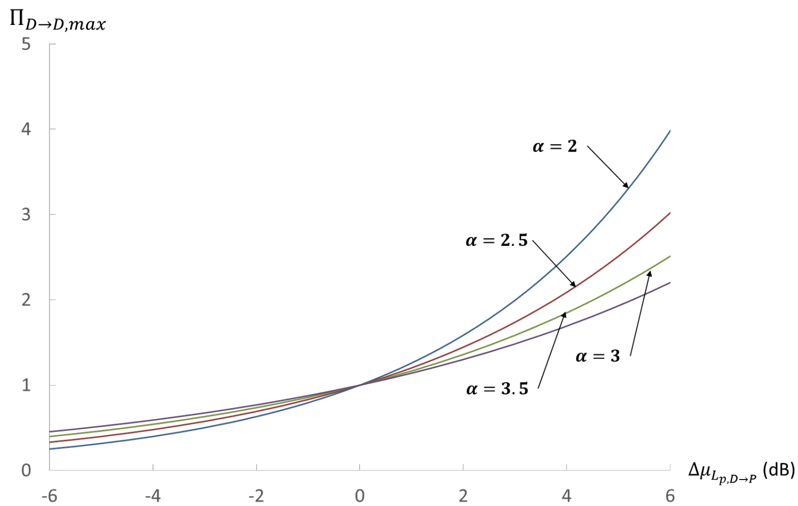

Figure 3.16: DSA coverage area ratio as a function of DSA→PU path loss mean change $\Delta\mu_{L_{p,D\to P}}$ and path loss decay α.

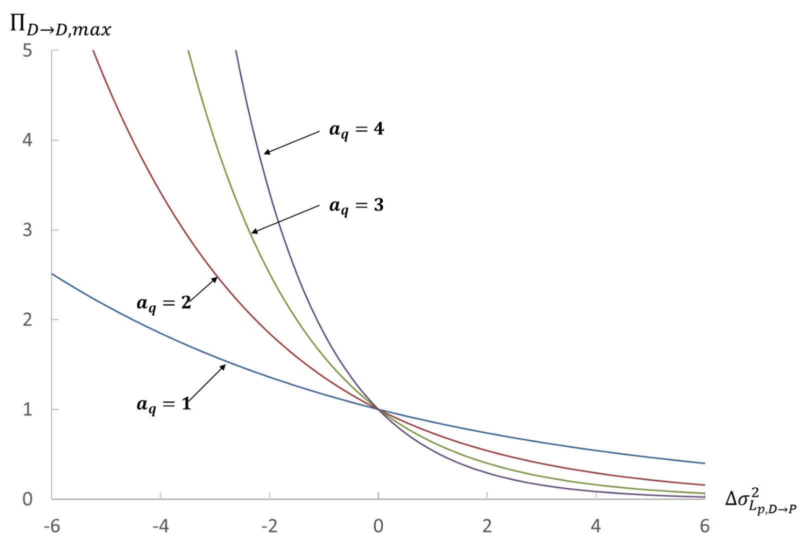

Figure 3.17: DSA coverage area ratio as a function of DSA→PU path loss uncertainty change $\Delta\sigma^2_{L_{p,D\to P}}$ and a_q.

by the minimum interference-free DSA$\rightarrow$PU distance achievable at some specified DSA transmit power. Thus rather than asking, "What is the maximum possible capacity, link distance, or coverage area given a change in path loss belief?", this section asks, "What is the *minimum* possible DSA$\rightarrow$PU standoff distance and associated spectrum access density?"

For this analysis, suppose that the DSA system wishes to transmit some power $P_{tx,D}$. To avoid causing interfere to a PU having a threshold $P_{rx,int}$ requires a minimum path loss given by

$$L_{p,D\rightarrow P,min} = P_{tx,D} - P_{rx,int}. \tag{3.52}$$

The minimum DSA$\rightarrow$PU standoff distance $d_{D\rightarrow P,min}$ at which $L_{p,D\rightarrow P,min}$ occurs depends upon the propagation environment.

Suppose that some path loss model is used in determining the distance a priori. As with the link range analysis, let the model be defined as in (3.47). The distance is then given by

$$d_{D\rightarrow P,min} = \frac{c}{4\pi f} 10^{-0.1\alpha^{-1} L_{p,D\rightarrow P,min}}. \tag{3.53}$$

Once the DSA system attains an updated path loss, the minimum standoff distance $d_{D\rightarrow P,min}$ may change. The relative change between prior and posterior can be defined by

$$\delta_{D\rightarrow P} = \frac{d_{D\rightarrow P,min,post}}{d_{D\rightarrow P,min,prior}} = 10^{-0.1 L_{p,D\rightarrow P,min}\left(\alpha_{post}^{-1} - \alpha_{prior}^{-1}\right)}. \tag{3.54}$$

If the DSA$\rightarrow$PU distance is known at the time of the DSA observation, then α_{prior} and α_{post} are found by

$$\alpha = \frac{L_{p,D\rightarrow P,q}}{10 \log_{10}\left(\frac{c}{4\pi f d}\right)}, \tag{3.55}$$

where the prior and posterior values of $L_{p,D\rightarrow P,q}$ are used to determine α_{prior} and α_{post}, respectively.

If the distance is not known, then α_{prior} and α_{post} cannot be found directly. An upper bound, however, can be used here for analysis. To do so, assume that the observation leading to the posterior belief in $\phi(L_{p,D\to P})$ is attributed only to an update in the path loss model (i.e., α). Thus the belief for $\phi(d_{D\to P})$ is unchanged from prior to posterior. The relative change in α can then be defined from (3.53) as:

$$\begin{aligned}\frac{\alpha_{post}}{\alpha_{prior}} &= \frac{L_{p,D\to P,q,post}}{10\log_{10}\left(\frac{c}{4\pi fd}\right)}\frac{10\log_{10}\left(\frac{c}{4\pi fd}\right)}{L_{p,D\to P,q,prior}},\\ &= \frac{L_{p,D\to P,q,post}}{L_{p,D\to P,q,prior}}.\end{aligned} \tag{3.56}$$

Solving for α_{prior} and substituting into the relative standoff distance ratio in (3.54) gives

$$\begin{aligned}\delta_{D\to P,min} &= 10^{-0.1L_{p,D\to P,min}\left(\alpha_{post}^{-1}-\frac{L_{p,D\to P,q,post}}{L_{p,D\to P,q,prior}}\alpha_{post}^{-1}\right)}\\ &= 10^{-0.1L_{p,D\to P,min}\alpha_{post}^{-1}\left(1-\frac{L_{p,D\to P,q,post}}{L_{p,D\to P,q,prior}}\right)}.\end{aligned} \tag{3.57}$$

Note that (3.57) represents an upper bound on the standoff distance ratio $\delta_{D\to P,min}$. If the posterior updated belief in $\phi(L_p)$ results in an update in $\phi(d_{D\to P})$, then the ratio in (3.56) is reduced, which produces a smaller change in standoff distances. The lower bound is logically given when all the updated belief in $\phi(L_{p,D\to P})$ is attributed to an update in $\phi(d)$. Under those conditions, $\alpha_{prior} = \alpha_{post}$ and it is easily shown from (3.54) that the standoff distance ratio $\delta_{D\to P,min} = 1$.

Given the standoff distance ratios in (3.54) and (3.57), the required exclusion zone area can be determined. Since the standoff distance $d_{D\to P,min}$ defines the minimum DSA→PU separation, it also defines the radius of the exclusion zone area:

$$\Pi_{D\to P,min} = \frac{A_{D\to P,min,post}}{A_{D\to P,min,prior}} = \delta^2_{D\to P,min},$$
$$= 10^{-0.2L_{p,min}\left(\alpha^{-1}_{post}-\alpha^{-1}_{prior}\right)}. \tag{3.58}$$

The coverage area ratio $\Pi D \to P, min$ can be used to evaluate changes in potential network density due to increased geographic sharing. Let each network require a geographical area A. Density ρ is the number of networks per area, i.e., $\rho = A^{-1}$ networks per unit area:

$$\Omega_{max} = \frac{\rho_{max,post}}{\rho_{max,prior}} = \frac{A_{min,prior}}{A_{min,post}} = \Pi^{-1}_{D\to P,min} = \delta^{-2}_{D\to P,min},$$
$$= 10^{0.2L_{p,D\to P,min}\left(\alpha^{-1}_{post}-\alpha^{-1}_{prior}\right)}. \tag{3.59}$$

In closing out this section, it should be noted that the spectrum efficiency metrics developed here are approximations designed to provide a first-order analysis. Numerous path loss models exist that define the change in total signal attenuation (i.e., path loss) as a function of distance [6, 7, 66, 68–70]. Each is based on a particular set of assumptions and empirical observations. The one selected in (3.53) provides a convenient representation that enables an assessment of uncertainty impacts on DSA system performance and spectrum access. The interpretation of the metrics should be viewed within the correct context. Specifically, the intent and application of the metrics is threefold:

1. To provide quantitative support to the thesis, illustrating that in situ reasoning provides the potential for greater spectrum access than existing a priori determinations

2. To approximate the relative magnitude of changes in spectrum access efficiency as a function of uncertainty regarding DSA→PU path loss.

3. To gain some general insight into permitted DSA system behaviors given sets of beliefs

As first-order approximations, the accuracy of the gains (or loss) magnitudes may not immediately translate to achievable performance levels, which are subject to factors such as equipment limitations (e.g., demodulator capabilities) as well as service-specific factors associated with the range of wireless users [8, 71–74].

Nonetheless, important insights can be gleaned from the metrics and associated findings for given scenarios. First and foremost, they are able to distinguish whether a difference between a prior and posterior belief results in a gain or loss. An increase in path loss at risk level q (i.e., $L_{p,D\to P,q}$) means that the DSA can either transmit more power, move closer to the PU, or some combination of the two. Conversely, a reduction in path loss $L_{p,D\to P,q}$ means that the DSA must either transmit less power, move further from the PU, or some combination of the two. Second, the variation of the metrics with their respective variables such as path loss uncertainty provides insight regarding how they affect the metric. Some can be understood by direct observation of the various equations; others—particularly relative changes in metric values between risk levels—may be best understood in the context of the simulation examples provided in the next section.

Chapter 4: Simulation and Analysis of DSA the Situational Awareness Model

A simulation model and associated analyses are presented in this section to demonstrate the DSA probabilistic reasoning process, illustrate the theoretical foundations developed in the prior section, and support the thesis. The model is depicted in Figure 4.1 and is principally Java-based, using the Netica Java API [75] as the basis for BN functionality. Custom Java code (labeled "FCMNet") was developed for constructing and managing the FCMs in a MEBN-like fashion [58].[1] FCMNet builds the FCMs from a library of MFrags as described in Section 3.2 and composes them into a DSA SA FCM. For the purposes of this study, FCMNet implements only the modular BN composition aspect of MEBN; the ontological aspects [76, 77] are not explicitly modeled as they are easily managed for a BN model of the scope presented here. JSON-formatted script files are generated from MATLAB code that defines each node's prior probability characteristics as well as any observations made by the DSA system (e.g., sensed P_{I+N}). The MATAB script generator uses various probabilistic models of physical world phenomenology such as signal attenuation and fading. The FCM Analysis module processes the script files, using the FCMNet module for functions such as instantiating the BN model, applying prior probabilities and observations to nodes, and querying the BN to extract node probability distributions. FCM Analysis also manages the creation of data files containing probability distribution statistics of FCM nodes.

The FCM built and analyzed for each of the cases below is shown in Figure 4.2. It is derived from the DSA SA FCM defined in (3.13). The Netica model excludes SINR and capacity due to probability distribution accuracy limitations associated with the exponential

[1]FCMNet was conceived under this effort and funded partly under National Science Foundation Grant 1250521 and United States Air Force Research Laboratories Grant FA9453-15-C-0401.

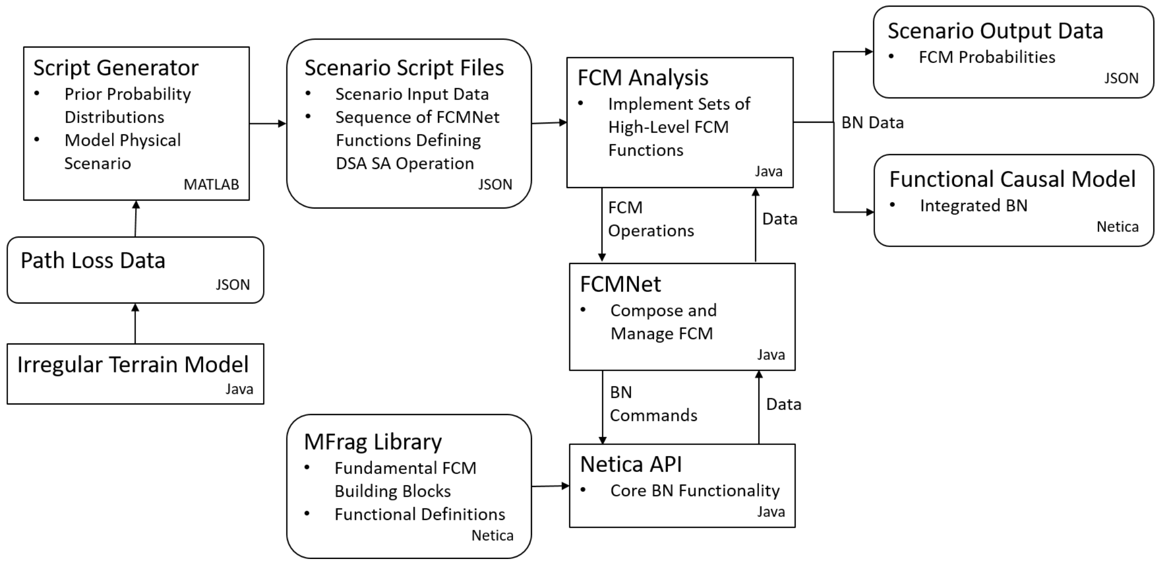

Figure 4.1: Simulation model block diagram.

functions required to convert from decibel to linear scale.[2] The model enables the core of the DSA SA FCM to be conducted within the model; calculations of SINR and capacity are easily conducted outside the model (e.g., using MATLAB).

All scenarios use a common DSA process for in situ situational observation and reasoning about the environment. Each scenario begins with a set of prior beliefs that can be derived from some set of a priori information or analyses. For example, potential PU device characteristics such as transmitter power levels and receiver interference thresholds can be extracted from published knowledge bases such as those used for TV Whitespace access [30]. Propagation environment characteristics can be extracted from a piori assessments or data from local sensors [78–100]. Once the priors are established, a DSA learning cycle is initiated. Each cycle contains a sensing period and BN update. Multiple received power samples are collected within a given sensing window, converted to probability distribution over the received power levels, and then applied to the DSA SA FCM as an observation of P_{I+N} (represented by "rxPwr_PU_DSA_tot" in Figure 4.2). The updated beliefs are then

[2]Netica must discretize the probability distributions at each node. Resulting small estimation differences are typically negligible with linear transformations between parameters. The exponential function associated with SINR* amplifies the errors.

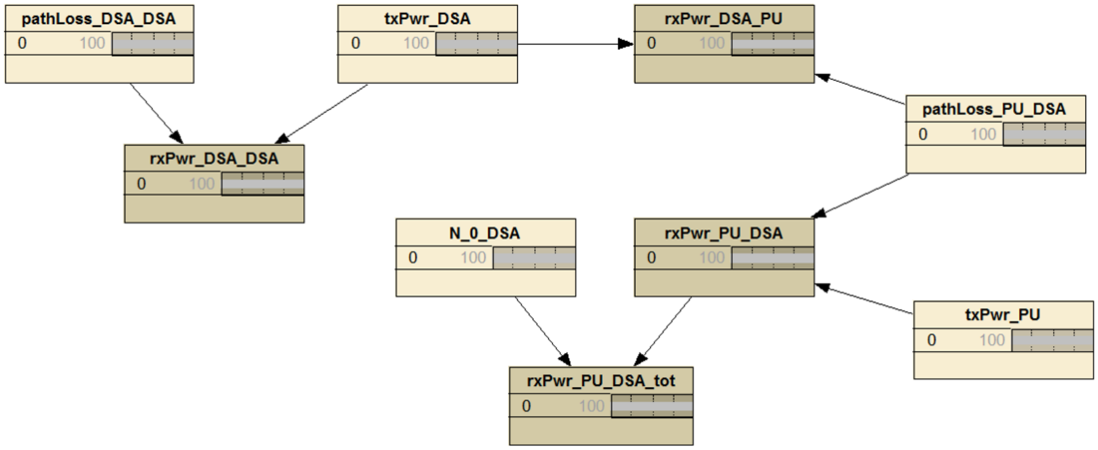

Figure 4.2: DSA SA FCM used for simulation and analyses (as depicted in the Netica GUI).

propagated to the other nodes. The resulting posterior probability distributions for each node are queried and used as prior probability distributions for the next observation-update cycle. The resulting change in parameter probabilities are then assessed to evaluate the effect of in situ observations and probabilistic reasoning on DSA system performance and spectrum access efficiency.

The path loss model used in the simulation includes large-scale propagation effects as well as small-scale fading. The ITM is used for generating large-scale path loss, and a Ricean model is used for determining the small-scale fades [6, 36, 37]). ITM inputs are provided in Table 4.1. Parameter specifications are representative of mobile and fixed-mobile spectrum usage in a temperate environment with moderate terrain. Site selections are specified as random placement to indicate that they may either be mobile or not purposely located to maximize signal strength. The variability parameters t_q and l_q are specified to maximally account for all possible location and time variability factors included in the model [36, 37]). ITM data is generated from $q = [0.01, \ldots, 0.99]$ in steps of 0.01 for link ranges of $d = [0.01, \ldots, 10]$ km in increments of 0.01 km; examples for $q = [0.01, 0.05, 0.5, 0.95, 0.99]$ are shown in Figure 4.3.

Because the DSA system modeled here uses spectrum sensing to provide in situ estimates

Table 4.1: ITM path loss model parameter settings

Parameter	Values
Distance (d)	$[1, \ldots, 10]$ km
Frequency (f)	556 MHz
Transmitter Height (h_t)	3 m
Receiver Height (h_r)	3 m
Transmitter Site Selection	0 (Random)
Receiver Site Selection	0 (Random)
Radio Climate	5 (Continental Temperate)
Polarization	1 (Vertical)
Time Variability Quantile (t_q)	0.99
Location Variability Quantile (l_q)	0.99
Confidence Quantile (s_q)	[0.01,...,0.99]
Terrain Type	3 (Hills)
Relative Permitivity	15 (Average Ground)
Conductivity	0.005 Siemens/m (Average Ground)
Surface Refractivity	301 (Continental Temperate)

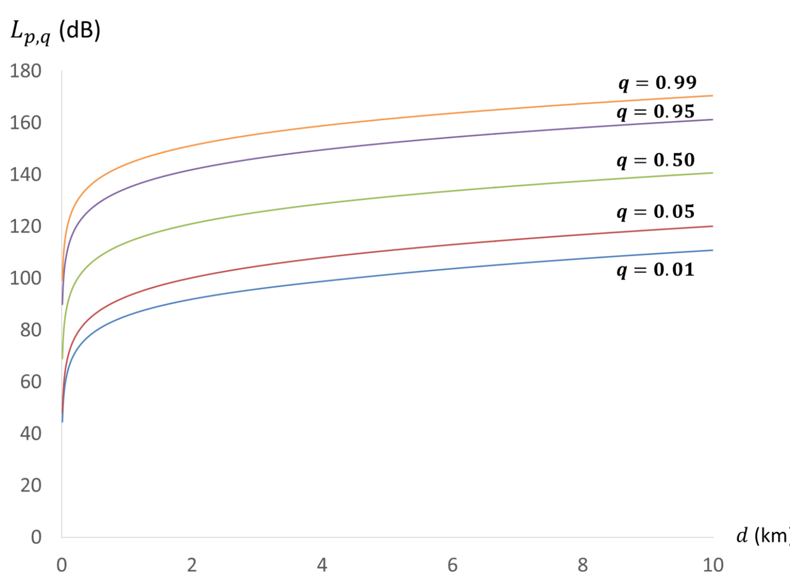

Figure 4.3: ITM path loss data as a function of distance and confidence quantiles $q = (0.01, 0.05, 0.50, 0.95, 0.99)$).

of path loss, sample-to-sample variations in received power that occur due to various signal propagation phenomenology need to be included. These small-scale variations result from transmitter-to-receiver geometry changes on the order of a wavelength as well as variations of reflectors along the signal path [6, 101]. The statistical characteristics of small-scale fading are typically modeled by Rayleigh, Ricean, or Gaussian distributions. Rayleigh fading is generally characterized by a signal that has many reflected components without any one single dominant one. If reflections are minor and a strong signal component exists, then a Gaussian fading model can be used. If a dominant signal component exists along with significant reflected power, then the Ricean distribution provides a good model of the fading characteristics. The Ricean can also be shown to approximate both the Rayleigh and Gaussian under low and high signal dispersion and is selected as the small-scale fading model for this study [6, 51, 102].

The Ricean distribution is given by

$$\phi(r) = \begin{cases} \frac{r}{\sigma^2} \exp^{\frac{-\left(r^2+A^2\right)}{2\sigma^2}} I_0\left(\frac{Ar}{\sigma^2}\right), & \text{for } A \geq 0, r \geq 0 \\ 0 & \text{for } r < 0 \end{cases} \tag{4.1}$$

where

- σ^2 is the total reflection power
- A is the amplitude of the dominant direct component
- I_0 is the modified zero-order Besssel function of the first kind (see e.g., [103]).

A common parameter for expressing the ratio of dominant to multipath power is the Ricean factor K defined as

$$K = 10\log_{10}\left(\frac{A^2}{2\sigma^2}\right) \text{ dB}. \tag{4.2}$$

Examples of Ricean probability distributions for several values of K are shown in Figure

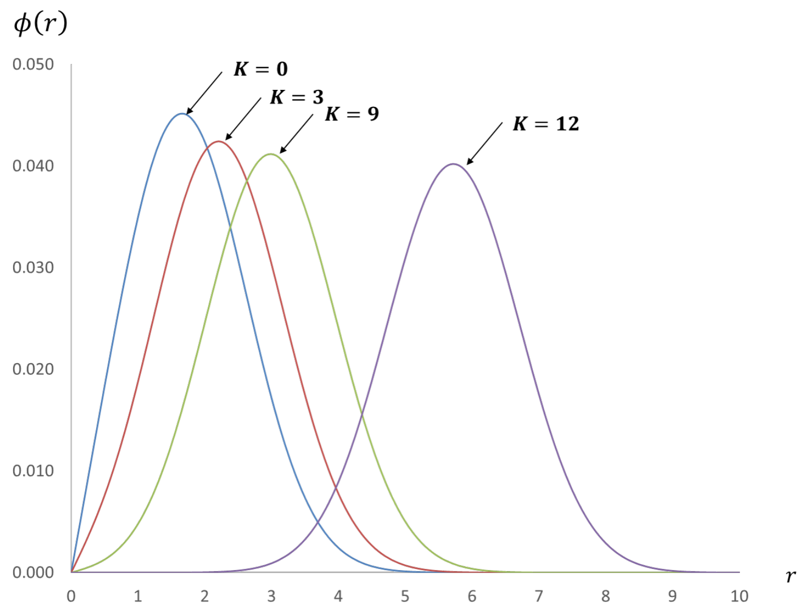

Figure 4.4: Ricean small-scale fading probability distributions for $K = [0.3.9.12]$, $\sigma^2 = 1$.

4.4. The corresponding fading depths for 1000 samples are shown in Figure 4.5 relative to the large-scale path loss value derived from the ITM.

It is important to connect the model used here to the framework defined in Sections 2.2 and Section 2.3. Note that the variability and confidence quantiles, link range uncertainty, and other probabilistic characterizations such as PU transmit power capture the time, location, situation, and environment uncertainty attributes defining the state space $\chi = \{T, L, S, E\}$ as presented in Section 2.3. The first three attributes are provided by the ITM itself; environmental uncertainty encompasses the remaining uncertainty factors included in the model. The model uses the defined state space, prior probability assessments, and observations to evaluate the probability of the various state spaces consistent with Section 2.3. Thus the DSA system modeled here falls within the framework of the logical argument as well as the conditions of Chen's theorem connecting variance reduction with uncertainty reduction [48, 49]. Demonstrating variance reductions and ties the corresponding effects on DSA behaviors and spectrum access efficiencies to uncertainty reductions in support of the thesis.

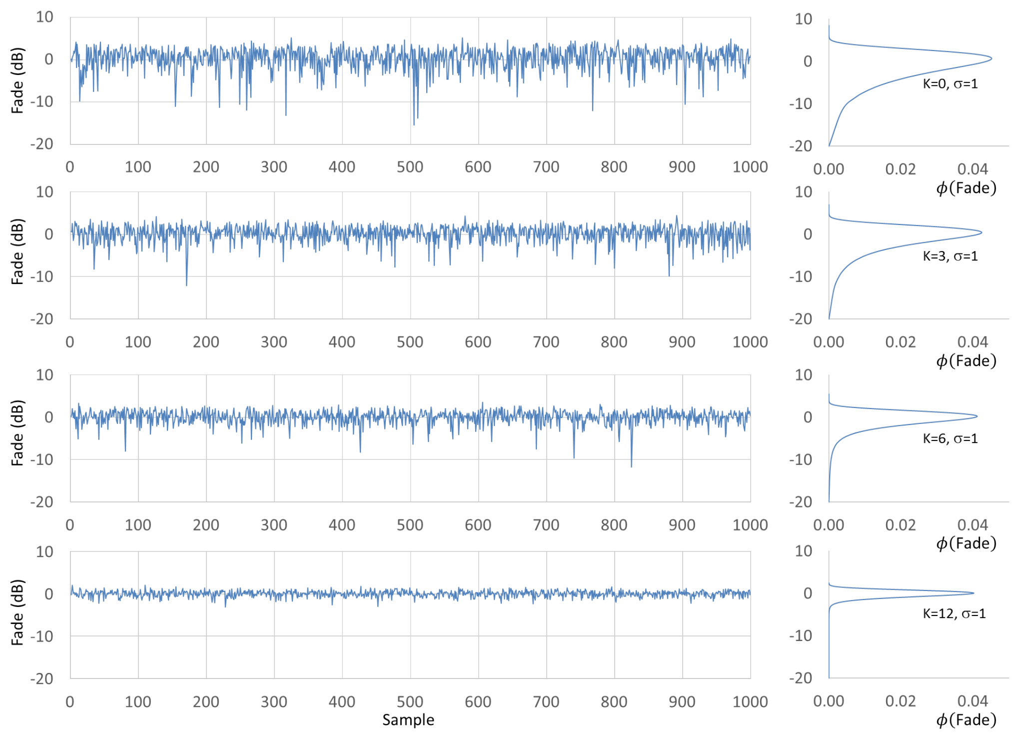

Figure 4.5: Ricean fading as a function of time (left) and the corresponding theoretical probability distribution distribution (right) for $K = [0, 3, 6, 12]$ dB.

Analyses are provided in the following sections for two scenario categories. The first category represents a mobile PU environment. It investigates model behavior and parameter estimation capabilities when significant prior uncertainty exists for the DSA→PU distance $d_{D\to P}$, path loss $L_{p,D\to P}$, and PU transmit power $P_{tx,P}$. The second category evaluates FCM capabilities in a situation similar to the TVWS scenario. It models a known PU transmit power $P_{tx,P}$ and small uncertainties with respect to the distance $d_{D\to P}$.

4.1 Scenario 1: Unknown PU Location, Transmit Power, and Path Loss

The first category of scenarios is the most general DSA scenario, in which the PU location, transmit power, and corresponding DSA→PU are not known. Thus the DSA system must rely on a priori data to establish initial beliefs for those parameters and use spectrum sensing with in situ probabilistic reasoning to improve its estimates of the local environment.

The prior DSA→PU path loss probability $\phi\left(L_{p,D\to P}\right)$ is derived from ITM data. The data discussed above is sampled at 1 dB increments along the entire 10 km path in 10 m increments. Given that no PU location is known, a uniform distribution is applied across all distances. The resulting histogram is normalized, producing the path loss prior distribution $\phi\left(L_{p,D\to P}\right)$ shown in Figure 4.6. The resulting mean and standard deviation are $\mu_{L_{p,D\to P}} = 127.8$ dB, $\sigma_{L_{p,D\to P}} = 13.15$ dB.

Other parameter prior beliefs are specified as shown in Table 4.2. The PU transmit power $P_{tx,P}$ is specified with equal probability at three possible power levels, providing a 12 dB range between the minimum and maximum values. The distribution represents cases where multiple transmitter types can be used or the existence of a single transmitter having variable transmit power. Such data would be made available from a database containing PU equipment characteristics [1,32–34] . The DSA transmit power $P_{tx,D}$ prior is given a uniform distribution, which allocates equal probability accross the range of possible transmit powers of the selected device. The receiver noise and the DSA→DSA path loss $L_{p,D\to D}$ prior beliefs

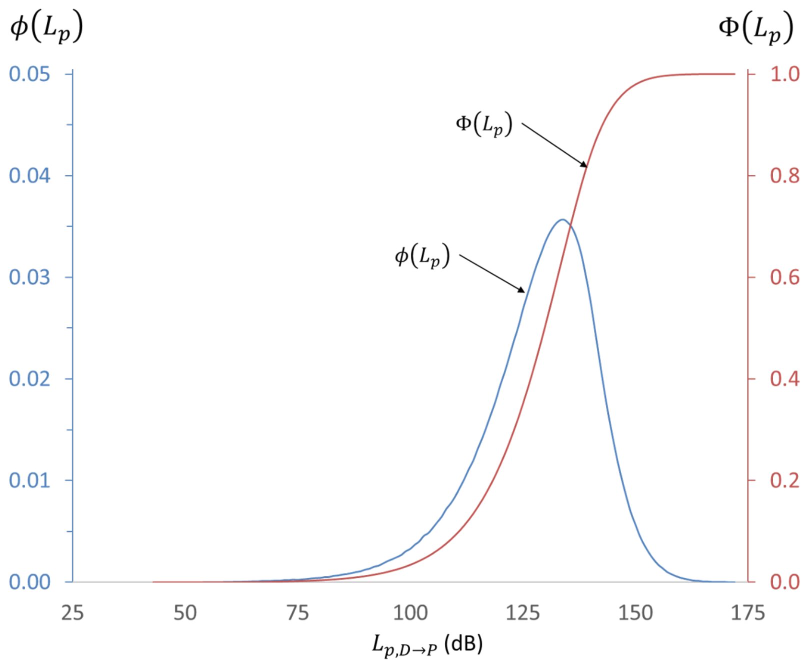

Figure 4.6: DSA→PU path loss prior probability density function $\phi\left(L_{p,D\to P}\right)$ and cumulative density function $\Phi\left(L_{p,D\to P}\right)$.

Table 4.2: Spectrum SA model parameter prior belief settings.

Parameter	Prior Belief
PU Transmit Power $\phi\left(P_{tx,P}\right)$	U[24,30,36] dBm
DSA Transmit Power $\phi\left(P_{tx,D}\right)$	U(0,36) dBm
Noise $\phi\left(N\right)$	N(-110, 1.5) dBm
DSA-DSA Path Loss $\phi\left(L_{p,D\to D}\right)$	N(80, 3) dB

are both specified as normal distributions. The noise power distribution models additive white Gaussian noise (AWGN). Additionally, the Ricean fade model is given by $K = 6$ and $\sigma = 2$.

At the start of the scenario, the prior beliefs are established in the FCM and propagated to the endogenous variables (e.g., $P_{rx,P\to D}$, P_{I+N}). The DSA then senses the spectrum, taking 1000 samples of the channel. The spectrum sensing observations measure the aggregate received power P_{I+N}. The samples taken during the sensing window are then used to generate a probability distribution $\phi\left(P_{I+N}\right)$, which becomes the noisy observation. The FCM is then updated to reflect the spectrum observation, updating the prior beliefs of the other nodes.

Within this general scenario framework, four distinct cases are examined—each defined by the relative difference between the means of the prior and observed sensed power $\mu_{P_{I+N},prior}$ and $\mu_{P_{I+N},obs}$, respectively. Scenario 1-1 evaluates a situation where $\mu_{P_{I+N},prior} \approx \mu_{P_{I+N},obs}$, providing the ability to directly evaluate the effects of uncertainty reductions absent any gain or loss from a change in $\mu_{L_{p,D\to P}}$. Scenario 1-2 investigates the condition where $\mu_{P_{I+N},obs} < \mu_{P_{I+N},prior}$, while Scenario 1-3 addresses the condition $\mu_{P_{I+N},obs} > \mu_{P_{I+N},prior}$. Scenario 1-4 investigates the condition where the received power is below the noise, i.e., $\mu_{P_{I+N},obs} < \mu_N$.

4.1.1 Scenario 1-1: Equivalent Observed and Expected Sensed Power

Figure 4.7 shows the prior along with the posterior power for the first time step for this first case. Given the observed power distribution, the FCM beliefs are updated to produce posterior uncertainties for the affected nodes. Of primary interest is the effect on $\phi_{L_{p,D\rightarrow P}}$; in particular the change in path loss associated with the risk threshold $L_{p,D\rightarrow P,q}$. As can be seen in Figure 4.8, $\phi_{L_{p,D\rightarrow P}}$ changes significantly. The standard deviation is reduced from 13.15 to $\approx$ 5.4. The distribution also now shows three peaks; each of which corresponds to one of the PU transmit powers $P_{tx,P}$ in Table 4.2 with a span corresponding to that of the sensed power P_{I+N}. The CDF in Figure 4.9 shows that the mean remains largely unchanged, and it is found that risk thresholds $L_{p,D\rightarrow P,q}$ have changed from 104 dB to 120 dB at $q = 0.05$, and from 89 dB to 120 dB at $q = 0.01$.

Figure 4.10 illustrates how $L_{p,q}$ changes over time. The plot shows contours for $q = 0.01, 0.05, 0.5, 0.95, 0.99$ over the 25 simulation time steps. It is seen that the distribution changes significantly after the first observation-update cycle and remains approximately the same for the remainder of the simulation. The mean ($q = 0.5$) is shown to have little change in this scenario due to the fact that $\mu_{P_{I+N},prior} \approx \mu_{P_{I+N},obs}$. The other percentiles are pulled closer to the mean due to the reduced variance that resulted from the observation. It can also be seen that the path loss associated with $q = 0.01$ and $q = 0.05$ are nearly equivalent following the observation.

The results can be used for validating the theoretical relationships derived in Chapter 3. Validation of the priors begins with the exogenous parameters ($P_{tx,P}$, $L_{p,D\rightarrow P}$, and N), using the equations in Section 3.3.1 to derive the theoretical values for the endogenous parameters ($P_{rx,P\rightarrow D}$ and P_{I+N}). The simulation prior values specified in Table 4.3 are taken directly from the model data files. Validation of the posterior results is performed by calculating the parameter values in reverse order beginning with the observed P_{I+N}. The data show close agreement between the simulation results and theoretical expectations.

The DSA$\rightarrow$PU path loss belief updates derived from the observations can be used to assess system performance and spectrum access efficiency impacts as defined in Chapter 3. The change in risk constrained transmit power $\Delta P_{tx,D,q}$ from (3.35) is defined as:

$$\Delta P_{tx,D,q} = \Delta\mu_{L_{p,D\rightarrow P}} - \left(a_{q,2}\sigma_{L_{p,D\rightarrow P},2} - a_{q,1}\sigma_{L_{p,D\rightarrow P},1}\right). \tag{4.3}$$

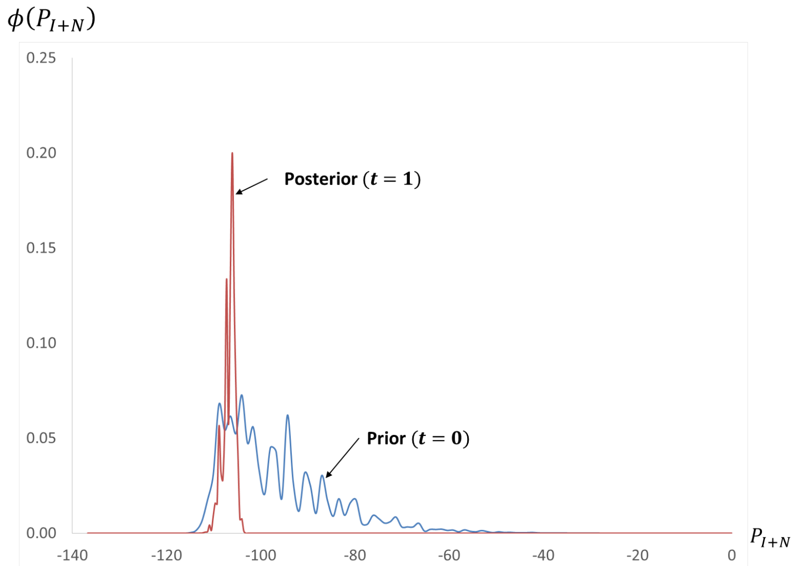

Figure 4.7: Scenario 1-1 DSA→PU sensed power P_{I+N} prior and posterior PDFs for the first time step.

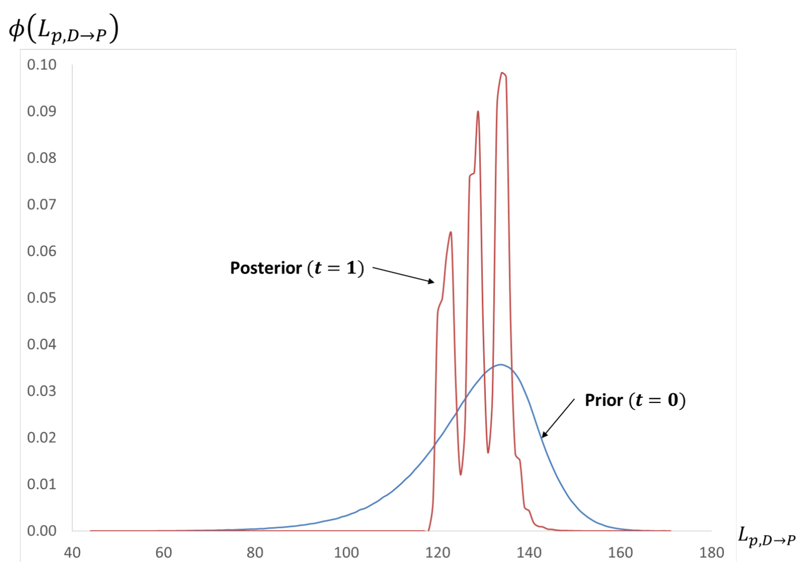

Figure 4.8: Scenario 1-1 DSA→PU path loss prior and posterior PDFs.

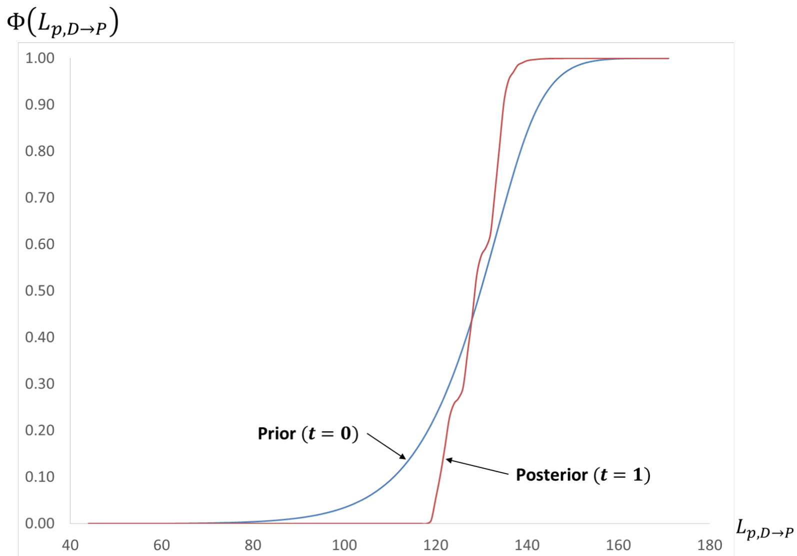

Figure 4.9: Scenario 1-1 DSA→PU path loss prior and posterior CDFs.

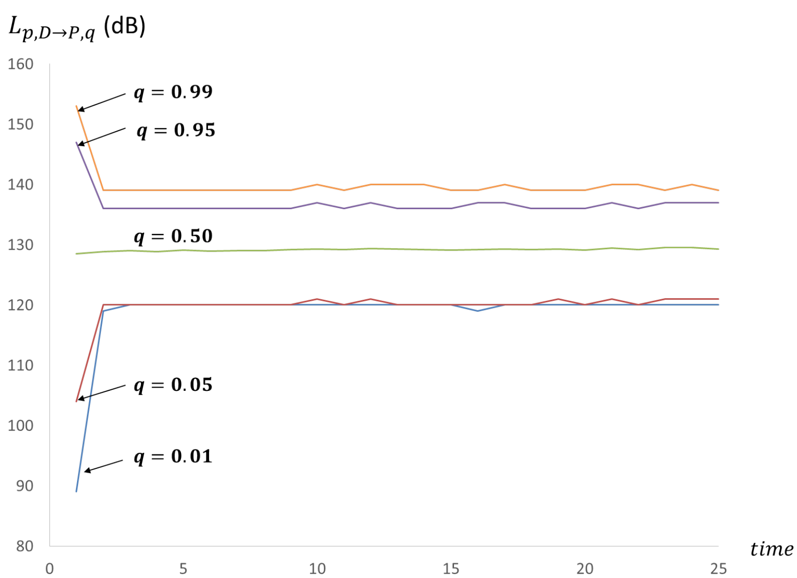

Figure 4.10: Scenario 1-1 DSA→PU path loss percentiles $q = \{0.01, 0.05, 0.50, 0.95, 0.99\}$ as a function of time

Table 4.3: Scenario 1-1 DSA SA model validation data.

Parameter	Prior Belief		Posterior Belief	
	Theory	Simulation	Theory	Simulation
$\mu_{P_{tx,P}}$ (dBm)	30.0	N/A	30.0	30.0
$\mu_{L_{p,D\to P}}$ (dB)	127.8	N/A	129.0	129.2
$\mu_{P_{rx,P\to D}}$ (dBm)	-97.8	-98.5	-99.0	-98.7
μ_N (dBm)	-110.0	N/A	-110.0	-110.0
$\mu_{P_{I+N}}$ (dBm)	-97.5	-98.7	N/A	-98.7

Recall from Section 3.3.1 that the terms $a_q\sigma_{L_{p,D\to P}}$ define the path loss associated with some risk level (i.e., percentile) q. The values of $a_q\sigma_{L_{p,D\to P}}$ changed from 24.50 dB to 8.88 dB at $q = 0.05$, and from 39.50 dB to 9.26 dB at $q = 0.01$. The values of $\mu_{L_{p,D\to P,q}}$ changed slightly, from 128.50 to 129.17. Thus the changes in risk constrained transmit power for Scenario 1-1 are

$$\Delta P_{tx,D,q} = \begin{cases} 0.67 - (8.88 - 24.50) = 16.29 \text{ dBm} & \text{for } q = 0.05, \\ 0.67 - (9.26 - 39.50) = 30.24 \text{ dBm} & \text{for } q = 0.01. \end{cases} \tag{4.4}$$

The increased transmit power potential is directly applied to (3.41). Normalizing for an arbitrary bandwidth W gives the change in expected capacity in b/s/Hz:

$$\Delta\mu_c \approx \begin{cases} 0.1\log_2(10)\left[16.29 - 10\log_{10}\left(\frac{10^{-9.87}+10^{-11})}{10^{-9.85}+10^{-11})}\right)\right] = 5.8 & \text{for } q = 0.05, \\ 0.1\log_2(10)\left[30.24 - 10\log_{10}\left(\frac{10^{-9.87}+10^{-11})}{10^{-9.85}+10^{-11})}\right)\right] = 10.7 & \text{for } q = 0.01. \end{cases} \tag{4.5}$$

While the theoretical capacity gains are significant, the higher range of gains may be impractical for actual DSA systems due to various channel effects and system design limitations. The increased power $\Delta P_{tx,D,q}$, however, could enable use of additional DSA system and service types.

Potential link range increases due to increased transmit power potential enabled by the change in path loss are defined by the link ratio given in (3.49) and are found as:

$$\delta_{D\to D,max} = \begin{cases} 10^{1.629\alpha^{-1}} & \text{for } q = 0.05, \\ 10^{3.092\alpha^{-1}} & \text{for } q = 0.01. \end{cases} \tag{4.6}$$

The corresponding area coverage increase for a DSA network resulting from the increased power and link range are

$$A_{D\to D,max} = \begin{cases} 10^{3.258\alpha^{-1}} & \text{for } q = 0.05, \\ 10^{6.183\alpha^{-1}} & \text{for } q = 0.01. \end{cases} \tag{4.7}$$

Spectrum efficiency gains can be determined as described in Section 3.3.2 by assessing the minimum standoff distance with the prior and posterior conditions. In this manner the prior acts as the a priori assessment while the posterior is the in situ assessment. The ratio of posterior to prior standoff distances is given as $\delta_{D\to P,min}$ in (3.54), which requires α for the prior and posterior beliefs. Since distance is not known, (3.57) is used to provide an estimate. Note that since the prior condition is used to specify the minimum path loss in this analysis, $L_{p,D\to P,min} = L_{p,D\to P,q,prior}$. Thus $\delta_{D\to P,min}$ becomes

$$\delta_{D\to P,min} = 10^{-0.1 L_{p,D\to P,min}\alpha_{post}^{-1}\left(1-\frac{L_{p,D\to P,q,post}}{L_{p,D\to P,q,prior}}\right)}, \tag{4.8}$$

$$= 10^{-0.1\alpha_{post}^{-1}\Delta L_{p,D\to P,q}}. \tag{4.9}$$

The standoff distance ratios for the two risk thresholds is then found to be

$$\delta_{D\to P,min} = \begin{cases} 10^{-1.629\alpha_{post}^{-1}} & \text{for } q = 0.05, \\ 10^{-3.092\alpha_{post}^{-1}} & \text{for } q = 0.01. \end{cases} \tag{4.10}$$

Table 4.4: Scenario 1-1 spectrum access gains from probabilistic reasoning.

Parameter	Prior to Posterior Change	
	$q = 0.05$	$q = 0.01$
$\Delta\mu_{L_{p,D\to P,q}}$ (dB)	0.67	0.67
$a_q \Delta\sigma_{L_{p,D\to P,q}}$ (dB)	-15.62	-30.24
$\Delta P_{tx,max}$ (dB)	16.29	30.92
Δc (bits/s/Hz)	5.8	10.7

The corresponding area ratios are then found from (3.58) as

$$\Pi_{D\to P,min} = \begin{cases} 10^{-3.258\alpha_{post}^{-1}} & \text{for } q = 0.05, \\ 10^{-6.138\alpha_{post}^{-1}} & \text{for } q = 0.01, \end{cases} \tag{4.11}$$

with the network density ratios given by (3.59) becoming

$$\Omega_{D\to P,min} = \begin{cases} 10^{3.258\alpha_{post}^{-1}} & \text{for } q = 0.05, \\ 10^{6.138\alpha_{post}^{-1}} & \text{for } q = 0.01. \end{cases} \tag{4.12}$$

Table 4.4 provides a summary of Scenario 1-1 results. In this scenario, probabilistic reasoning from in situ observations significantly reduces uncertainty in the path loss estimate, giving the potential for increased link ranges, DSA channel capacity, or spectrum access efficiencies. Because the prior and posterior mean path losses $\mu_{L_{p,D\to P,q}}$ are nearly identical, the majority of the changes are a direct result of reduced path loss uncertainty $\sigma_{L_{p,D\to P,q}}$.

4.1.2 Scenario 1-2: Observed Power Lower than Expected

Scenario 1-2 investigates a scenario where the observed power P_{I+N} is less than the prior estimate. This situation represents a case where signal attenuation is greater than expected, the PU may be at a further distance or transmitting at a lower power, or some combination.

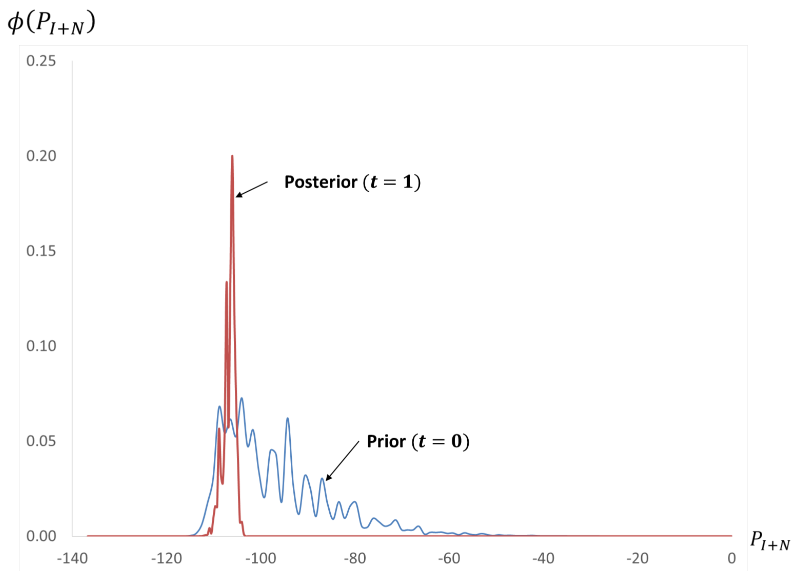

Figure 4.11: Scenario 1-2 DSA→PU sensed power P_{I+N} prior and posterior PDFs for the first time step.

The measured power is as shown in Figure 4.11, with the difference $\Delta P_{I+N} = -10$ dB. This results in a posterior path loss mean $\mu_{L_{p,D\to P,q}}$ that is less than the prior as shown in Figures 4.12 and 4.13.

Figure 4.14 shows the change in path loss distribution percentile levels over time. As with Scenario 1-1, the distribution converges to a steady state after the first observation. This scenario, however, exhibits more frequent small fluctuations between time steps that found in Scenario 1-1 (see Figure 4.10). The cause of the increased fluctuations is due to the increased influence of noise N in P_{I+N} due to the weak PU signal $P_{rx,P\to D}$. The influence of the noise—which fluctuates with each observation as previously described—is more pronounced at the higher percentiles ($q = 0.05, 0.01$) where noise begins to dominate the sensed power.

The various parameters and metrics are calculated as with Scenario 1-1 and presented in Table 4.5. The change in expected path loss $\Delta\mu_{L_{p,D\to P,q}}$ due to the -10 dB difference in expected vs. observed P_{I+N} is 9.46 dB. The change in uncertainty $\Delta\sigma_{L_{p,D\to P,q}}$ is comparable to Scenario 1-1. The cumulative effect of increased path loss mean and reduced variance

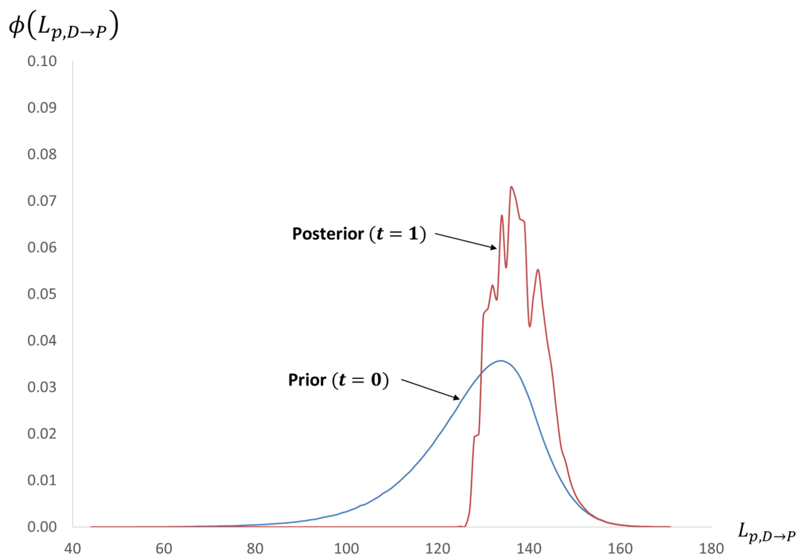

Figure 4.12: Scenario 1-2 DSA→PU path loss prior and posterior PDFs.

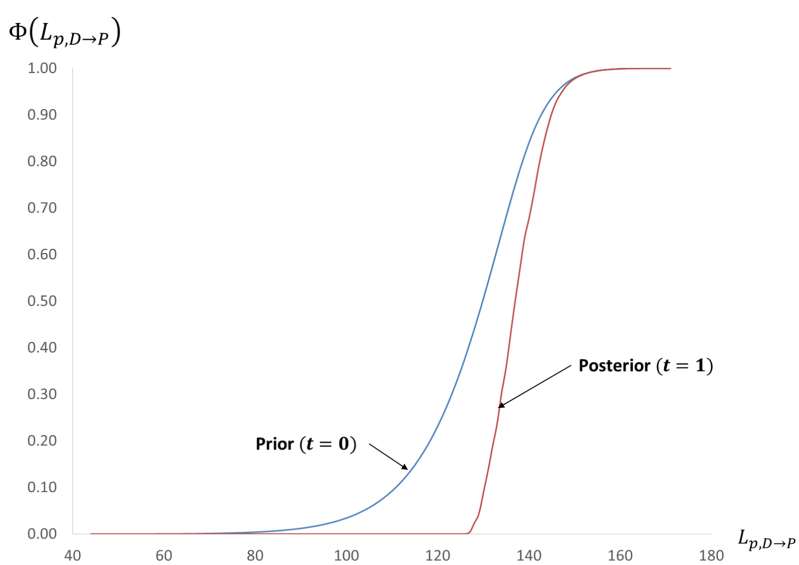

Figure 4.13: Scenario 1-2 DSA→PU path loss prior and posterior CDFs.

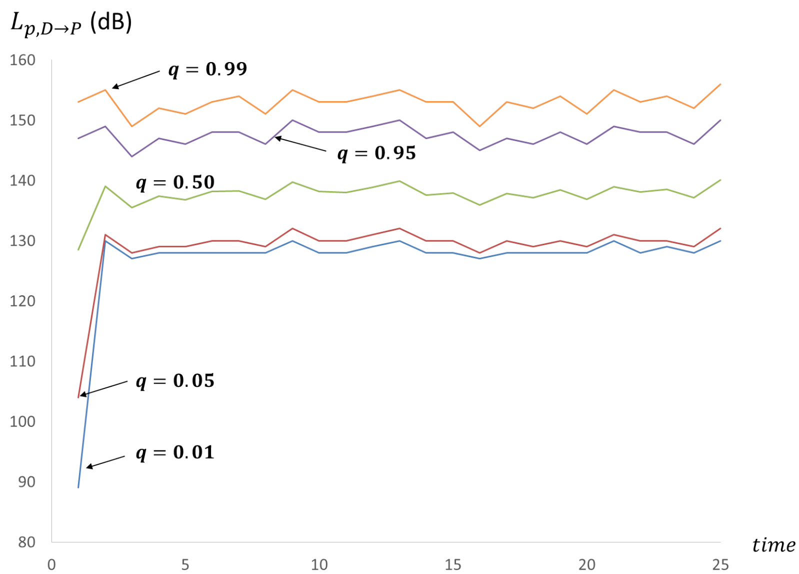

Figure 4.14: Scenario 1-2 DSA→PU path loss percentiles q={0.01, 0.05, 0.50, 0.95, 0.99} as a function of time

Table 4.5: Scenario 1-2 spectrum access gains from probabilistic reasoning.

Parameter	Prior to Posterior Change	
	$q = 0.05$	$q = 0.01$
$\Delta\mu_{L_{p,D\to P,q}}$ (dB)	9.46	9.46
$a_q\Delta\sigma_{L_{p,D\to P,q}}$ (dB)	-16.49	-29.95
$\Delta P_{tx,max}$ (dB)	25.96	39.42
Δc (bits/s/Hz)	11.2	15.6

allow for an increased transmit power of $\Delta P_{tx,max} = 25.96, 39.4$ dBm. The majority of the difference relative to Scenario 1-1 ($\Delta P_{tx,max} = 16.29, 30.92$ dBm) can be traced to the difference in $\Delta \mu_{L_{p,D\rightarrow P,q}}$ between the two scenario, which is ultimately caused by differences in $\mu_{P_{I+N}}$.

As with Scenario 1-1, the increased path loss estimate enables greater capacity, link range, and coverage area. Similarly, the potential for increased spectral efficiency is greater. Thus the in situ observations provide for gains in all aspects under this scenario.

4.1.3 Scenario 1-3: Observed Sensed Power Higher than Expected

Unlike the prior scenario where the sensed power was lower than expected, this scenario evaluates the effects on potential DSA behaviors with the sensed power P_{I+N} is higher than expected. This situation represents a case where signal attenuation is less than expected, the PU may be closer or transmitting at a higher power, or some combination of situational differences. The measured mean power is shown in Figure 4.15 and is 30 dB greater than the expected. This results in a posterior path loss mean $\mu_{L_{p,D\rightarrow P,q}}$ that is approximately 27 dB less than the prior as shown in Figures 4.16 and 4.17 and in Table 4.6.

Figure 4.18 shows the change in path loss distribution percentile levels over time. As with the previous scenarios, the distribution converges to a steady state after the first observation. The change in expected path loss $\Delta \mu_{L_{p,D\rightarrow P,q}}$ due to the 30 dB difference in expected vs. observed P_{I+N} is -27.38 dB. Interestingly, the change in uncertainty $a_q \Delta \sigma_{L_{p,D\rightarrow P,q}} = 15.34, 28.88$ dB is comparable to the prior scenarios. This consistent reduction in uncertainty regardless of ΔP_{I+N} is due to the low variance of the received power relative to the prior belief.

The cumulative effect of reduced path loss mean and variance for this scenario exhibit an interesting effect. At $q = 0.05$, the 27.38 dB reduced path loss outweighs the 15.34 dB gain due to reduced uncertainty for a net -12.04 change in path loss. At $q = 0.01$, however, the 28.88 dB gain due to reduced path loss uncertainty is greater than the change in the mean. This latter case results in a 1.5 dB increase in path loss. Thus the DSA system

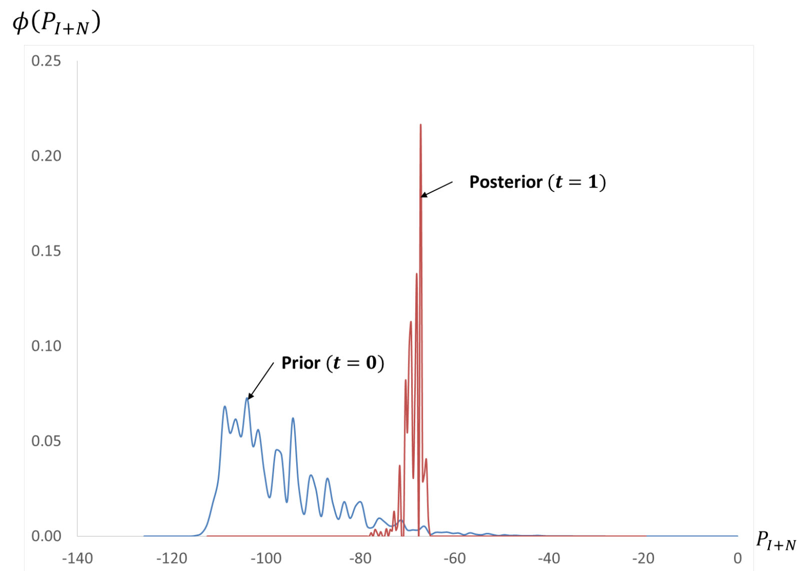

Figure 4.15: Scenario 1-3 DSA→PU sensed power P_{I+N} prior and posterior PDFs for the first time step.

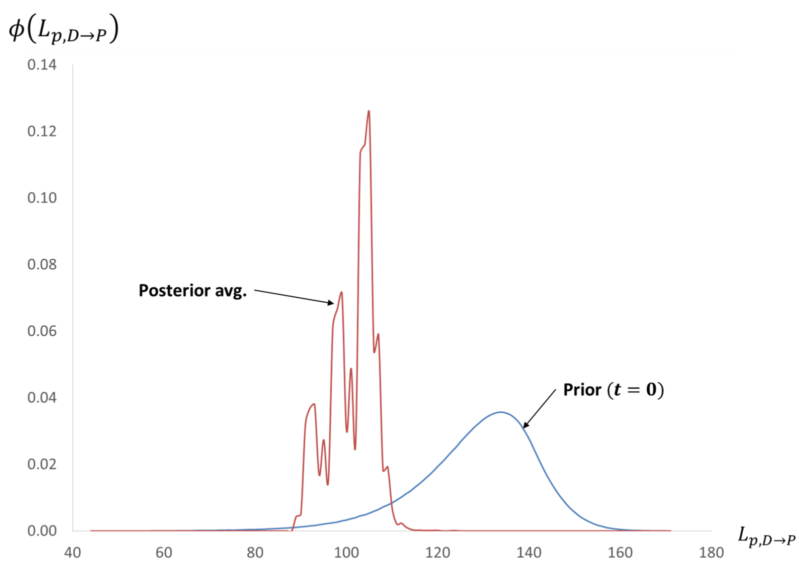

Figure 4.16: Scenario 1-3 DSA→PU path loss prior and posterior PDFs.

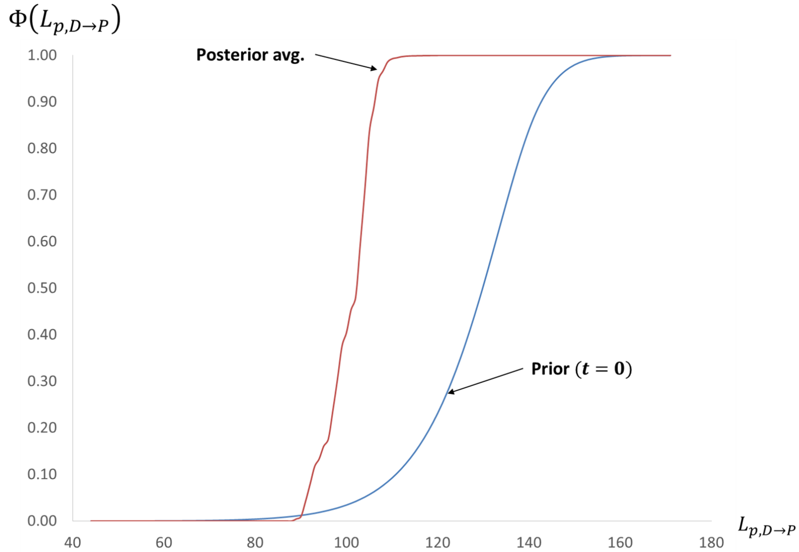

Figure 4.17: Scenario 1-3 DSA→PU path loss prior and posterior CDFs.

Table 4.6: Scenario 1-3 spectrum access gains from probabilistic reasoning.

Parameter	Prior to Posterior Change	
	$q = 0.05$	$q = 0.01$
$\Delta\mu_{L_{p,D\to P,q}}$ (dB)	-27.38	-27.38
$a_q\Delta\sigma_{L_{p,D\to P,q}}$ (dB)	-15.34	-28.88
$\Delta P_{tx,max}$ (dB)	-12.04	1.05
Δc (bits/s/Hz)	-13.0	-8.5

would need to reduce its power by $\Delta P_{tx,max} = -12.04$ dB relative to the prior condition for a policy that specifies the 5% risk threshold, while it could increase it by 1.5 dB or a policy that specifies the 1% risk threshold.

The different net changes in path loss at the two risk thresholds also creates different spectrum access efficiency results. At $q = 0.05$, a greater standoff distance is required in the posterior case relative to the prior belief. This in turn results in reduced network density potential. The opposite is found at $q = 0.01$; standoff distance can be reduced and network density increased. Thus different DSA system behaviors are generated based on differences in prior vs. posterior beliefs coupled with differences in risk thresholds.

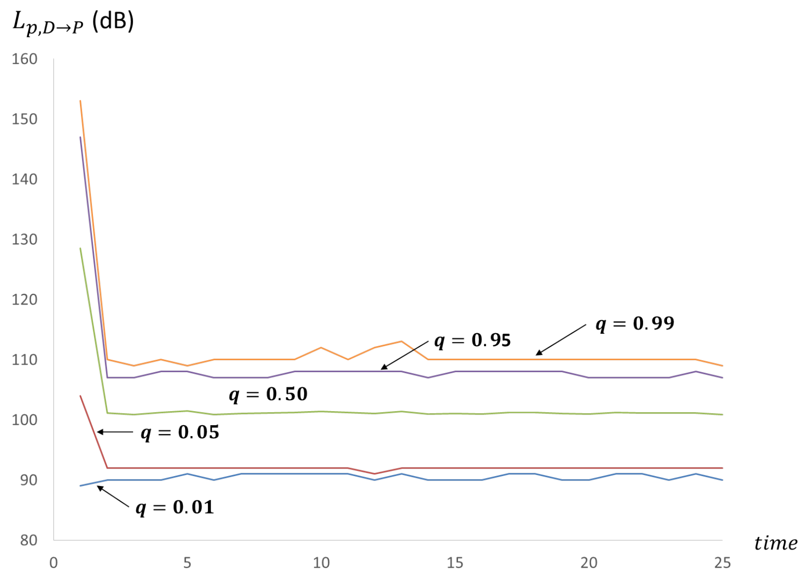

Figure 4.18: Scenario 1-3 DSA→PU path loss percentiles q={0.01, 0.05, 0.50, 0.95, 0.99} as a function of time

The key insight to this outcome is that the probabilistic reasoning model developed here is able to govern system behaviors according to the in situ conditions. Observations that call for decreased transmit power and/or increased standoff distance are able to be identified. These cases that result in greater constraints on DSA system behavior are vital for spectrum sharing and coexistence. Thus the probabilistic reasoning approach provides an effective method for establishing efficient spectrum access.

4.1.4 Scenario 1-4: PU Signal Power Less than Noise Power

This fourth and final case under Scenario 1 explores the behavior of the probabilistic reasoning model when the received PU signal $P_{rx,P\to D}$ becomes exceedingly week. Here the sensed power is shown in Figure 4.19, which includes noise N as well as the PU signal component. The mean received PU signal level is $\mu_{P_{rx,P\to D}} = -116$ dBm, while the average noise is $\mu_N = -110$ dBm for a composite $\mu_{P_{I+N}} = -112$ dBm and $SNR = -6$ dB.

Figures 4.20 and 4.21 illustrate the resulting change in path loss belief. Note that the posterior belief depicted in the figure is the average result. It's apparent variance is

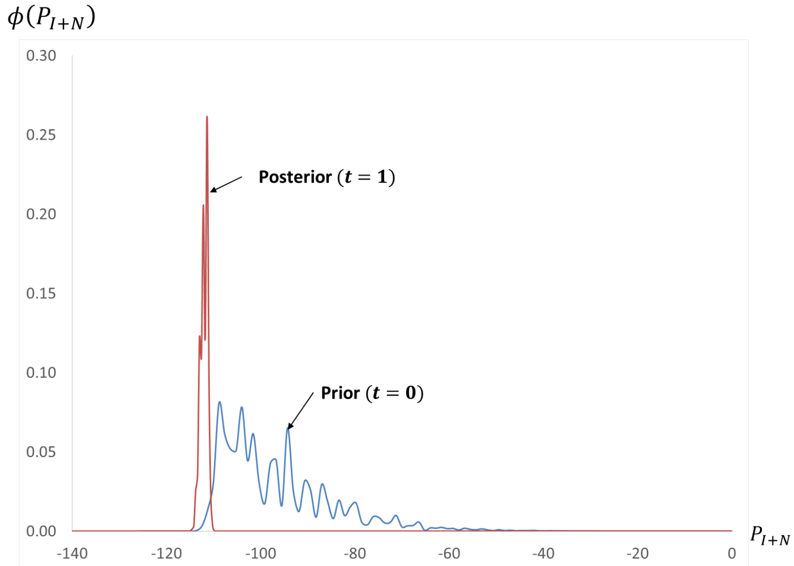

Figure 4.19: Scenario 1-4 DSA→PU sensed power P_{I+N} prior and posterior PDFs for the first time step.

much greater than the prior cases, which is the result of the significant fluctuations in the distribution mean between samples as can be seen in Figure 4.22. As with Scenario 1-2, the variations come from the significant influence of N and its associated random characteristics incorporated into the simulation model. For each sample, however, the variance is on par with the other cases.

While the metrics in Table 4.7 provide the results in terms of the average of each sample, they may require adjustment to account for the sample-to-sample variation in $\mu_{P_{I+N}}$. Large swings in $L_{p,D\to P}$ seen in Figure 4.22 (exceeding 10 dB at low percentiles) would cause the DSA radio to make frequent adjustments to its behaviors (e.g. transmit power) on short timescales that may diminish the channel's benefit. Further, the significant variations create risk that the DSA would cause interference to a PU. Thus the addition of a filtering or averaging process (e.g., Kalman Filter) for extracting the statistics across multiple sensing windows may be needed.

As the SNR of the PU signal decreases, it will eventually be overtaken completely by the noise N. From the theoretical assessment, one would expect the path loss (and resulting

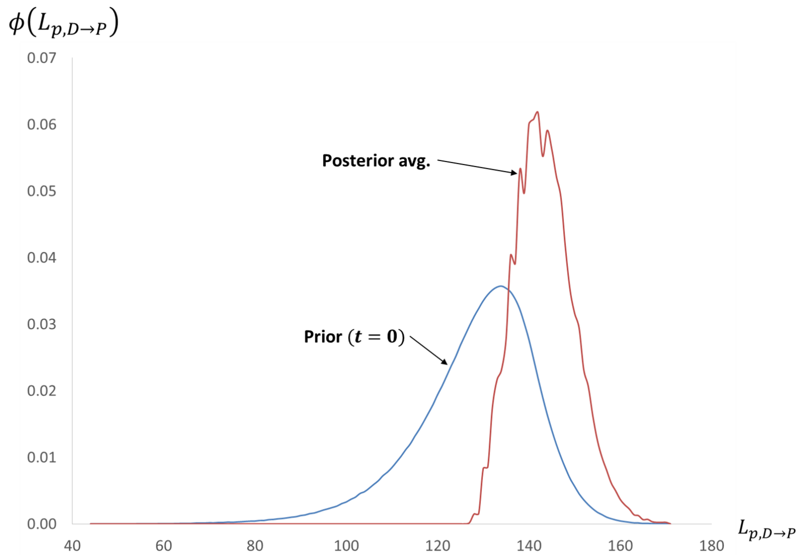

Figure 4.20: Scenario 1-4 DSA→PU path loss prior and posterior PDFs.

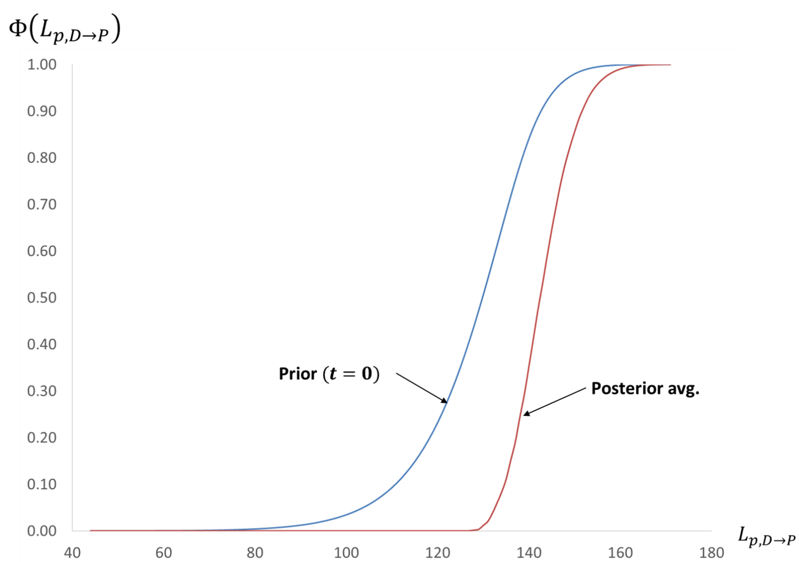

Figure 4.21: Scenario 1-4 DSA→PU path loss prior and posterior CDFs.

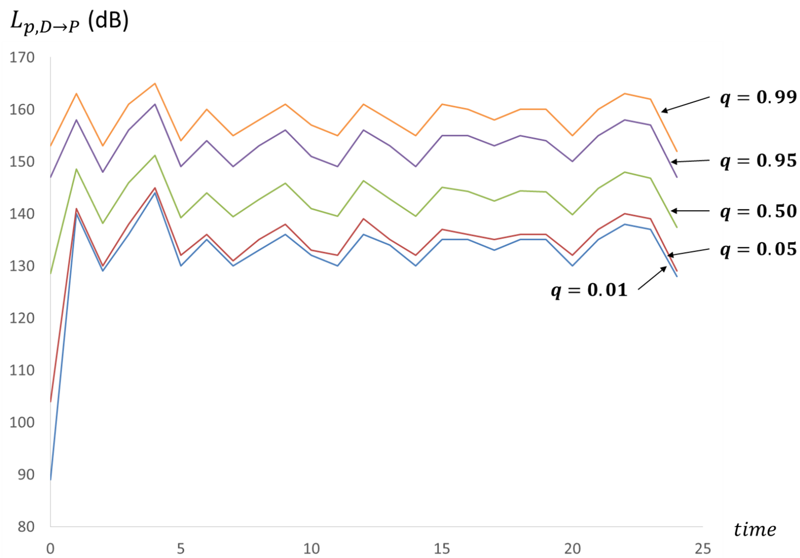

Figure 4.22: Scenario 1-4 DSA→PU path loss percentiles q={0.01, 0.05, 0.50, 0.95, 0.99} as a function of time

Table 4.7: Scenario 1-4 spectrum access gains from probabilistic reasoning.

Parameter	Prior to Posterior Change	
	$q = 0.05$	$q = 0.01$
$\Delta\mu_{L_{p,D\to P,q}}$ (dB)	14.88	14.88
$a_q \Delta\sigma_{L_{p,D\to P,q}}$ (dB)	-16.70	-30.12
$\Delta P_{tx,max}$ (dB)	31.58	45.00
Δc (bits/s/Hz)	13.9	18.3

metrics) to approach $\pm\infty$. That condition is comparable to the typical logic employed in Listen-Before-Talk (LBT) spectrum access schemes: if no detection is made, then the process concludes that a PU is absent (see e.g., [90, 104]). Thus missed detections and very weak PU signals present problems in those cases.

The DSA FCM, however, may be able to mitigate such cases. For the FCM to produce a significantly large transmit power, the sensed noise probability $\phi(N)$ would need to match very closely to the noise prior. Even if such a match were to occur, recall that the path loss has been defined with non-zero probability over a limited range. In this set of scenarios, that range was determined by the range of path losses that could occur out to 10 km, which corresponds roughly to a maximum non-zero probability path loss of 170 dB. Any observation that exceeds that limit would be deemed inconsistent with the model, either indicating that the model is incorrect or that no signal is present.

Recall, however, that the priors for path loss and PU transmit power were based on a consistent set of assumptions; the path loss prior $\phi(L_{P,D\to P})$ was specified based on the PU→DSA distance $d_{P\to D}$ over which a DSA sensor would detect a PU transmitting at its maximum power $P_{tx,P,max}$. Thus changes to those exogenous parameters would require that those priors (which are associated with some model of the world external to the FCM) be adjusted consistently.

More practically, however, is an interpretation that the maximum path loss specified for $\phi(L_{P,D\to P})$ is the sensing or awareness horizon of the the DSA. Beyond that horizon, the DSA can only assume that a PU possibly exists. Thus, it must make it's decision based on the limits of $\phi(L_{P,D\to P})$ (and the other exogenous parameters). In this sense, the probabilistic reasoning model developed here would have an implicit limit on the maximum DSA transmit power of

$$Ptx, D, max \leq P_{rx,int} + \max\left(L_{p,D\to P}\right) \tag{4.13}$$

4.1.5 Scenario 1 Summary

The analyses of the four Scenario 1 cases provides validation to the theoretical relationships developed in Chapter 3 and significant insight into the characteristics of the DSA FCM. First and foremost is the ability of the probabilistic reasoning model to improve the theoretical performance of DSA. In most cases presented here, the significant reduction in uncertainty led to increases in performance (e.g., capacity and link range) as well as decreased standoff distance and increased network density. One case, however, did demonstrate the ability to improve interference prevention capabilities when updated beliefs indicated that the path loss was lower than indicated by the prior.

It was further demonstrated that the potential for improved spectrum access efficiency scales with the difference between the a priori and in situ assessments. Figures 4.23 and 4.24 illustrate the standoff distance ratio $\delta_{D\rightarrow P,min}$ and network density Ω_{min} metrics as functions of the difference in prior to observed received power for each of the scenarios. It is found that required standoff distances decreased (i.e., lower $\delta_{D\rightarrow P,min}$) with decreasing sensed power. Consequently, the potential density of networks increases with decreasing sensed power. The magnitude of those changes are dependent upon the path loss model applied. Overall, the results from this scenario support the thesis.

4.2 Scenario 2: Known PU Location

For this set of scenarios, the location of the transmitter is known and the DSA is able to determine its own position to within ± 50 m as illustrated in Figure 4.25. The parameters from Scenario 1 are used here (see Tables 4.1 and 4.2), with the exception of path loss $\phi(L_{p,D\rightarrow P})$, which must be re-defined to account for the change in $\phi(d_{D\rightarrow P})$. A uniform distribution with respect to distance is applied to the ITM model within the ranges $350 \leq d_{D\rightarrow P} \leq 450$, giving $\phi(L_{p,D\rightarrow P})$ and $\Phi(L_{p,D\rightarrow P})$ shown in Figure 4.26.

As with Scenario 1, the DSA uses the a priori assessments as an initial set of prior beliefs. It then senses the spectrum and updates its beliefs based on the observations. The

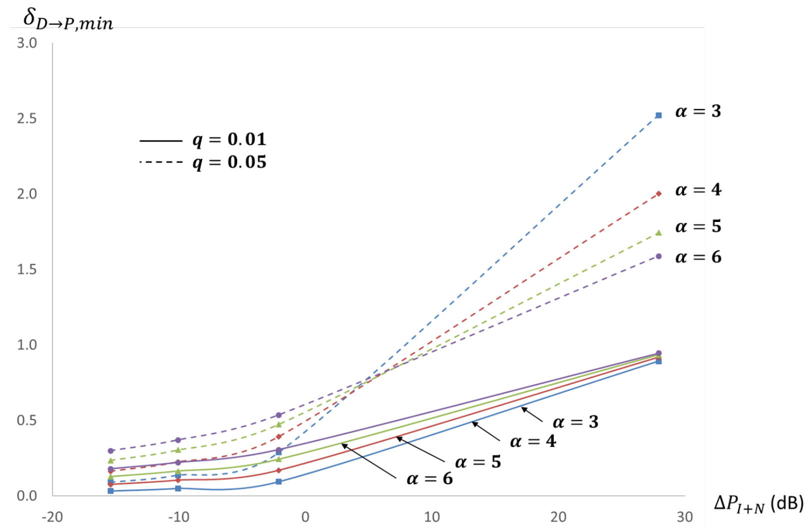

Figure 4.23: Scenario 1 prior to posterior distance ratio $\delta_{D\to P,min}$ as a function of sensed power P_{I+N} and α for $q = 0.05$ (dashed lines) and $q = 0.01$ (solid lines).

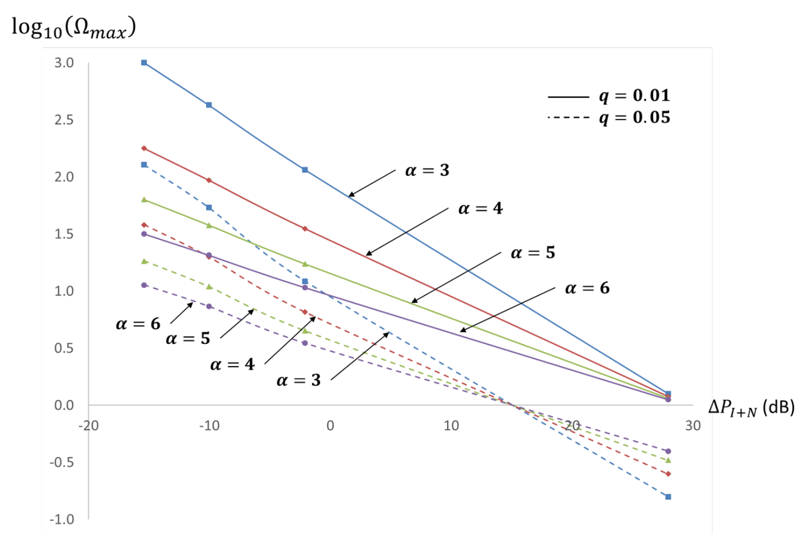

Figure 4.24: Scenario 1 prior to posterior density ratio Ω_{min} as a function of sensed power P_{I+N} and α for $q = 0.05$ (dashed lines) and $q = 0.01$ (solid lines).

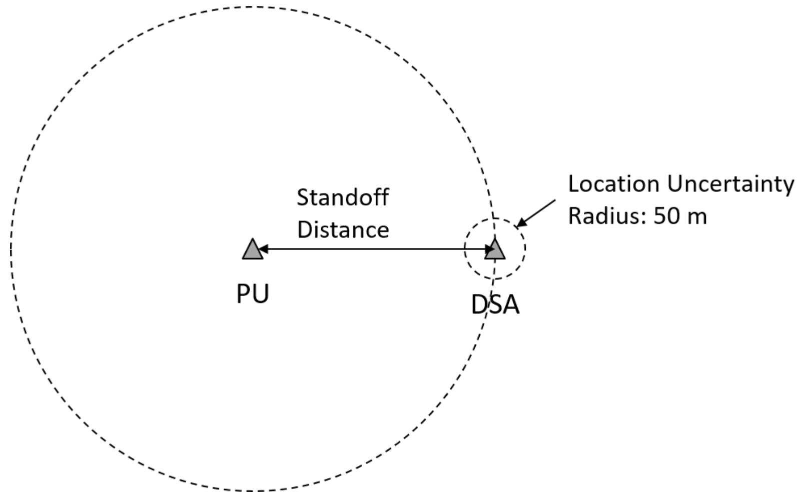

Figure 4.25: Geometry for a DSA policy with known PU location ± 50 m and 400 m exclusion zone radius.

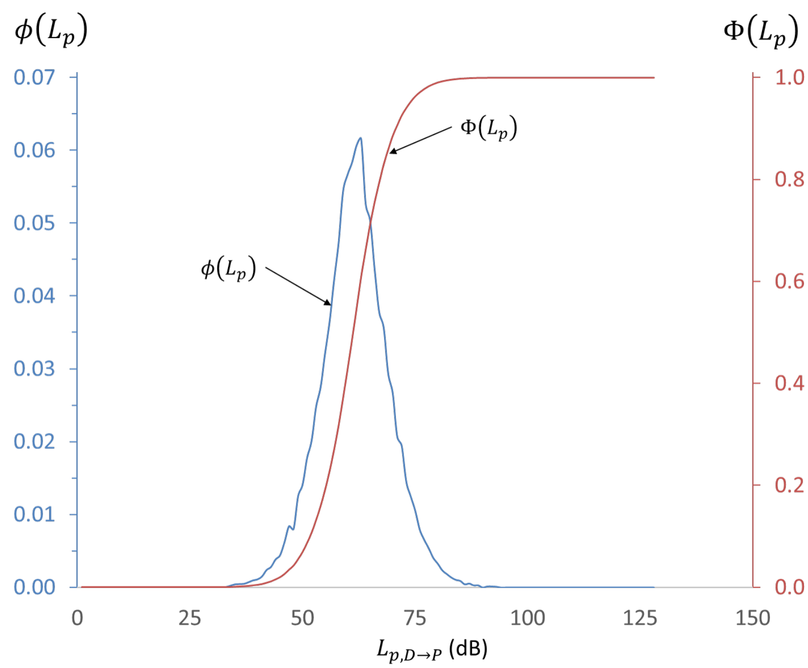

Figure 4.26: Scenario 2 DSA→PU path loss prior probability density function $\phi\left(L_{p,D\to P}\right)$ and cumulative density function $\Phi\left(L_{p,D\to P}\right)$ for distance to PU at 400 m ± 50 m.

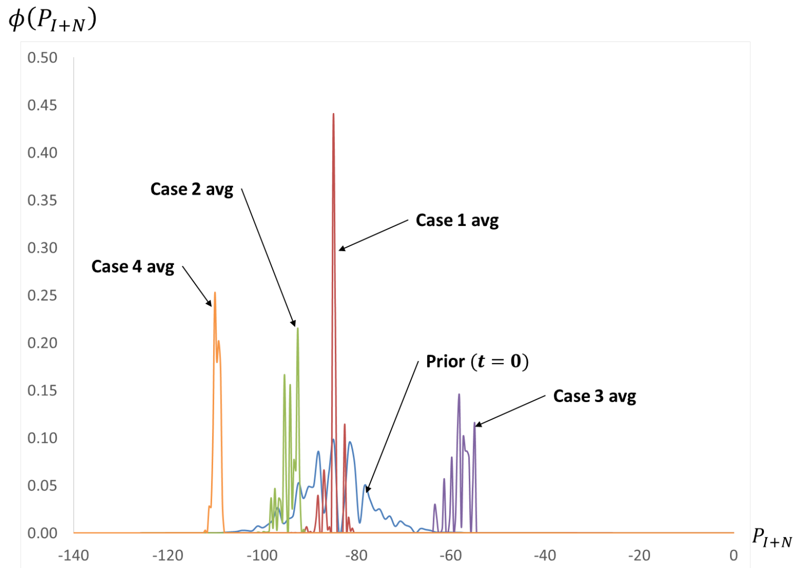

Figure 4.27: Scenario 2 DSA→PU sensed power P_{I+N} prior and posterior PDFs for the first time step.

posterior beliefs of one observation-update cycle then become the prior beliefs of the next.

The sensed power and resulting path loss beliefs for the four scenarios are shown in Figures 4.27 through 4.29. Similar to Scenario 1, the corresponding changes in path loss $\Delta L_{p,D\rightarrow P,q}$ are proportional to the difference in prior to posterior mean sensed power $\Delta\mu_{P_{I+N}}$. Additionally, the temporal characteristics of the estimates shown in Figures 4.30 through 4.33. The variances as shown in the figures and in Tables 4.8 and 4.9, however, are smaller, with risk threshold values ranging from approximately 10–15 dB below the mean as opposed to 15–30 dB in Scenario 1. Thus the impact of a greatly reduced prior distribution is seen here.

The spectrum access efficiency metrics $\delta_{D\rightarrow P,min}$ and Ω_{min} are presented in Figures 4.34 and 4.35, respectively. It is observed that—even though distance is known within a fairly small uncertainty—potentially significant gains can be found for reducing standoff distances and increasing network density. With the understanding that the data in the figures likely represent estimates of an upper bound, potential standoff distance reductions

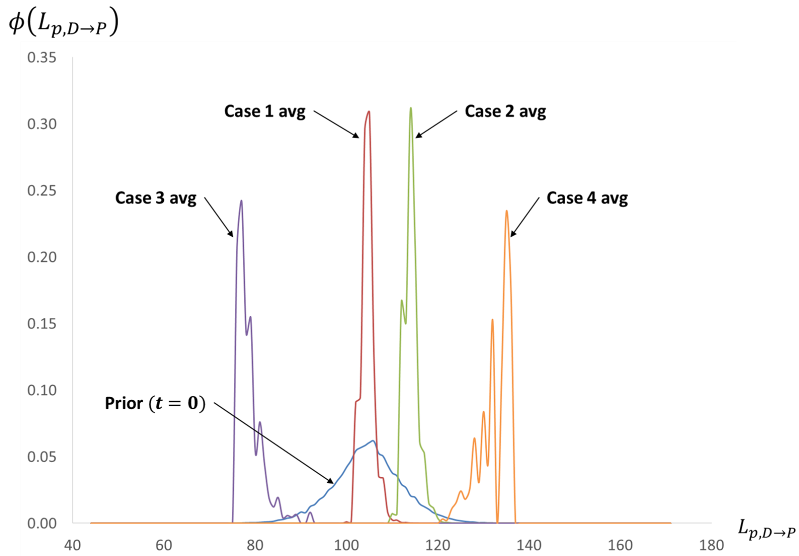

Figure 4.28: Scenario 2 DSA→PU path loss prior and posterior PDFs.

Table 4.8: Scenario 2 spectrum access gains from probabilistic reasoning, q=0.05.

Parameter	Prior to Posterior Change			
	Scenario 1-1	Scenario 1-2	Scenario 1-3	Scenario 1-4
$\Delta\mu_{L_{p,D\to P,q}}$ (dB)	-0.09	9.42	-26.06	27.69
$a_q\Delta\sigma_{L_{p,D\to P,q}}$ (dB)	-10.08	-10.58	-10.06	-10.02
$\Delta P_{tx,max}$ (dB)	10.08	20.00	-16.00	37.71
Δc (bits/s/Hz)	3.3	9.8	-14.0	21.5

Table 4.9: Scenario 2 spectrum access gains from probabilistic reasoning, q=0.01.

Parameter	Prior to Posterior Change			
	Scenario 1-1	Scenario 1-2	Scenario 1-3	Scenario 1-4
$\Delta\mu_{L_{p,D\to P,q}}$ (dB)	-0.09	9.42	-26.06	27.69
$a_q\Delta\sigma_{L_{p,D\to P,q}}$ (dB)	-16.00	-15.70	-16.06	-15.35
$\Delta P_{tx,max}$ (dB)	16.00	25.13	-10.00	43.04
Δc (bits/s/Hz)	5.3	11.5	-12.0	23.3

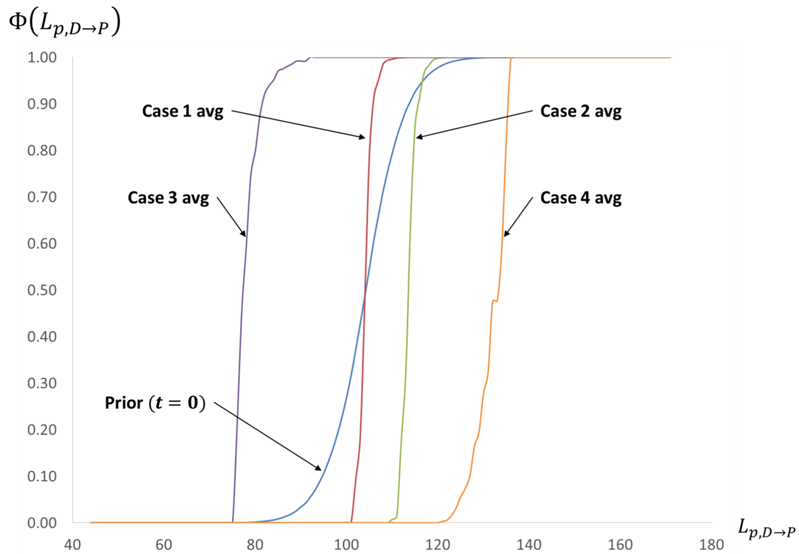

Figure 4.29: Scenario 2 DSA→PU path loss prior and posterior CDFs.

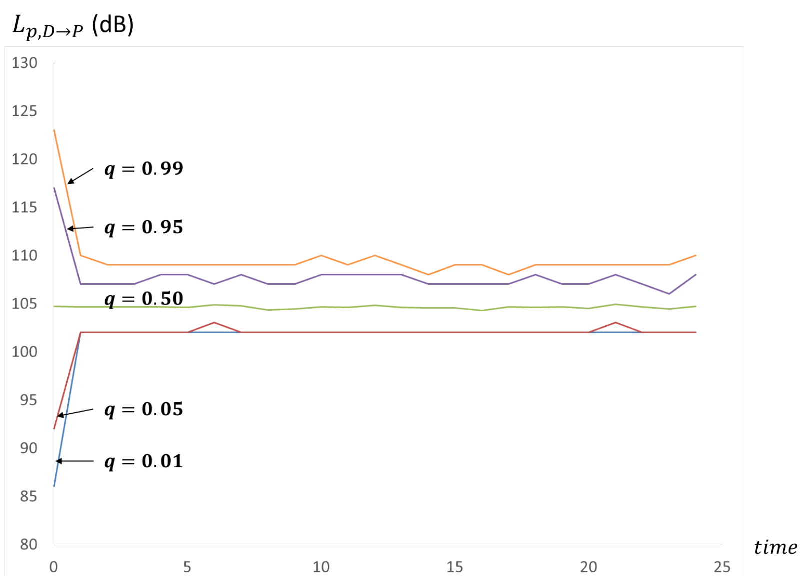

Figure 4.30: Scenario 2-1 DSA→PU path loss percentiles q={0.01, 0.05, 0.50, 0.95, 0.99} as a function of time

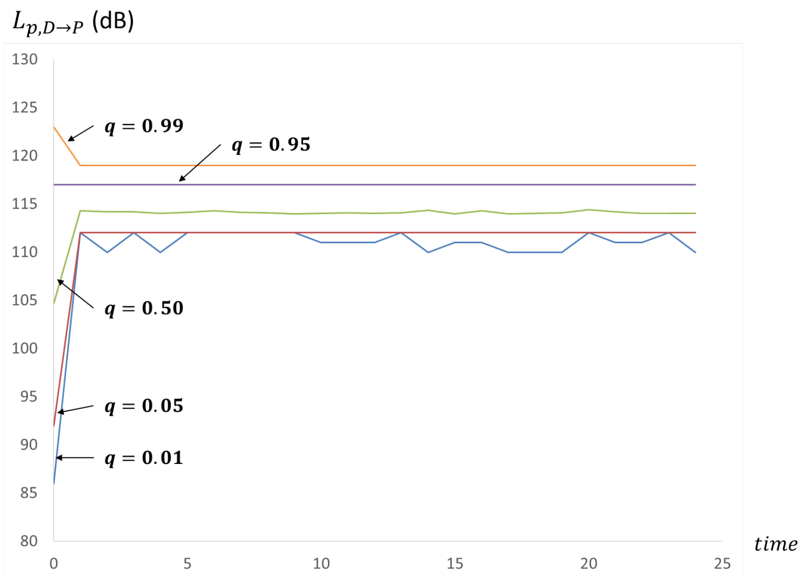

Figure 4.31: Scenario 2-2 DSA→PU path loss percentiles q={0.01, 0.05, 0.50, 0.95, 0.99} as a function of time

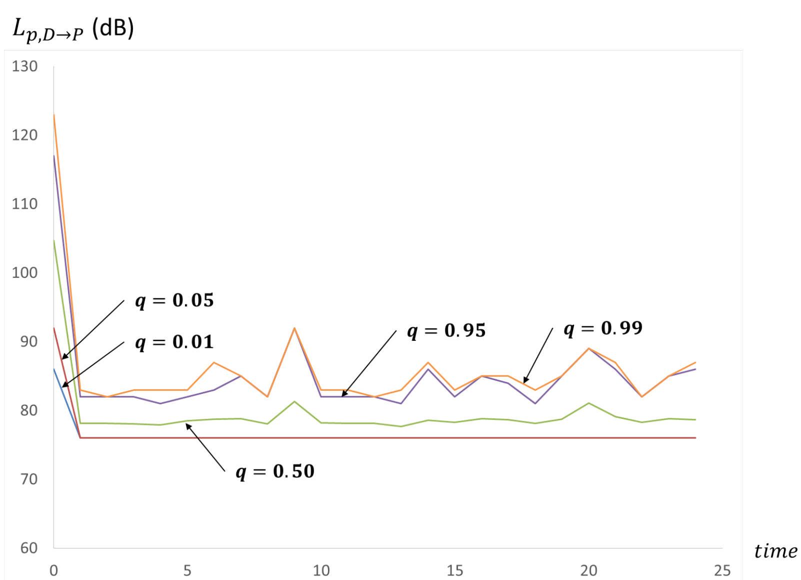

Figure 4.32: Scenario 2-3 DSA→PU path loss percentiles q={0.01, 0.05, 0.50, 0.95, 0.99} as a function of time

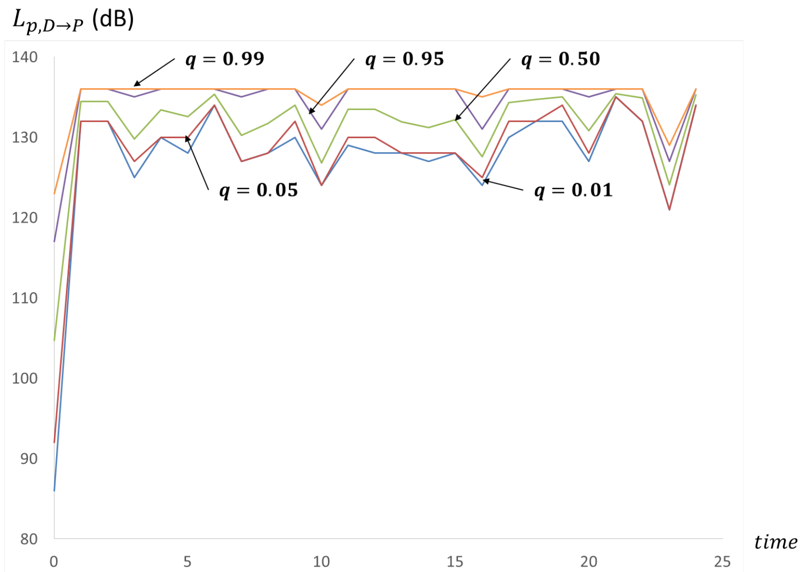

Figure 4.33: Scenario 2-4 DSA→PU path loss percentiles q={0.01, 0.05, 0.50, 0.95, 0.99} as a function of time

on the order of 25–50% are estimated due to the reduction in uncertainty in Scenario 2-1, which corresponds with the data at $\Delta P_{I+N} \approx -1$ dB. Thus the data indicate that a probabilistic reasoning model can produce significant spectrum access efficiency gains in cases such as the TV Whitespace conditions where location uncertainty is small but path loss uncertainty persists. It can be shown that the maximum spectrum access efficiency gains—i.e., minimum $\delta_{D\to P,min}$ and maximum Ω_{min}—are subject to the maximum risk-constrained path loss difference $\Delta L_{D\to P,q,max} = L_{D\to P,max} - L_{D\to P,q,prior}$, where $L_{D\to P,q,prior}$ represents the a priori threshold. Specifically, the minimum $\delta_{D\to P,min}$ and maximum Ω_{min} are given as

$$\delta_{D\to P,min} = 10^{-0.1\alpha_{post}^{-1}\left(L_{D\to P,q,prior} - L_{D\to P,max}\right)} \tag{4.14}$$

and

$$\Omega_{D\to P,min} = 10^{0.2\alpha_{post}^{-1}\left(L_{D\to P,q,prior} - L_{D\to P,max}\right)}. \tag{4.15}$$

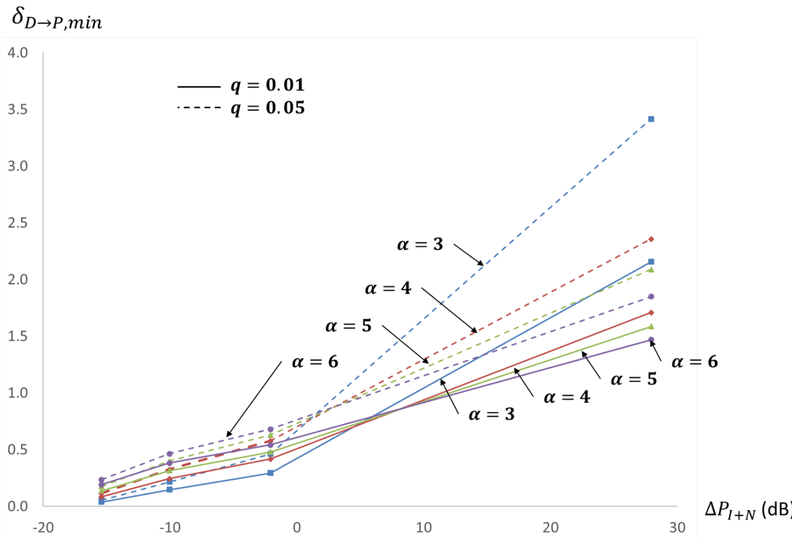

Figure 4.34: Scenario 2 prior to posterior distance ratio $\delta_{D\to P,min}$ as a function of sensed power P_{I+N} and α for $q = 0.05$ (dashed lines) and $q = 0.01$ (solid lines).

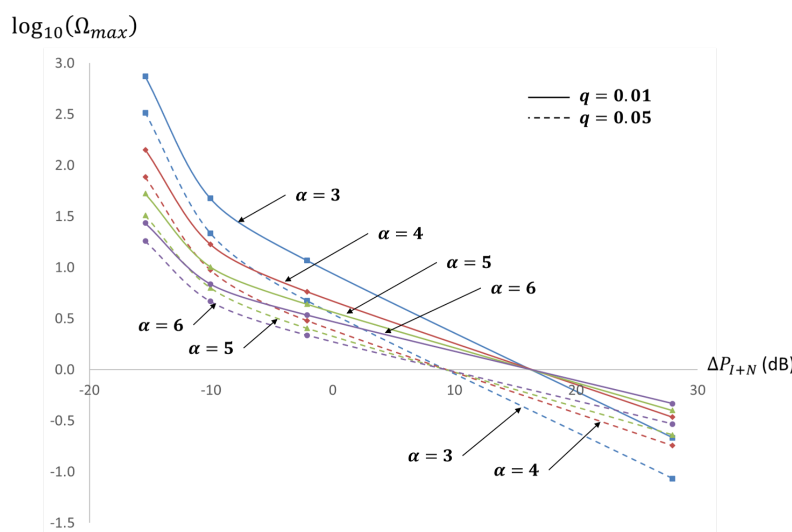

Figure 4.35: Scenario 2 prior to posterior density ratio Ω_{min} as a function of sensed power P_{I+N} and α for $q = 0.05$ (dashed lines) and $q = 0.01$ (solid lines).

4.3 Summary and Concluding Remarks

The simulations and analyses conducted here provide significant analytical and quantitative support for thesis. The results demonstrate the ability to establish a probabilistic reasoning model that can reduce situational awareness uncertainty relative to a priori assessments through in situ observation and probabilistic reasoning. The results corroborate the theoretical findings and analyses from Chapter 3. They demonstrate the relationships between path loss uncertainty and permitted system behavior limitations and the ability to govern behaviors as a function of risk.

With the risk-constrained behaviors, it was shown that aggregate changes in path loss mean and variance affect DSA behaviors in terms of permitted transmit power determination leading to corresponding changes in capacity and link range. Changes in spectrum access efficiency metrics such as standoff distance and network density are similarly affected. The model demonstrated the correct behavior; increasing capabilities when permitted by the updated findings and further restricting them when required. Specifically, capacity and link range potential were increased with corresponding increases path loss; required standoff distance and network density were likewise affected. The converse held true as well; the metrics indicated lower performance levels with path loss estimates were decreased as predicted by the theoretical assessments in Chapter 3.

Finally, the observations were shown to hold across a range of scenarios. Location uncertainty affected the extent of the gains achieved with uncertainty reduction, but the gains were still significant even with low levels of location uncertainty.

Chapter 5: Research Summary

As wireless demands increase, spectrum sharing techniques are becoming increasingly important. Research into methods for enabling Dynamic Spectrum Access (DSA) has made significant progress in many areas and has enabled some spectrum sharing capabilities. Current and emerging sharing policies, however, are limited in two aspects. First, they use centralized spectrum access mechanisms to compensate for a lack of trusted interference mitigation technique in distributed DSA systems. Second, they specify spectrum access behaviors (e.g., DSA transmit powers and exclusion zones) during the policy formulation process in advance of a specific operating context, which then potentially limits the behavior due to the risk of rare events.

Spectrum management can be cast (in part) as a risk management process. In this context, the current method of a priori behavior specification can be shown as *necessarily* and systemically inefficient:

1. In establish operating limits, a spectrum access policy must consider all possible conditions for which the policy applies (i.e., all times, locations, and situations);

2. Policies establish limits on spectrum access behaviors (e.g., transmitter power, bandwidth, and standoff distances) associated with a specified probability of interference, which can be characterized by a percentile threshold q;

3. These operating limits are only efficient when actual conditions correspond with those associated with q, and are by definition inefficient under more favorable conditions;

4. Given that more favorable conditions occur with a probability $1-q$, policies therefore *necessarily* lead to inefficient spectrum access in $1-q$ percent of conditions;

5. Since in general $q \ll 0.5$ to attain low interference risk, this process is *necessarily* inefficient in the majority of scenarios;

Reducing the magnitude of this inefficiency requires a reduction in the range between the mean and threshold percentiles. That reduction requires reducing uncertainty—i.e., reducing the variance of the underlying probability distribution. Reducing uncertainty therefore requires the ability to establish spectrum access behaviors using information focused on the specific operating context.

The research conducted under this effort addressed the thesis that in situ probabilistic reasoning coupled with policy specifications enables greater spectrum sharing efficiency than current a priori specification methods. The thesis is supported by theoretically, analytically, and quantitatively.

Theoretical support comes from the argument in Chapter 2 that in situ uncertainty assessments can be made within a more focused context than a priori assessment methods. Thus, the a priori state space χ_1 over which probability assessments are made is larger than that of the in situ process χ_2. If the in situ state space is a subset of the a priori state space ($\chi_2 \subseteq \chi_1$), it can be shown that $\text{Var}\{\chi_1\} \geq \text{Var}\{\chi_2\}$ by Chen's theorem [48]. Thus theory shows that in situ probabilistic reasoning in DSA systems enables greater spectrum access potential than existing methods, which establish operating limits using a priori information.

A probabilistic reasoning model is then developed and characterized in Chapter 3. The model builds on Pearl's Causality Theory [53] combined with well-established principles from communications theory. Viewing the DSA process in a causal context guides the development of the resulting Functional Causal Model (FCM), which describes the mathematical and logical relationships among DSA systems, protected users (PUs), and performance parameters such as transmit power, interference, and channel capacity. The method provides two key capabilities. First, it enables in situ assessment of uncertainties based on local conditions and observations. Second, extends the concept of risk-constrained spectrum access—determining spectrum access behaviors based on uncertainty and risk—from the current a priori process into in situ probabilistic reasoning.

It is shown through analysis of the underlying mathematical relationships that the probabilistic reasoning method enables DSA system behaviors to be governed by risk thresholds coupled with uncertainty assessments. Specifically, it is shown that DSA→PU path loss uncertainty is the fundamental characteristic that determines spectrum access capabilities. Given that a DSA system must operate at or below some permitted risk level q, spectrum access behaviors are governed by

$$L_{p,D\to P,q} = \mu_{L_{p,D\to P}} - a_q \sigma_{L_{p,D\to P}}.$$

All relevant DSA spectrum access behaviors, performance parameters, and spectrum efficiency metrics can be expressed as function of path loss uncertainty based on this expression. It is shown that higher levels of uncertainty $\sigma^2_{L_{p,D\to P}}$ result in reduced levels of DSA system behavior (capacity and link range) and spectrum access efficiency (standoff distance and network density).

The probabilistic reasoning model is developed into a computer model for simulation and analysis presented in Chapter 4. The analysis addresses eight different spectrum access conditions categorized into two scenario types. The first category represents mobile PU conditions, in which significant uncertainty exists regarding the DSA→PU distance and associated path loss. The second category represents conditions in which the DSA→PU distance is known with small uncertainty (similar to the TV Whitespace and 3.5 GHz band situations). Within each category, the sensed PU power was varied relative to the prior expectation so as to assess the resulting posterior beliefs and associated changes in spectrum access behaviors. Using the concept of risk-constrained behaviors, it was shown that the probabilistic reasoning model produced spectrum access behaviors corresponding with aggregate changes in path loss mean and variance. The model demonstrated increased capabilities when permitted by the updated findings and further restricting them when required. Specifically, capacity and link range potential were increased with corresponding increases path loss; required standoff distance and network density were likewise affected.

The converse held true as well; the metrics indicated lower performance levels with path loss estimates were decreased as predicted by the theoretical assessments in Chapter 3.

Thus the thesis is supported by theoretically, analytically, and quantitatively.

5.1 Applications

The concepts developed in this thesis enable additional capabilities in spectrum sharing. Appendix A develops a decision model for DSA based on the probabilistic reasoning approach in this thesis. Probabilistic decision-making is a natural extension of the probabilistic reasoning model. The decision model uses utility theory—specifically multi-attribute utility theory—to enable evaluation and choice among alternative DSA actions. Utility theory provides an axiomatic system of choice evaluation that captures the relationships among goals, constraints, and uncertainty in a decision-making process. The decision model incorporates DSA channel capacity, interference, and monetary cost for spectrum access as decision attributes into a joint utility function.

The utility function is simulated and analyzed to assess DSA decision behaviors and trades under a range of spectrum sharing options and degrees of situational uncertainty. The analyses demonstrate the impact of spectrum usage volatility on preferences between emerging usage options under the tiered access model. Formulations are developed that identify the impact of cost and spectrum access uncertainty on decision trades between General Authorized Access (access without guarantees) and fee-based Secondary Access (access with guarantees). Analysis also characterizes decision trades between fee-based and auction-based spectrum pricing, leading to the insight that auction-based pricing incurs a distinct disadvantage relative to fee-based pricing due to the inherent uncertainty and pricing volatility.

The underlying probabilistic reasoning model for spectrum access is also applied to a satellite communications (SATCOM) system in Appendix B. SATCOM systems and networks require reliable management decisions for efficient and effective use of SATCOM resources. High demand on a SATCOM payload increases resource allocation challenges and amplifies the impacts of service shortfalls from unforeseen changes in user demand or service capabilities due to issues such as weather. By applying the probabilistic reasoning with risk-based assessments, SATCOM operators can assess the impacts of uncertainty on SATCOM system performance. The probabilistic reasoning method enables the quantitative representation of SA uncertainties and probabilistic reasoning for prediction, planning, and diagnosis of SATCOM payload performance. Furthermore, it provides the ability to conduct risk-based decision-making.

5.2 Contributions

The research summarized in this dissertation provides several contributions to the existing body of research regarding spectrum sharing and communications system modeling.

First, the research characterizes the spectrum management process of interference mitigation as a risk management process. It recognizes the use of probabilities and confidence levels in the analyses process and associated models supporting spectrum access policy specifications. The processes and models essentially seek to characterize the level of risk and then develop rules that constrain spectrum access behaviors subject to desired risk levels. This process gives rise to the concept of risk-constrained spectrum access.

Second, the research builds on the risk management aspects to logically show that existing methods for specifying spectrum sharing behaviors *necessarily* lead to inefficient spectrum access. The issue is shown to be systemic and only resolvable if the context in which behaviors are specified can be limited to those associated with actual operational conditions.

Third, the research establishes a DSA probabilistic reasoning model that enables spectrum sharing subject to situational uncertainty and risk. The model builds on Causality Theory and wireless communications theory that allows a DSA system to reason about observations and make corresponding probability assessments regarding potential actions. The risk-constrained spectrum access concept is applied as a means for governing DSA system behaviors. It is demonstrated in theory and simulations that method adjusts behavior limits in accordance with uncertainty levels a risk thresholds.

Fourth, the FCM basis of the DSA probabilistic reasoning model can be extended to complex DSA decision-making and to more general wireless communications problems. Appendix A extends the DSA FCM developed in this thesis with a multi-attribute utility model, demonstrating how the probabilistic reasoning model enables greater DSA decision-making capabilities. Appendix B provides an example of its application to a satellite communications (SATCOM) system. The modeling technique enables risk-based assessments on parameters other than interference (e.g., channel capacity) and provides a general mechanism for performance assessment, risk-constrained system management, and decision-making.

5.3 Summary and Future Research

The research conducted here represents a starting point for further exploration of probabilistic reasoning in DSA and other wireless communications systems. The research established the fundamental capability to incorporate probabilistic reasoning into spectrum sharing as a means for improve system performance and overall spectrum sharing capabilities related to interference prevention and increased spectrum access efficiency. It develops the concept of risk-based spectrum access, which allows regulators to specify levels of interference risk thresholds that must be maintained for spectrum access behaviors. Together with situational uncertainty assessments, the risk thresholds govern DSA system behaviors according to estimations of operating conditions. Numerous extensions and applications follow from the results in addition to the decision-making and SATCOM applications presented in Appendices A and B.

One important area of additional research is the assessment of estimation capabilities. The research presented in this thesis is based on a DSA system's perception of the operating environment. Understanding how well a DSA system can estimate the propagation environment is critical in evaluating the viability of applying the concept to actual systems. The model approach assumes the ability to adequately assess important factors such as PU transmit powers using data published in regulator databases. The extent to which that data enables probabilistic assessments of prior distributions affects the difference between truth and perception and ultimately the effectiveness of the approach.

Within the context of DSA application, the model can be extended to temporal spectrum sharing. The scenarios evaluated here are principally focused on geographic sharing so that a relationship can be established with existing and emerging spectrum sharing policies. While each scenario encompasses multiple observation-update cycles, the assumption is that the mean signal levels are almost constant across the entire time period. The scenarios model a dynamic Bayesian Network where the priors of one time step are equivalent to the posteriors of the previous time step. A dynamic PU signal along with algorithms that predict channel usage and availability based on observations could be applied. Numerous such algorithms exist in literature (see e.g. [82, 90, 97, 105–108]).

Additionally, the model can be extended to multi-channel and multi-user scenarios. A multi-channel implementation may be more than simply replicating the DSA FCM for each channel, and may additionally include external process that apply sensing and channel selection strategies to optimize overall spectrum access. Additionally, multi-user scenarios enable cooperative sensing among collaborative DSA systems, and the process for evaluating permitted behaviors depends on collectively evaluating the impact that multiple DSA devices would have on multiple PUs. Some related work can be found in [79, 82–96, 98, 99].

Appendix A: DSA Decision-Making Under Uncertainty with Probabilistic Reasoning

Various decision processes can be applied for DSA spectrum access. The most basic is perhaps the declaration of a channels as “open” or “occupied”, then selecting one that is “best” among all radios wishing to directly communicate with each other [104]. In the simplest decision schemes, the valuation of best may be measured by a single parameter such as maximum transmit power (see e.g., [74,109]), which translates into channel capacity and link range as discussed in Chapters 3 and 4.

It is more likely, however, that DSA decisions will need to consider multiple attributes including capacity, interference, and perhaps even monetary cost among others. Therefore a DSA decision process needs to understand the relative importance of each decision attribute and how to reach a satisfactory or perhaps even optimal decision. Multi-attribute utility theory provides the foundation for developing joint utility functions that take into account multiple decision factors (attributes), each of which captures an essential element of the objectives and constraints [110]. The decision process evaluates multiple spectrum access options and selects the one having the greatest overall expected utility.

Probabilistic decision-making is a natural extension of the FCM approach [53]. The model presented here uses utility theory—specifically multi-attribute utility theory [110]—to enable evaluation and choice among alternative DSA actions. Utility theory provides an axiomatic system of choice evaluation that captures the relationships among goals, constraints, and uncertainty in a decision-making process.

The decision-making and situational awareness processing functions of a DSA system as depicted in Figure A.1 would use an FCM as discussed in Chapter 3 and associated queries in a complimentary manner. The Awareness Processing function would be responsible for estimating the relevant world state as defined by some FCM containing random variables and their relationships. A DSA system would directly update observable random variables through some data acquisition process (e.g., sensing or database access), and counterfactual

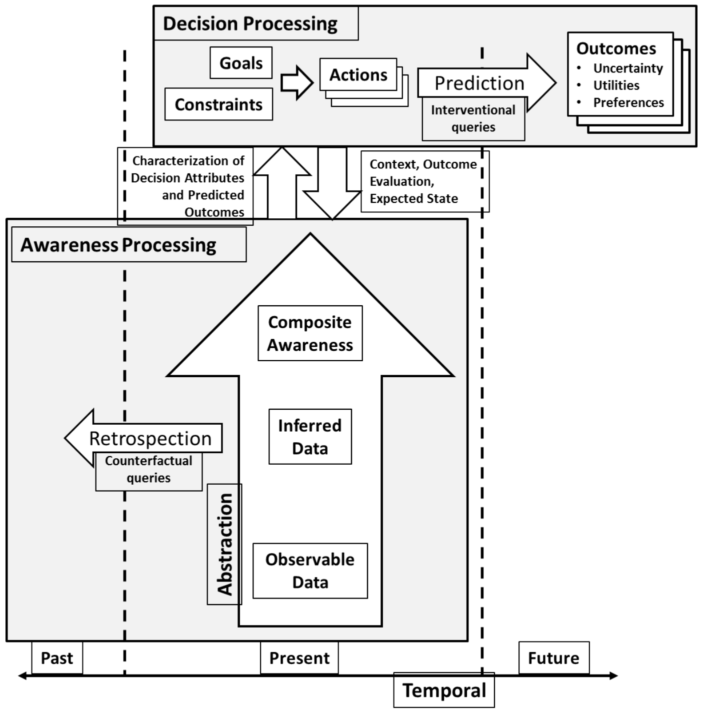

Figure A.1: Conceptual situational awareness and decision-making functional architecture.

queries (‘Would $Y = y$ in situation $U = u$ had X been x?”) could be used to learn from past observations. Unobserved random variables and higher-order (abstracted) concepts would be inferred to produce a composite situational awareness defining the DSA system’s belief about the relevant world state as demonstrated in Chapter 3. The Decision Processing function would use interventional queries (“What is the expected response of Y due to action $do(X = x)$?”) on the acquired information to evaluate possible outcomes and their expected utilities. The DSA system would select the action $do(x)$ with the greatest expected utility and inform the situational awareness function of the expected state to be used in evaluating the next set of observations and actions.

The intent of the overall process is to allow a DSA system to make decisions, which are choices among a set of options (or actions) that produce consequences (or outcomes) and are made with the intent of achieving some objective (e.g., channel capacity). In utility theory, the value or worth of alternative consequences is often placed in a relative rather than absolute context. That is, they are ordered according to preference. Furthermore, decisions may require the use of probability and inference due to uncertainties that exist regarding inputs to the decision process. As demonstrated in Chapter 3, the output of the SA model is a set of probability distributions for variables such as channel capacity. Utility theory uses a decision system comprised of a) a set of one or more attributes and probabilities comprising the essential elements of the objectives, b) a quantitative model reflecting the decision-maker's preferences for and among each of the attributes, and c) mechanisms allowing the decision-maker to make trades among alternative actions.

At an operational level, DSA systems must place importance on regulatory compliance for factors such as non-interference with protected users. DSA system users, however, need to attain sufficient levels of service, such as reliable link capacities and perhaps other measures of service quality. Additionally, DSA system use may need to make decisions related to cost such as could occur with secondary sharing and auction-based access. The following sections identify key principles in defining a DSA decision model, provide a derivation for a multi-attribute DSA utility function, and illustrate its integration with the SA model of the previous section for decision-making.

The next section identifies a core set of DSA decision attributes, which are developed into a DSA utility function in Section A.2. A theoretical assessment of the DSA utility function is conducted in Section A.3 supported by simulation results in Section A.4.

A.1 DSA Decision Attributes

Establishing a decision model for a DSA system requires sufficient definition of key operating elements of a DSA system. The elements encompass goals and desired outcomes, constraints, uncertainties, and preferences for making trades among the goals and optimizing the outcome among a set of alternative actions. The attributes selected for the decision model should possess several key characteristics [110]:

- Completeness: The set of attributes must collectively be adequate indicators of the degree to which an objective is met. Thus they are comprehensive in that they capture all the relevant aspects of the objective such that a decision-maker can understand the mapping between attaining a particular attribute level and achieving the overall objective.

- Operational: Each attribute must be observable and measureable by the decision-maker in a manner that supports timely decisions. The set of attributes should enable alternative actions to be assessed and compared, providing a sufficient degree of explanation to the decision-maker as to the trades to be made among the options. Each attribute must also enable the incorporation of uncertainty by expressing a probability or belief measure with each attribute level.
- Decomposable: Where large dimensionality exists in the problem, it should enable decomposition into manageable sets of tasks.
- Nonredundancy: Attributes should be defined to avoid incorporation of consequences in more than one attribute.
- Minimal: The set of attributes should be small in number to increase the operationality of the resulting decision model.

Three fundamental goals of DSA systems proposed as attributes for the spectrum utility model developed here are 1) the availability of sufficient (reliable) wireless channel capacity; 2) avoidance of harmful interference to other spectrum users; and 3) monetary cost (or profit). The following sections describe the rationale for selecting capacity, interference, and cost as the attribute set in the spectrum utility. Examples of the attributes are presented with a focus on their elements and why they (individually and collectively) meet the desired criteria.

A.1.1 Capacity

A primary goal of a DSA system is to provide the user with a desired degree of information carrying capacity. That capacity goal comes with several qualifiers such as reliability and duration. Capacity also has a direct impact on other aspects of system performance such as latency. Thus capacity for a given amount of time is the goal and factors indicating how the capacity is achieved (e.g., bandwidth, power, and duration) as well as quality of service (QoS) characteristics are elements of the capacity attribute. The trade space within each of those elements define constraints upon capacity and can be used to qualify viable options.

The capacity formulation as defined by (3.10) provides a basic view of expected capacity and can be expanded to account for other essential factors in DSA system operation. For example, the DSA system may wish to understand the total data that can be transferred, which is the capacity integrated over time, e.g., $\int_t C(t)dt$. The DSA system may also include other factors affecting throughput such as overhead from reliability mechanisms (e.g., error correction coding, retransmission). Detailed models can be developed for various protocols and combined with channel capacity to either determine a) the resulting throughput offered to the user for a given spectrum usage option, b) the capacity characteristics needed to meet a specified level of user throughput, c) or the quality of service that can be provided to data flows and applications. Those capacity-related concepts would be reflected as augmentations to the DSA FCM shown previously in Figure 3.4. Thus capacity in some form provides extensive insight for extent to which spectrum use opportunities meet user data transport needs.

A.1.2 Interference

The second metric of interest for DSA operation is the effect on other spectrum users. Several interference metrics have been proposed in literature, including interference temperature, increased error rates, reduced coverage areas, and outage times [5, 109, 111–113]. The appropriate metric depends on technical and regulatory considerations and must correlate with interference effects on the protected system. Metrics could include energy into a receiver, signal structures (e.g., harmonics), relative frequency spacing of signals, protocols (e.g, media access control, error correction coding), time (durations and rates), and application responses to disruptions (e.g., radar detection range loss, increased data retransmissions).

One primary issue shared among all interference monitoring techniques is difficulty in establishing DSA system awareness of the interference potential at any given physical location. Any RF device has a limited ability to accurately determine spectral energy at a distance. Furthermore, interference results from the *aggregated* power from multiple sources; thus DSA interference assessments or policies must account for possible emissions from multiple RF sources in determining the allowable transmission power characteristics. Remote measurement and reporting of interference via a dedicated sensor network, feedback from an affected user, or from other devices [78–100] can increase the accuracy of energy estimates and account for energy from all RF sources, but implementation complexity imposes engineering challenges and system costs.

Nonetheless, managing signal levels and avoiding harmful interference is a fundamental requirement for a DSA system. The specific FCM attribute used for the decision model will be $P_{rx,D\rightarrow P}$, which is the signal power that the DSA imposes on the PU.

A.1.3 Monetary cost

The broad scope of economic considerations for DSA spans all facets of system development and operation including costs for device and infrastructure development, regulatory compliance, and spectrum leasing [20, 114, 115]. While all three of those factors are interconnected, the focus here is on economic elements influencing in situ operational trades among various decisions. The type of cost model desired here relates to the cost that a user would be required to pay for access. Thus system costs such as infrastructure costs are not relevant to the decision process once a particular spectrum access model and system design are implemented.

Under the emerging tiered access concept being developed for the 3.5 GHz sharing rules (see Figure 1.7), DSA systems may incur varying costs for accessing spectrum on a secondary basis [2]. Some portions of the spectrum will have free access while others may require payment for access, perhaps with contractual guarantees of quality in return for payment. Peha and Panichpapiboon [115] point out that spectrum quality guarantees are a fundamental motivation for users to pay for secondary access rather than utilize uncoordinated access with no QoS guarantees. Other contractual guarantees such as access duration, transmit power, and channel bandwidth are other likely elements of any secondary sharing agreement. The DSA user could then make trades between coordinated and uncoordinated access based on cost versus benefit. Thus a DSA system would reasonably need to make preference judgments that include monetary cost.

Three alternative spectrum sharing options result from the mix of access guarantees and access pricing models:

1. Access at no cost. Access to spectrum is provided at no cost similar to existing ISM bands used for 802.11 systems. Access mechanisms will most likely be uncoordinated, but regulators could impose a lightweight coordination protocol or common etiquette to ensure fair access. No quality guarantees would exist other than those that result from regulatory constraints for fair access.

2. Auction-based pricing. Secondary users compete for access from spectrum brokers by placing bids for spectrum resource guarantees (e.g., bandwidth and transmit power).

3. Fixed pricing. Spectrum providers use defined pricing models that are known to users in advance.

Several common pricing aspects exist for the latter two . Principally, spectrum providers would seek to maximize profit while spectrum users would seek to minimize cost [20, 115, 116]. It's reasonable to expect spectrum cost models to specify a minimum price with real-time prices determined in accordance with spectrum supply and demand [117]. Furthermore, it is reasonable to expect that the service agreements established via auction or fixed pricing are legal contracts that define the constraints imposed on the secondary user (e.g., bandwidth, duration, transmit power) of the lease as well as spectrum quality guarantees from the provider (e.g., maximum interference levels that secondary users could incur). Practical pricing models would likely incorporate bandwidth, duration, spectrum quality, spectrum availability (supply v. demand), and transmit power. While conceptually discussed in literature, a spectrum pricing model covering that scope, however, is not yet established [115–117].

A greater understanding of DSA users' attitudes toward cost in relation to capacity and interference will help better define cost utility functions, but is not a prerequisite for creating a general model to demonstrate the fundamental concepts. Moreover, the spectrum utility model developed here can be used to further an understanding of DSA users' attitudes toward cost and impact on trades among various spectrum access and cost models.

Whereas capacity and interference are explicitly modeled in the DSA FCM from Figure 3.4, monetary cost is not. Cost could easily be integrated into the model. For example, suppose a rate-based cost (cost per unit time) is established as a function of DSA transmit power P channel bandwidth W, as well as guarantees regarding interference levels P_{int} from other spectrum users. Such a model would be represented as

$$G\left(M = \langle U, V, F \rangle\right) \text{ for } \begin{cases} U \equiv \{P_{tx}, P_{int}, W\} \\ V \equiv \{M\} \\ F \equiv \{M = f\left(P_{tx}, P_{int}, W\right)\} \end{cases} \tag{A.1}$$

and shown in Figure A.2.

If cost is a linear function of $P_{tx,D}$, W, and $P_{rx,P\rightarrow D}$, with associated cost rates m_1 \$/dBm, m_2 \$/Hz, and m_3 \$/dBm, the cost M can be expressed as

$$M = m_1 P_{tx,D} + m_2 W + m_3 P_{rx,P\rightarrow D}. \tag{A.2}$$

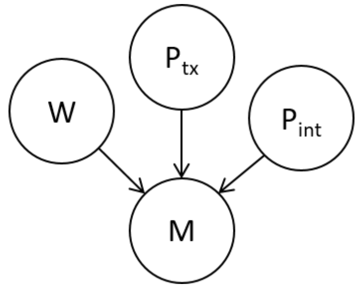

Figure A.2: Spectrum sharing cost functional causal model.

The mean and variance μ_M and σ_M^2 are given by

$$\mu_M = m_1 \mu_{P_{tx,D}} + m_2 W + m_3 \mu_{P_{rx,P \to D}} \tag{A.3a}$$

$$\sigma_M^2 = \sigma_{P_{tx,D}}^2 + \sigma_{P_{rx,P \to D}}^2 \tag{A.3b}$$

for a known bandwidth W. $P_{tx,D}$ is a controlled variable in that the DSA system evaluates each option by $do(P_{tx,D})$, so the mean here is simply $P_{tx,D}$ with no variance, which is defined in terms of path loss characteristics and the PU interference threshold in (3.22).

A.1.4 Further Attribute Considerations

Capacity, interference, and monetary cost provide a set of attributes for a spectrum utility model that capture the fundamental elements of DSA operation. Together, the attributes generally meet the criteria for attribute selection. Interference monitoring presents some operational challenges but is a primary metric for assessing a DSA system's impact on other spectrum users. Furthermore, uncertainty models can be developed for the attributes as discussed above and shown in Sections 3.2 and 3.3. The set of attributes is certainly manageable and will be shown to impose little complexity.

The completeness of the proposed attributes in comprehensively characterizing all relevant decision-making attributes may vary by user or application. Some users may wish to include other attributes relevant to a particular DSA system implementation, architecture, or usage. The attributes propose here, however, do provide sufficient insight in assessing and characterizing the use of the FCM and multi-attribute decision-making for DSA systems.

A.2 Defining a Spectrum Utility Function

Each of the three attributes correlates to a distinct utility in the DSA decision process. Collectively they create a set of potentially conflicting objectives, requiring a joint utility function that defines trades among them and produces a joint utility assessment. This section identifies the relevant characteristics of the individual utility functions and derives the joint utility function as a multi-attribute utility function built upon the three individual utility functions.

A.2.1 Spectrum Utility Function Derivation

Determining the form of the joint spectrum utility function requires an understanding of the relationships among the attributes as well as insight into desired behavior of the joint utility function. Principle among the attribute relationships is utility independence, which is a necessary and sufficient condition for establishing a joint utility function composed of individual utility functions [110]. If two attributes are mutually utility independent, then individual utility functions established over each attribute can be combined to generate a joint utility function. Defined formally, attribute X is *utility independent* of attribute Y when conditional preferences for lotteries on X do not depend upon the particular value Y. As an example utility independence assertion, the relative preference of capacity levels for a radio or user is based on the ability to fulfill throughput demand and does not vary based on a given cost or interference potential. Similar utility independence assertions are made for the other attributes.

While those conditions are necessary for mathematical consistency, other constraints are needed from the DSA context to ensure logical consistency. Specifically, it is necessary that the joint utility function have a non-zero value if and only if all of the individual utilities are non-zero. A spectrum utility value of 0 must be found if either the expected capacity is insufficient, expected interference levels are too high, or expected costs are unacceptable.

A multi-attribute utility function with mutual utility independence as asserted here can be shown to have the form

$$ku(x) + 1 = \prod_{i=1}^{n} [ku_i(x_i) + 1] \tag{A.4}$$

where $u(x)$ is the joint utility function and $u_i(x_i)$ are marginal utility functions for $x_i \in X$ [110, 118]. The marginal utility functions are defined as $u_i(x_i) = u(x_i, x^0_{\neg i})$, which means that $u_i(x_i)$ is evaluated with all attributes $x \in X$ except x_i set to their minimum utility values x^0. According to the desired constraints, the joint utility function must exhibit the characteristic:

$$u_i(x_i^0) \Rightarrow u(x) = 0. \tag{A.5}$$

That is, the joint utility $u(x) = 0$ when any of the individual utilities $u_i(x_i) = 0$. Evaluating (A.5) under the specified conditions of $u(x_i, x^0_{\neg i})$ yields

$$1 = ku_i(x_i) + 1. \tag{A.6}$$

But $u_i(x_i)$ cannot be 0 everywhere, and the multiplicative form of (A.4) is conditioned upon $k \neq 0$. The result in (A.6) indicates the existence of a "null condition" such that the decision-maker is indifferent to the values of the complimentary attributes when one or more of the other attribute values is x_i^0 [118].

To continue the derivation, a reversal can be applied [118] such that $u(x_i^0) = 1, u(x_i^1) = 0$, and $k = -1$. The joint utility function $u(x)$ also takes on the same reversal. Applying the constraint of (A.5) with the reversal now gives

$$u(x_i^0) = 1 \Rightarrow u(x) = 1. \tag{A.7}$$

Applying the constraint as before produces the desired result

$$[1 - u(x_i, x_{\neg i}^0)] = [1 - u(x_i)] \prod_{j \in \neg i} [1 - u_j(x_j^0)] = 0. \tag{A.8}$$

The resulting utility function is now given by the multiplicative form of (A.4) with $k = -1$:

$$1 - ku(x) = \prod_{i=1}^{n} (1 - ku_i(x_i)) \tag{A.9}$$

With $k < 0$ the substitution $u^{'}(x) = -[ku(x) + 1]$ can be applied [118], which gives the final form

$$u^{'}(x) = \prod_{i=1}^{n} u_i^{'}(x_i). \tag{A.10}$$

The preference ordering can also be expressed in the more traditional frame of $u^{'}(x_i^0) = 0, u^{'}(x_i^1) = 1$.

For the decision attributes used here—capacity C, interference I, and monetary cost M—the joint utility function becomes

$$u(C, I, M) = \prod_{i=C,I,M} u_i(x_i) = u_C(c)u_i(I)u_M(m). \tag{A.11}$$

The form of the resulting function matches intuition, which is supported by formal decision and preference theory. The joint utility is 0 if any of the individual attribute utilities is 0. Thus if interference potential is unacceptably high for a given action, the interference and joint utilities will both be 0. The DSA system can then discard the option from consideration. Conversely, if all the individual utilities are maximized, the joint utility is also maximized.

To use the spectrum utility function for decision-making, a DSA system would evaluate the expected utility of each option under consideration and select the the optimum. Given the expected utility definition in (A.15), the expected utility of the spectrum utility function given some candidate decision $do(x)$ (e.g., channel selection and transmit power) then becomes

$$\mathrm{E}\left[U(C,I,M)|do(x)\right] = \int_{C,I,M} u_C(c)u_I(i)u_m(M)\phi\left(C,I,M|do(x)\right) dc\, di\, dm. \tag{A.12}$$

The joint probability $\phi(C,I,M|do(x))$ is derived from the DSA SA model from Figures 3.4 and A.2 as shown in Figure A.3. It can be observed from the FCM that capacity C, interference I, and cost M probabilities are all independent given some transmit power $P_{tx,D}$. This (conditional) independence indicates that the joint probability of the spectrum utility function can then be represented as

$$\phi(C,I,M|P_{tx,D}) = \phi\left(C|P_{tx,D}\right)\phi\left(I|P_{tx,D}\right)\phi\left(M|P_{tx,D}\right). \tag{A.13}$$

The expected value of the spectrum utility function is then the product of the expected values of the individual utility functions [119]

$$\mathrm{E}\big[u(C,I,M)\big] = \mathrm{E}\left[u_C(c)\right]\mathrm{E}\left[u_I(i)\right]\mathrm{E}\left[u_M(m)\right]. \tag{A.14}$$

A.2.2 Characteristics of Utility Functions

Utility functions are subjective characterizations of the decision-maker's preferences and attitudes toward gains and risks. The decision process uses the utility functions in conjunction with their associated probability distributions to determine the expected utility of various options, then selects the optimal option. Expected utility indicates the average level of utility (i.e., worth) that a decision-maker could expect if selecting that particular option, and provides as a means for evaluating, preference ordering, and decision-making

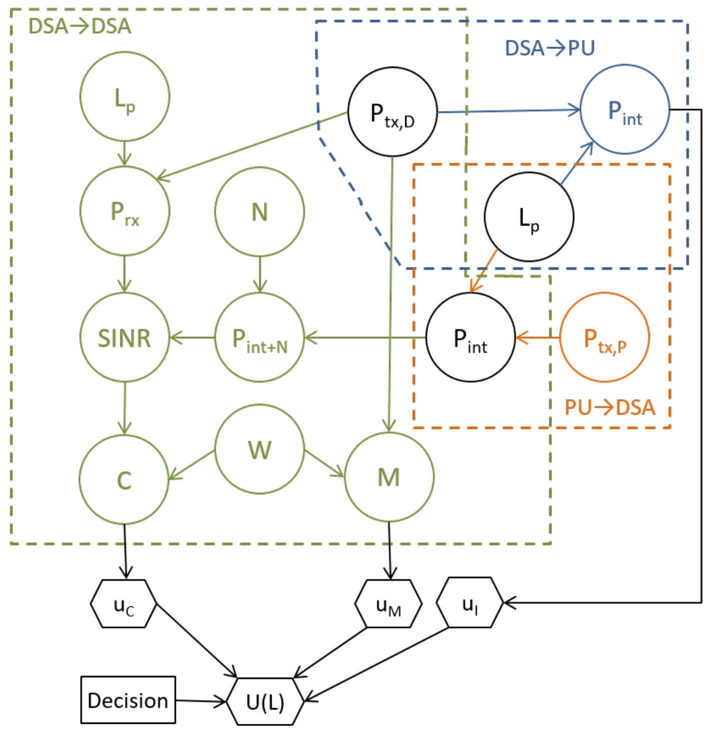

Figure A.3: DSA probabilistic reasoning and decision-making model.

among a set of alternative options when uncertainty exists in the decision process (see e.g., [120]). Given a utility function $U(x)$ that specifies the preference ordering of values of some attribute x having a probability density of $\phi(x)$, the expected utility is given as

$$\mathrm{E}\left[U(x)\right] = \int_x U(x)\phi(x)dx. \tag{A.15}$$

To make decisions among alternative options in a given decision, the DSA system would prefer the option with the best expected utility. That is, given two options L_1 and L_2, the DSA would prefer L_1 only if its expected utility was greater than that of L_2:

$$L_1 \succ L_2 \Leftrightarrow \mathrm{E}\left[\mathrm{U}\left(L_1\right)\right] > \mathrm{E}\left[\mathrm{U}\left(L_2\right)\right]. \tag{A.16}$$

The risk attitudes associated with utility functions reflect the behavior that stems from them. Risk behavior can be characterized using a few basic concepts. The first is that of a *certainty equivalent*, which is the attribute level $\hat{x}$ at which the decision-maker is indifferent between a guarantee of getting $\hat{x}$ or proceeding with a decision under uncertainty with an expected outcome of $\mathrm{E}\left[U(L)\right]$ and the possibility of attaining a value of x that is better or worse than $\hat{x}$ [110]. The certainty equivalent is formally defined as the attribute value $\hat{x}$ such that

$$u(\hat{x}) = \mathrm{E}\left[u(x)\right]. \tag{A.17}$$

The concept of *risk attitude* indicates the relative value that the DSA user applies to the range attribute levels within the context of uncertainty [110]. The function ultimately encodes risk aversion, risk proneness, or risk neutrality.[1] Risk aversion indicates a preference to bypass a decision made under uncertainty in exchange for the guarantee of having the expected attribute level μ_x. The result, however, is that the expected utility of the uncertain

[1] Utility functions can also be piecewise combinations of the three fundamental risk attitudes.

decision is greater than the utility of the expected attribute level, that is

$$u(\hat{x}) = \mathrm{E}\left[u(x)\right] > u(\mu_x) = U\left(\mathrm{E}\left[x\right]\right). \tag{A.18}$$

Thus the risk-averse decision-maker is willing to settle for less than the certainty equivalent $\hat{x}$ to avoid the risks associated with the decision. Conversely, risk proneness indicates a preference for proceeding with the decision under uncertainty rather than a guarantee of having the expected attribute level. It follows that the certainty equivalent for a risk prone function is preferred to the expected attribute level. The three risk attitudes are then defined in terms of the expected outcome utility relative to the certainty equivalent utility:

$$\text{Risk Averse: } u(\hat{x}) < u(\mu_x) \tag{A.19a}$$

$$\text{Risk Prone: } u(\hat{x}) > u(\mu_x) \tag{A.19b}$$

$$\text{Risk Neutral: } u(\hat{x}) = u(\mu_x). \tag{A.19c}$$

For monotonically increasing or decreasing functions,[2] the shape of the utility function indicates a decision-maker's attitudes toward risk [110]. A concave, convex, or linear utility function indicates risk aversion, risk proneness, or risk neutrality—respectively—as shown in Figure A.4.

The concept of a *risk premium* indicates the degree of risk aversion or proneness existing in a decision option [110]. It defines how much of an attribute a decision-maker is willing to give up relative to the average to avoid uncertainty-related risks. It is positive for risk averse utility functions and negative for risk prone utility functions. Risk premium is defined as

[2]The principles here can easily be extended to other functions that are piecewise monotonic.

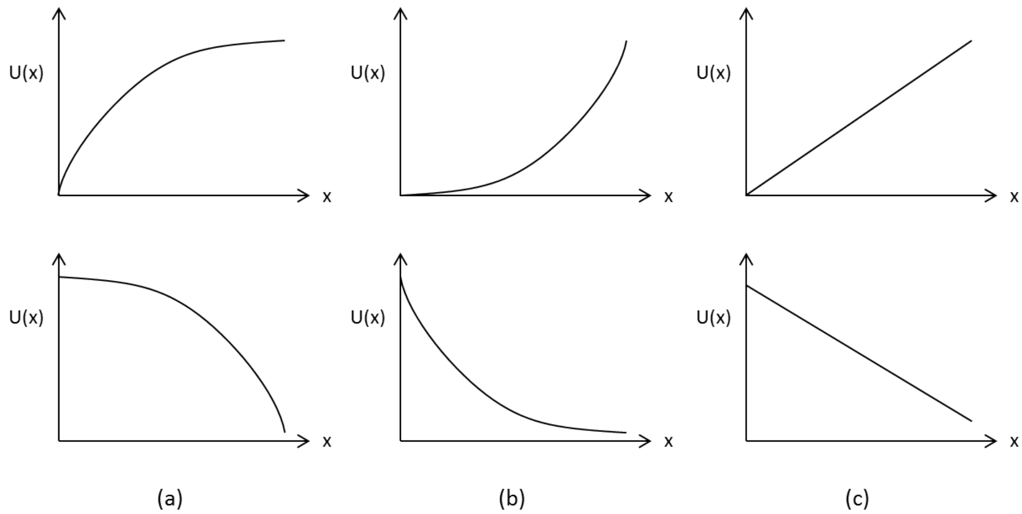

Figure A.4: Examples of monotonically increasing (top) and decreasing (bottom) utility functions exhibiting a) risk aversion, b) risk proneness, c) and risk neutrality.

the difference between the expected attribute value and certainty equivalent

$$RP(x) = \bar{x} - \mu_x \tag{A.20a}$$

$$RP(x) = \hat{x} - \mu_x \tag{A.20b}$$

for monotonically increasing and decreasing utility functions, respectively.

Risk premium can also be expressed in terms of an attribute's variance σ_x^2 for some forms of utility functions. Arrow [121] and Pratt [122] established the relationship between an attribute's variance and the associated risk premium as

$$RP \approx -\frac{\sigma_x^2}{2} \frac{U''(x)}{U'''(x)} \tag{A.21}$$

across some region of x having constant risk attitude and non-distorted probability [123–125]. A utility function has a constant risk attitude if the risk premium is constant across the attribute range. The class of utility functions having the form $a + b \cdot \mathrm{e}^{cx}$ are shown to have a constant risk attitude, with the risk attitude determined by the constant c [110]. For such a utility function, the Arrow-Pratt measure of risk aversion in (A.21) becomes

$$RP \approx -\frac{c\sigma_x^2}{2}. \tag{A.22}$$

A direct assessment of uncertainty on the decision trades can also be made in some cases. Consider again a comparison of two spectrum access options L_1 and L_2. Applying the definition of preference ordering in (A.16) with the certainty equivalent from (A.18) provides

$$L_1 \succ L_2 \Leftrightarrow U\left(\hat{X}_{1,k}\right) > U\left(\hat{X}_{2,k}\right). \tag{A.23}$$

Given the positive affine transformation nature of the utility functions used here [120], the relationship can be mapped from the utility domain to the attribute domain:

$$\text{Increasing U}(X)\text{: } L_1 \succ L_2 \Leftrightarrow \hat{X}_1 > \hat{X}_2 \tag{A.24a}$$

$$\text{Decreasing U}(X)\text{: } L_1 \succ L_2 \Leftrightarrow \hat{X}_1 < \hat{X}_2. \tag{A.24b}$$

The preference ordering conditions of (A.24) can further be defined in terms of the expected value μ_{X_i} and uncertainty $\sigma_{X_i}^2$ by applying the risk premium definition from (A.20) to (A.24) defines the ordering for a monotonically increasing utility function in terms of the expected costs and risk premiums:

$$\text{Increasing U}(X)\text{: } \mu_{X_1} - RP_{X_1} > \mu_{X_2} - RP_{X_2} \tag{A.25a}$$

$$\text{Decreasing U}(X)\text{: } \mu_{X_1} - RP_{X_1} < \mu_{X_2} - RP_{X_2} \tag{A.25b}$$

If the region of interest across X meets the criteria for the Arrow-Pratt measure of risk aversion [123], (A.21) can be applied to (A.25), allowing its expression in terms of μ_X and

σ_X^2:

$$L_1 \succ L_2 \Leftrightarrow$$

$$\text{Increasing U}(X)\text{: } \Delta\mu_X > \frac{\Delta\sigma_X^2}{2}\frac{U''(X)}{U'''(X)} \tag{A.26a}$$

$$\text{Decreasing U}(X)\text{: } \Delta\mu_X < \frac{\Delta\sigma_X^2}{2}\frac{U''(X)}{U'''(X)}. \tag{A.26b}$$

This formulation enables direct assessment of attribute trades as a function of uncertainty, such as that associated with price volatility.

The final concept of a *utility gain* is developed and proposed here and offers a means for quantifying the difference between two multi-attribute utilities specified by a multiplicative utility function. Utility gain specifies the magnitude of utility improvement needed in one subset of attributes to overcome the shortfall existing in others. Indifference between two options L_1 and L_2 exists if their expected utilities are equivalent:

$$L_1 \sim L_2 \Leftrightarrow E\left[U(L_1)\right] = E\left[U(L_2)\right] \tag{A.27}$$

If the utility of some subset of attributes $X_S \subset X$ is known for the two options, has he multiplicative form, and independent probabilities as shown in (A.14), then the gain required in the remaining attributes $X_{\neg S} \subset X$ for choice indifference is specified by the ratios of the expected utilities:

$$\prod_{X_{\neg S}} \frac{\mathrm{E}\left[u(L_1)\right]}{\mathrm{E}\left[u(L_2)\right]} = \prod_{X_S} \frac{\mathrm{E}\left[u(L_2)\right]}{\mathrm{E}\left[u(L_1)\right]} \tag{A.28}$$

Using this relationship, assessments can be made regarding the utility gain of one set of attributes X_S required to compensate for shortfalls in the utility levels of the other attributes $X_{\neg X}$ relative to an alternative options. As will be shown in the following section, (A.28) can also be used to evaluate the impact of uncertainty on utility assessments.

The concepts of risk attitude, certainty equivalent, risk premium, and utility gain presented in this section enable assessments of DSA decision-making and behavior with imperfect awareness. The following section develops a joint utility function, to which the concepts presented here are applied in Sections A.3 and A.4 to demonstrate the relationship between uncertainty and decision-making concepts.

A.3 Theoretical Assessment of DSA Decision-Making

Two comparisons are of particular interest given emerging dynamic spectrum access regulatory and economic concepts as described in Chapter 1 [1,2]. Uncertainties associated with imperfect situational awareness as well as spectrum usage and cost volatility may force spectrum sharing users to make decisions under uncertainty as to the preferred type of spectrum access. Decisions could include choices among the three spectrum sharing modes. Section A.3.1 analyzes spectrum user decision-making between General Authorized Access and fee-based secondary sharing; Section A.3.2 assesses trades between fixed pricing and auction-based pricing models.

A.3.1 Decision Trades between General Authorized Access and Secondary Access

General Authorized Access requires no monetary cost in exchange for spectrum access, but it has no guarantee of spectrum access. Therefore its ability to access sufficient spectrum to attain the desired channel capacity is subject to the volatility of spectrum availability. If volatility is high, then the user may be required to make frequent adjustments to aspects such as frequency selection, bandwidth, and transmit power, which directly affect the overall achievable channel capacity. High volatility may affect both the expected capacity μ_C and uncertainty σ_C^2. Alternatively, the spectrum user may elect to use a Secondary Access option having mechanisms enabling guaranteed capacity C at a specified price M. Given the spectrum utility function (A.11) and preference ordering, a Secondary Access option

L_S is preferable to a General Access option L_G if:

$$L_S \succ L_G \Leftrightarrow \mathrm{E}\left[U(L_S)\right] > \mathrm{E}\left[U(L_G)\right]. \tag{A.29}$$

Using utility gain (A.28), the expected monetary cost utility E[U(M)] can be defined as a function of the other expected utilities as:

$$\mathrm{E}\left[U_M(m_S)\right] > \frac{\mathrm{E}\left[U_C(c_G)\right]\mathrm{E}\left[U_I(i_G)\right]\mathrm{E}\left[U_M(m_G)\right]}{\mathrm{E}\left[U_C(c_S)\right]\mathrm{E}\left[U_I(i_S)\right]} \tag{A.30}$$

Recognizing that no monetary cost is associated with the opportunistic access option, its expected cost utility E[$U_M(m_G)$] $= 1$. Similarly, E[$U_I(i_S)$] $= 1$ because the centralized spectrum access manager is responsible for managing interference [1, 2]. Those insights simplify (A.30) to

$$L_S \succ L_G \Leftrightarrow \mathrm{E}\left[U_M(m_S)\right] > \mathrm{E}\left[U_I(i_G)\right]\frac{\mathrm{E}\left[U_C(c_G)\right]}{\mathrm{E}\left[U_C(c_S)\right]} \tag{A.31}$$

Thus for a secondary sharing service to be preferred over an opportunistic access option, its monetary cost utility E[U(M)] must be greater than the ratio of the remaining opportunistic and secondary sharing expected utilities.

To illustrate the trades on preference ordering, consider uncertainty in the form of Beta probability distributions with mean and variance $\mu_x = 0.5$, σ_x^2 as shown in Figure A.5. Let utility functions be constant risk with decay constant c. Monetary cost M and Interference I utilities are assumed to be monotonically decreasing functions, such as those illustrated in Figure A.6. Figure A.7 shows the expected General Access cost utility as a function of the various utility function decay constants. For a given $\mathrm{E}\left[U_I(i_G)\right]$ and $\mathrm{E}\left[U_C(c_S)\right]$, the expected monetary cost utility E[U(M)] will have similar behavior. The impact of spectrum volatility is shown to increase expected utility in risk prone utility functions (negative decay constant) and decrease it in risk averse utility functions. The magnitude of the impact can

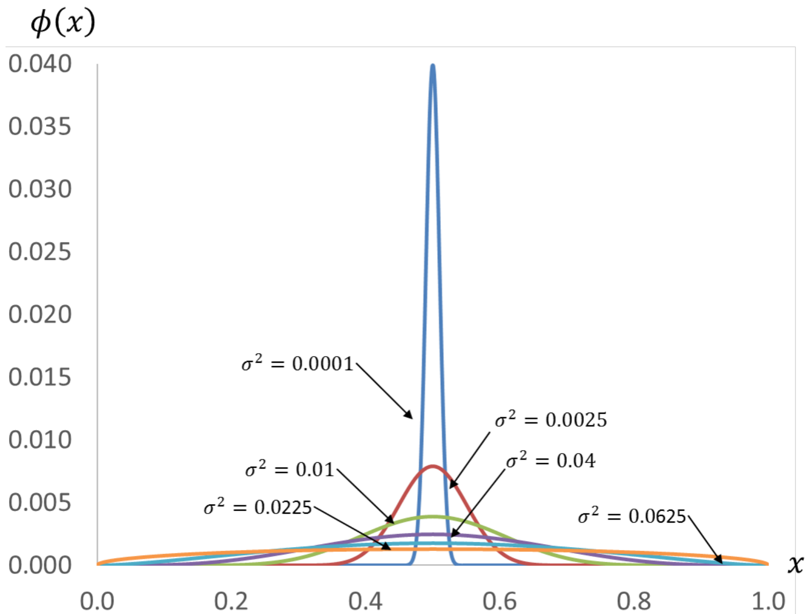

Figure A.5: Beta pdfs for a range of variances.

be characterized by the risk premium of (A.20), which is shown in Figure A.8.

A.3.2 Decision Trades between Fixed and Auction Pricing

A similar assessment can be made for trades between a Secondary Access sharing option using fixed pricing L_F and one using auction-based pricing L_A. Let both options provide identical operating environments, providing equivalent interference risk and associated expected utility. Thus the decision trades depend upon the expected utilities for cost and capacity with the preference ordering of $L_A \succ L_F$ given:

$$\mathrm{E}\left[U_M(m_A)\right]\mathrm{E}\left[U_C(c_A)\right] > \mathrm{E}\left[U_M(m_F)\right]\mathrm{E}\left[U_C(c_F)\right] \tag{A.32}$$

Thus spectrum user preferences for auction price is only preferable to a fixed price option if

$$L_A \succ L_F \Leftrightarrow \frac{\mathrm{E}\left[U_M(m_A)\right]}{\mathrm{E}\left[U_M(m_F)\right]} > \frac{\mathrm{E}\left[U_C(c_F)\right]}{\mathrm{E}\left[U_C(c_A)\right]} \tag{A.33}$$

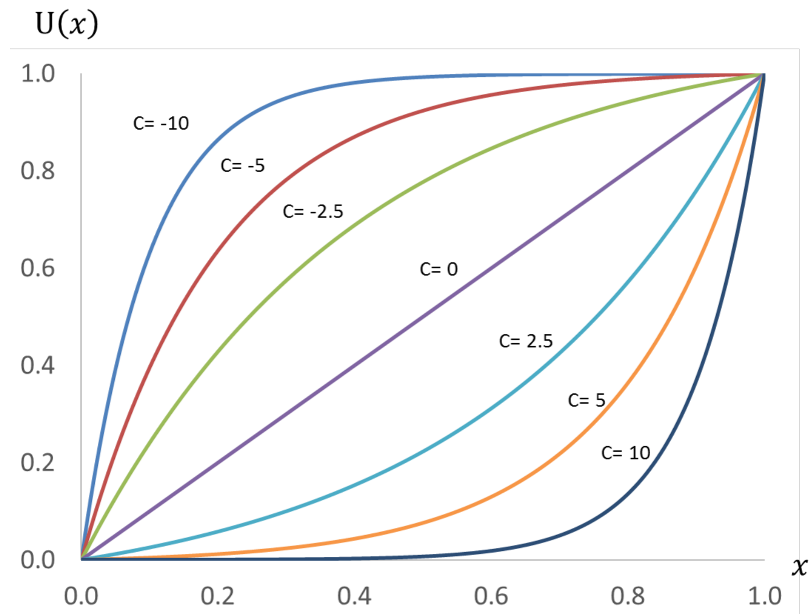

Figure A.6: Constant risk, monotonically increasing utility functions.

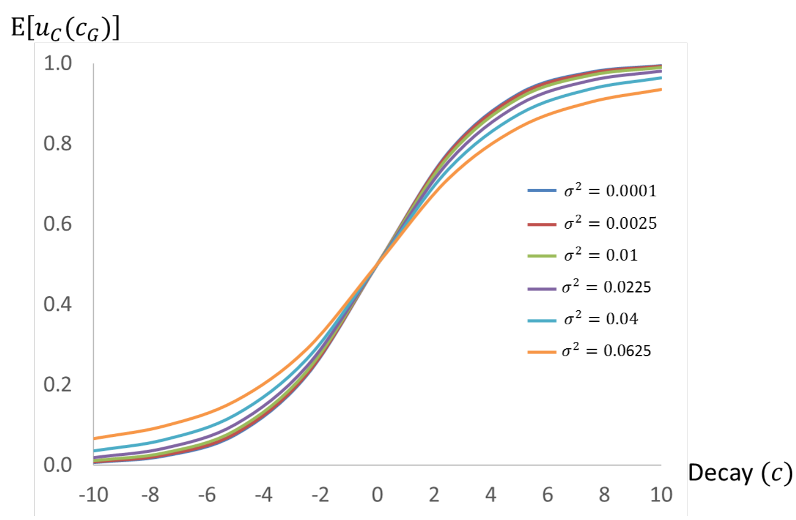

Figure A.7: Expected capacity utility for General Access as a function of utility function decay c and spectrum access volatility σ^2.

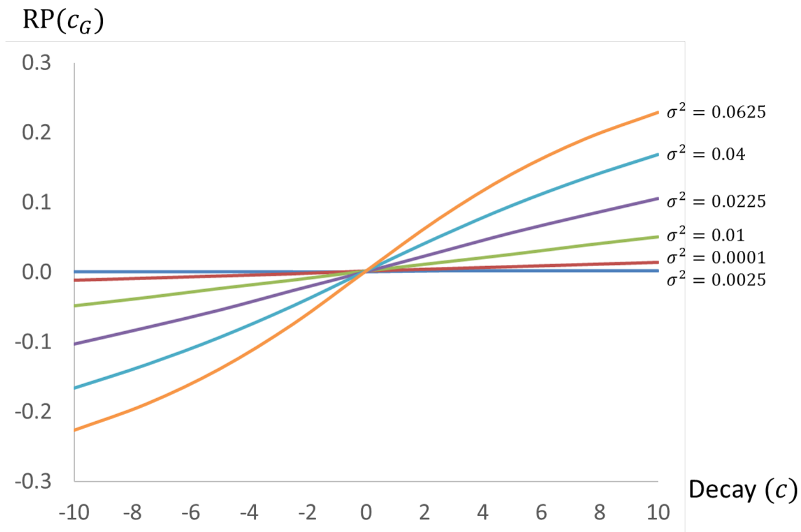

Figure A.8: Risk premium for General Access as a function of utility function decay c and spectrum access volatility σ^2.

This finding is significant, as it states that there is a distinct disadvantage of the auction option. If the spectrum user is risk averse, the uncertainty of the auction price drives down the expected cost utility $\mathrm{E}\left[U_M(m_A)\right]$. This can be seen by considering the case of equivalent capacity utilities and applying (A.26) to the cost utilities:

$$L_A \succ L_F \Leftrightarrow \mu_{M_A} + \frac{c_M \sigma^2_{M_A}}{2} < \mu_{M_F}. \tag{A.34}$$

Thus it can be shown that the auction pricing option will only be selected by Secondary Access users under one of the following conditions:

1. If the capacity utilities of the two options are equal, the expected cost of the auction price μ_{M_A} must be lower than that of the fixed price option by more than the risk premium $\frac{c_M \sigma^2_{M_A}}{2}$. Applying (A.26) provides the difference in terms of the variance:

$$\Delta\mu_M > \frac{\sigma^2_{M_A}}{2} c_M. \tag{A.35}$$

2. If the cost utilities of the two options are equal, the expected capacity utility of the auction option must be greater than that of the fixed price option.

3. If capacities and expected costs are different between the two options, the auction must have some combination of lower expected cost *and* increased expected capacity to overcome the penalty paid for cost uncertainty.

The following section presents a simulation of the spectrum sharing decision model. It illustrates a decision among four different spectrum access options and discusses the results in the context of the theoretical findings presented in this section.

A.4 Decision-Making Simulation, Analysis, and Insights

Consider a DSA system that seeks to make a choice among four different spectrum access alternatives. Each alternative has some unique characteristic that is representative of the three spectrum access methods discussed previously. While the cases presented here are notional, they highlight the general insights regarding decision trades among alternative spectrum access models that were developed in the previous section.

The DSA system considered here will have two basic components; namely the awareness model and decision model. The awareness model uses the FCM shown in Figure A.3, which enables the DSA system to assess expected performance and spectrum policy compliance given uncertain and imprecise information regarding the operating environment and characteristics of other spectrum users as illustrated in Chapter 4. The model captures the mutual influences between the DSA and protected users (PUs) as well as the probabilities associated with the three decision attributes: Capacity C, monetary cost M, and interference I to PUs.

The three attributes map to marginal utility functions $u_i(x_i)$, which are represented as hexagonal nodes and inform the decision. Capacity will be characterized by the aggregate capacity over time, which indicates the expected amount of data in megabytes (Mb) that is transferred over a specified period of time. Interference will be measured in terms of the

Table A.1: Utility function parameters for the example.

Attribute x_i	Parameter Values		
	$x(0)$	$x(1)$	c
C (Mb)	0	70 Mb	-3
I (dBm)	$P_{int} - 3$ dB	P_{int}	5
M ($)	0	1	5

DSA power received at the PU. Monetary cost indicates any payment required for accessing spectrum (e.g., spectrum leasing) and will be measured as a function of transmitted power P_{tx}, bandwidth W, and time in terms of cost per dBm-MHz-sec. Thus using a given amount of spectrum for a period of time results in a specific total cost.

Each marginal utility function selected for the study uses a constant risk attitude. The minimum and maximum utility values used for the example are given in Table A.1. Capacity is given a utility of 0 if no data can be sent; the maximum utility is assigned to the ability to send the desired amount of data within the prediction window. For interference utility, a utility of 0 is given to any DSA power received at the PU that is greater than the risk-constrained interference power threshold P_{int} specified by the policy. The maximal utility is mapped to a received power P_{rx} that has a 3 dB margin below the threshold P_{int}; the margin influences the DSA to provide additional interference mitigation beyond the policy specification. Resource usage utility is given a utility value of 1 for no energy expended and 0 for completely expending the remaining energy of the battery. Similarly, monetary cost has the highest utility value at $M = 0$ and lowest utility value at $M = M_{max}$. The cost scale is normalized, giving $M_{max} = 1$. The decay constants c used for the marginal utility functions are also provided in Table A.1. The functions indicate risk aversion for each attribute, which influence the DSA behavior to make conservative decisions in seeking greater capacity while avoiding interference and cost risks.

The decision process evaluates the expected utility $\mathrm{E}[U(L)]$ of each option. The marginal utility functions are combined with the probability measures derived from Figure A.3 using context-specific uncertainties described below. It can be shown that the probability distributions for each decision attribute are mutually independent given the DSA transmit power P_{tx} (P_{tx} d-separates the attributes). The expected value of the spectrum utility function is therefore given by (A.12). This methodology is applied to the utility valuations made using the scenario-specific values.

The four spectrum access options in this example include two General Authorized Access and two Secondary Access alternatives. For General Access, the DSA system can choose from geographic sharing and geo-temporal sharing options. For geographic sharing, the DSA system would transmit at a maximum power P_{tx} such that all PU networks would be beyond the interference range of its signal. For geo-temporal sharing, the DSA system would employ temporal sharing with other nearby PUs, transmitting only when the channel is available. In geographic sharing, the DSA may need to transmit at a lower power and operate at a low channel capacity, but has a lower risk of interruption due to the presence of other spectrum users. For geo-temporal sharing, the DSA may need to pause transmissions while other spectrum users are transmitting, but it can potentially transmit at a higher power to provide higher instantaneous capacity.

The DSA system can also access spectrum by Secondary Access, in which it leases spectrum from a spectrum provider. One option provides for fixed pricing while the other uses auction-based pricing, both of which include transmit power limits, bandwidth, duration, and quality (e.g., limits on interference from other users). With the exception of cost for the auction-based pricing option, the terms of the agreements are assumed to be known at the time of the decision assessment.

For this example, the DSA system uses a 10 sec prediction window for evaluating each of four possible spectrum access options. The parameters differentiating the four spectrum access options are given in Table A.2. A frequency $f = 1$ GHz and bandwidth $B = 2$ MHz are used for all options. The basis of the geo-temporal sharing option is identical to the geographic sharing case, but the DSA system seeks to transmit only during periods in which the nearest PU is not accessing the channel. The secondary sharing options use

Table A.2: Scenario parameters for the four spectrum access options.

Param.	General Access		Secondary Access	
	Geographic	Geo-temporal	Fixed Price	Auction
$P_{tx,pu}$	Beta(1.167,1.167)		N/A	
d	Unif(0,10) km			
α	Beta(1.08,4.32)			
T_{sen}	10%			
P_{rx}	N(-80,1) dbm	N(-102,1) dBm		
T_{win}	T_{pred}	Beta(8.625,2.875)	T_{pred}	T_{pred}
C	0		$\frac{1}{B}$	N(1,0.1)

the same inference structure as the opportunistic strategies, but specify the probability of P_{int} as 0 to reflect that the DSA system would pay for (temporary) access with specified guarantees. The fixed price option is therefore determined by the DSA-DSA portion of the FCM from Figure A.3. The auction pricing option, however, must also make a probability assessment of the spectrum price, which is characterized using the monetary cost node M. The total cost of each secondary sharing option will therefore depend upon the transmit power, bandwidth, and access duration. A transmit power P_{tx} of 27 dBm is derived such that 70 Mb can be transmitted within the 10 sec prediction window.

The expected utilities calculated for each option are shown in Table A.3, and the corresponding expected values are shown in Table A.4. Based on the overall expected utility $\mathrm{E}[U(L)]$, the DSA system would prefer the Geo-temporal sharing option, with an expected utility of 0.981. The DSA predicts that it can transmit a maximum power of 37 dBm at greater than 99% confidence of no harmful interference for an expected duration of almost 8 sec. The expected capacity of 72.5 Mb would exceed the desired capacity of 70 Mb. By comparison, the Geographic option is predicted to allow a transmit power near 20 dBm for the entire 10 sec prediction window, sending about 39.5 Mb.

Note that the expected capacity utility $\mathrm{E}[u_C] < 1$ for the Geo-temporal option despite the expectation of exceeding the desired aggregate capacity. The reduced expected utility results from the presence of capacity uncertainty, which produces a risk premium. The

Table A.3: Expected utilities for the four spectrum access options

Expected Utility	General Access		Secondary Access	
	Geographic	Geo-temporal	Fixed Price	Auction
E[$u_C(L)$]	0.857	0.987	1.000	1.000
E[$u_I(L)$]	0.984	0.994	1.000	1.000
E[$u_M(L)$]	1.000	1.000	0.847	0.839
E[$U(L)$]	0.843	0.981	0.847	0.839

Table A.4: Expected values for the four spectrum access options

Expected Value	Opportunistic Access		Secondary Sharing	
	Geographic	Geo-temporal	Fixed Price	Auction
E[C]	39.5 Mb	72.5 Mb	72.5 Mb	72.5 Mb
E[I]	-96.8 dBm	-97.5 dBm	N/A	N/A
E[M]	0	0	0.6	0.6

capacity uncertainty of $\sigma_C^2 = 4.43$ Mb^2 is calculated from the FCM, producing a risk premium of $RP_C \approx 7.35$ Mb per (A.22). The approximation matches well with $RP_C = 7.75$ Mb calculated using (A.20).

The two Secondary Access options also exhibit the effects of uncertainty on utility valuation and preference ordering. As shown in Table A.4, the two options are predicted to produce the same expected outcomes (values) for all attributes. The Fixed Price option, however, has a greater expected utility, which can easily be traced to the cost uncertainty incurred by the Auction Pricing option. While the auction is shown to have the same expected cost as the Fixed Price option, the DSA system incurs cost risk if choosing to enter the auction. The model produces an auction price uncertainty of $\sigma_C^2 = 0.001$, which by (A.26) requires an expected auction price $\mu_M < 0.598$ for the auction to be preferred over the fixed-pricing option.

The utility gain analysis of (A.31) can be applied to determine preference conditions for the Secondary Access options over the geo-temporal option. With the expected utility values from Table A.3, the cost utility of a Secondary Access option must be E[U(M_S)] > 0.98, which is a significant increase over the cost utilities of 0.847 and 0.839 shown in Table A.3.

The application of the theoretical formulations from Sections A.2 and A.3 presented here illustrate the trades that must be considered in evaluating spectrum sharing architectures. It can be seen that user preferences and situational uncertainty can have significant effects on the decisions behaviors of spectrum users.

A.5 DSA Decision-Making Summary

Dynamic Spectrum Sharing architectures under development will implement various forms of spectrum sharing. The spectrum sharing models have significant implications on business models for those that administer the sharing process as well as those that use it. The work presented here identifies the fundamental elements for assessing dynamic spectrum user behaviors and identifies decision trades that impact their use and viable business models for secondary spectrum providers.

A spectrum utility model using multi-attribute utility theory forms the users' decision model. The model allows a user to make trades among preferences for key attributes such as channel capacity, monetary cost, and interference potential. The model is used here to demonstrate the impact of spectrum usage volatility on preferences between free spectrum access without access guarantees and fee-based spectrum access with access guarantees. Analysis also characterizes decision trades between fee-based and auction-based spectrum pricing. Analysis indicates that auction-based pricing incurs a distinct disadvantage relative to fee-based pricing due to the inherent uncertainty and pricing volatility.

Appendix B: Application of Function Causal Modeling for a Communications Satellite Link

Satellite communication (SATCOM) systems and networks require reliable management decisions for efficient and effective use of SATCOM resources. SATCOM systems that support dynamic user demands such as disaster relief require frequent and sometimes rapid reconfigurations. Disaster relief SATCOM demands are particularly difficult to manage due to high geographic concentrations of users, often correlated resource demands, and need to adapt to evolving situations and plans. Furthermore, emerging end-user technology and applications such as imagery and high-rate video dissemination place significant demands on payload resources. The high demand on a SATCOM payload increases resource allocation challenges and amplifies the impacts of service shortfalls from unforeseen changes in user demand or service capabilities due to issues such as weather.

Recent and ongoing research efforts are investigating autonomous adaptation capabilities for SATCOM to enhance man-in-the-loop payload management processes. Some efforts explore the potential for intelligent/cognitive SATCOM payloads (specifically packet-switching payloads) to self-manage higher layer functions such as dynamic bandwidth allocation, dynamic channel selection, and quality of service (QoS) provisioning [126, 127]. Other efforts seek to increase the effectiveness and responsiveness of centralized payload control centers (see e.g [128]), particularly for older SATCOM systems with limited on-board processing capability. Dynamic SATCOM resource management studies have also been extended to include anti-jamming capabilities [129]. In either case, the expectation is that autonomous adaptation will react faster than a human-in-the-loop system and decrease service degradations. Autonomous resource management capabilities, however, would need to be highly trusted by SATCOM operators and users before implementation.

Policy-based approaches can provide high degrees of trust and have been proposed for dynamic SATCOM resource management [126, 127], which can provide a provable decision-making capability similar to those developed for dynamic spectrum management systems

[32–34]. While the policy-based reasoning process is shown to be trustable in a computational sense, trusting these types of systems in an operational setting is hindered by the imperfect and often incomplete information that is available for decision-making.

Decision quality—whether by human operators or an autonomous algorithm—is affected by the aggregate degree of SA information uncertainty. Increased uncertainty leads to increased risks associated with decisions. While policy-based management capabilities provide a framework for establishing trusted decision-making, they do not readily address the characterization of SA uncertainty. This capability requires a probabilistic SA model to be integrated with the policy-based reasoning system.

The probabilistic SA approach proposed in Chapter 3 can be extended to SATCOM resource management. The FCM method enables the quantitative representation of SA uncertainties and probabilistic reasoning for prediction, planning, and diagnosis of SATCOM payload performance. Furthermore, it provides the ability to conduct risk-based decision-making within a policy-based resource management scheme [126, 127] and assess the impact of SA uncertainties on SATCOM resource management risks.

This appendix explores the FCM approach in the context of SATCOM resource management and planning. Sec. B.1 provides the theoretical relationships that define a SATCOM FCM along with an example. Sec. B.2 applies the model to SATCOM resource management; specifically the relationship between uncertainty, risk, and SATCOM resource allocation.

B.1 A SATCOM Probabilistic SA and Reasoning Model

Models used for communication systems including SATCOM payloads are founded on probabilistic concepts [7, 130–132]. Phenomena affecting communications link characteristics—attenuation, polarization loss, scintillation, etc.—and information capacity are based upon stochastic concepts and are generally expressed in probabilistic terms. SATCOM resource management decision processes must therefore account for the stochastic characterizations affecting system performance in order to appropriately implement strategies and behaviors.

Within the context of a SATCOM situational awareness capability, the received power FCM encodes information collected by the SATCOM monitoring system to infer the unobserved variables. The observation variables will depend upon the awareness acquisition capabilities of the system. Not all variables can be established directly from observations or other data, and those that can be observed will generally have some associated degree of uncertainty. Multiple factors such as weather, depolarization, and air moisture content affect the total path loss Lp of the link. The overall uncertainty is the aggregate of the uncertainties associated with each factor.

Figure B.1 is an FCM representation of a SATCOM link, which can be built from the MFrags shown in FiguresB.2 - B.5. The MFrags can be assembled to create FCMs of individual, regenerated, or transponded SATCOM links. Furthermore, they can be extended to build models containing multiple links and multiple satellites. Figure B.2 shows the MFrags associated with the transmitter characteristics in the model. Transmitter system loss L_{sys} for the example model is the aggregate of feed radome losses, L_{feed} and L_{rad}, respectively. Pointing errors are captured in the pointing offset loss MFrag and is a function of the pointing offset ω and aperture half-power beamwidth θ_{3dB}. In general, knowledge of θ_{3dB} will have high accuracy due to testing, but uncertainty regarding ω may have some notable effects, particularly in highly-mobile ground terminals. Finally, the equivalent isotropic radiated power (EIRP) is the combination of the transmitter power P_{tx}, aperture gain G_{tx}, and system loss L_{sys}.

Similarly, MFrags that characterize phenomenology affecting the transmitted signal power along the path from the transmitter aperture to the receiver aperture are shown in Figure B.3. These capture the signal strength losses due to atmospheric attenuation L_{atm}, ionospheric effects L_{ion}, and free-space loss L_{fs}. Those affects are each represented in separate MFrags, which are aggregated in the Path Loss MFrag to calculate the total path loss L_{path}. The total link loss L_{link} is calculated in the Link Loss MFrag, which combines the path loss L_{path} with the signal losses due to transmitter and receiver pointing errors Lpt. The signal power at the receiver aperture is then the $EIRP$ less the link loss L_{link}.

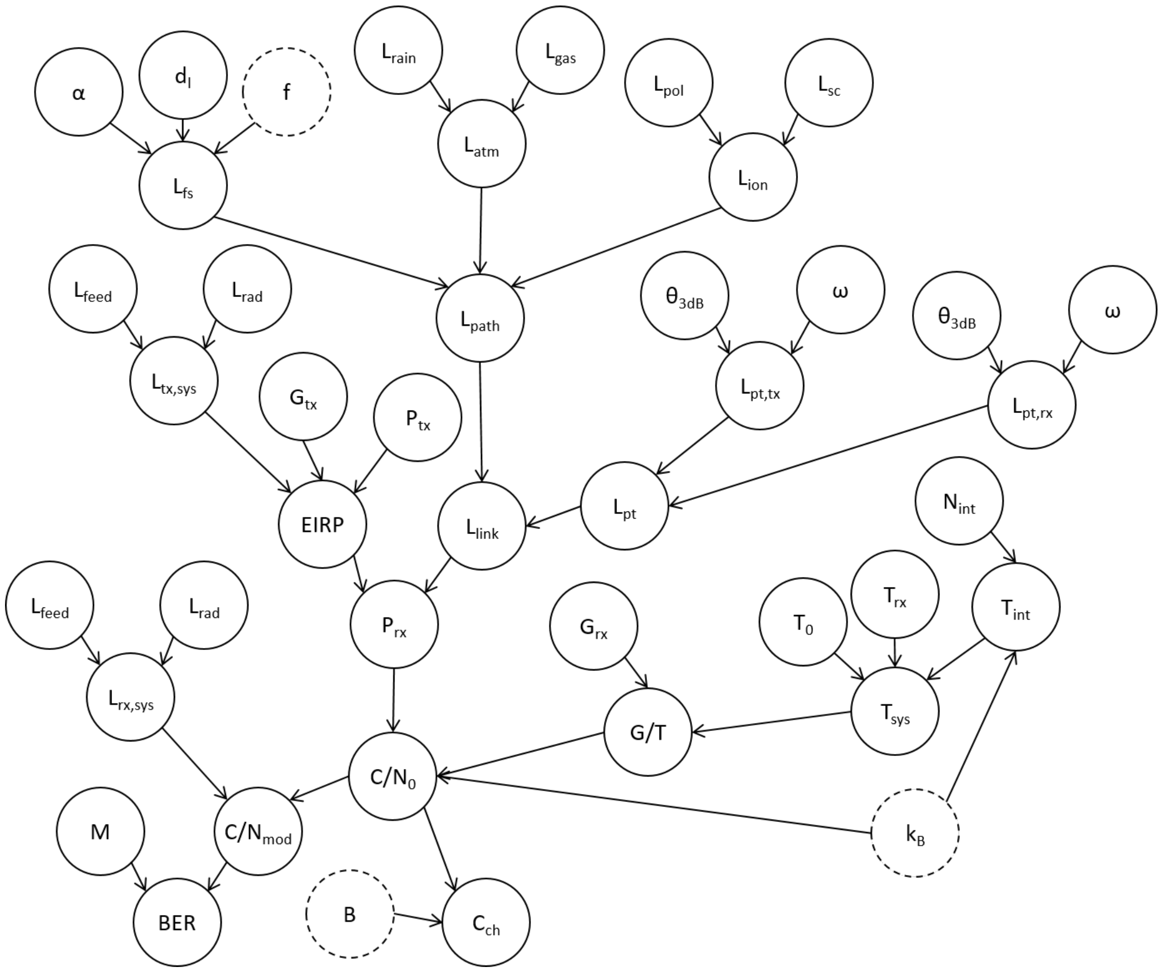

Figure B.1: SATCOM SA FCMs

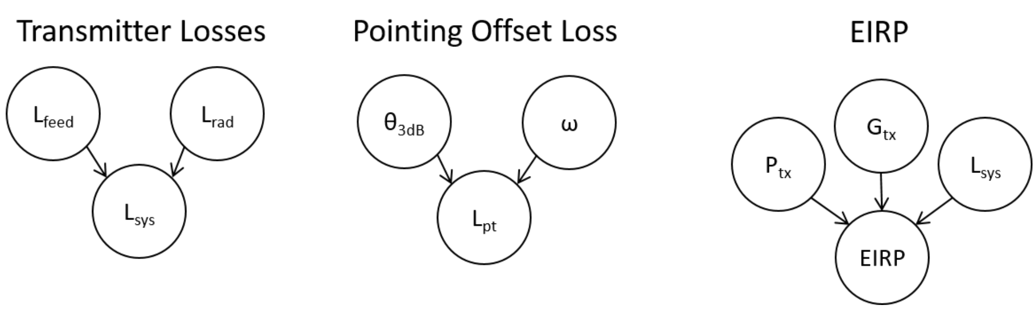

Figure B.2: SATCOM Transmitter FCMs

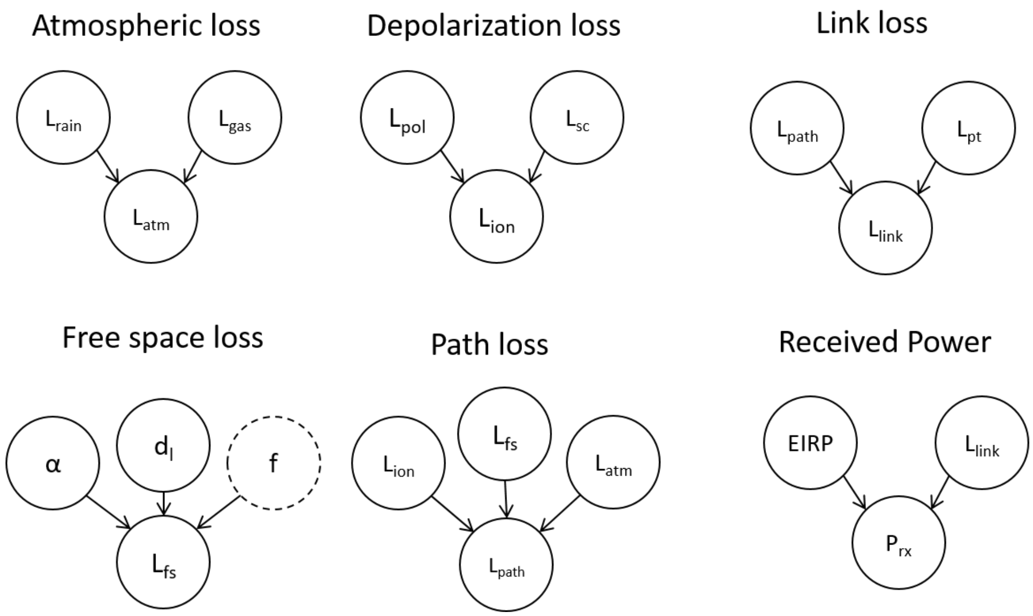

Figure B.3: SATCOM Link FCMs

Receiver MFrags are shown in Figure B.4, which include parameters needed to translate the received signal and noise at the aperture into the carrier to noise power spectral density ratio (C/N_0) sent to the modem. Potential interference (e.g., intermodulation, cosite, and jamming) is characterized here in terms of equivalent interference noise temperature T_{int}, which is given in degrees Kelvin by the following relationship

$$T_{int} = \frac{1}{k_B} 10^{0.1N_{int}} \tag{B.1}$$

where N_{int} is the interference noise in dBW and k_b is Boltzmanns constant in W/Hz-K. The Total System Noise Temperature MFrag combines the interference noise temperature, receiver component noise temperature T_{rx}, and environmental noise temperature N_0 to determine the total system noise temperature T_{sys}. The receiver gain-to-noise temperature ratio MFrag calculates the G/T figure of merit, which is then used to determine the C/N_0 in the Carrier-to-Noise PSD MFrag. For links that are transponded, the $C/N_{0,tot}$ can be

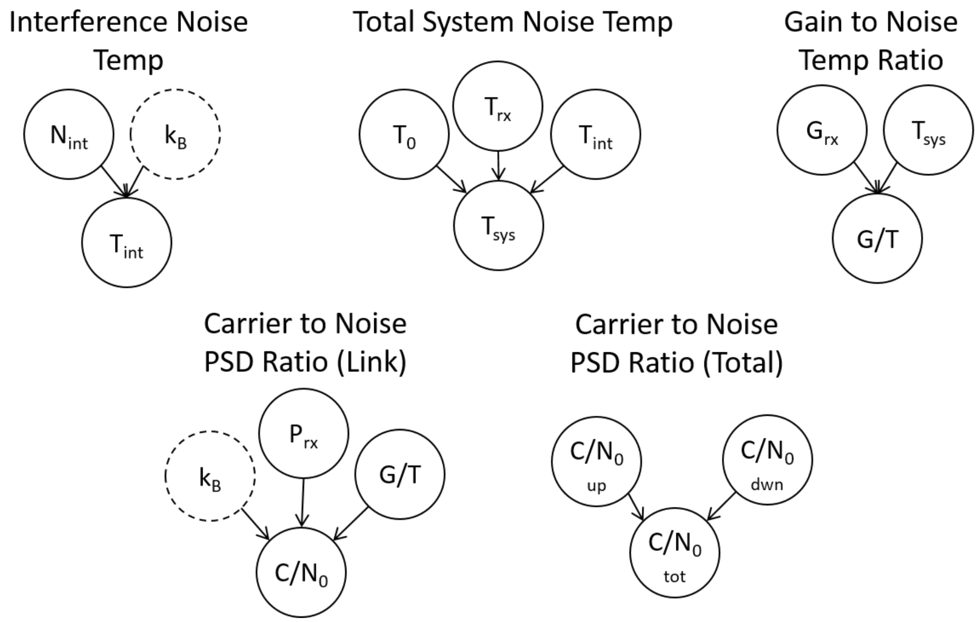

Figure B.4: SATCOM receiver FCMs

calculated in an MFrag as the combination of uplink and downlink C/N_0 as shown in Figure B.4.

MFrags that represent performance metrics of Bit Error Rate (BER) and channel capacity C are shown in Figure B.5. The C/N_0 at the demodulator (C/N_{mod}) incorporates the system losses such as line losses and modem component losses. This value is then used to determine the BER probability distribution, which is also a function of the modulation M. Other MFrags can be developed to calculate additional metrics and figures of merit such as link margin and data throughput, but are not necessary here to demonstrate the concept.

The MFrags from Figures B.2–B.5 are now used to build the single SATCOM link FCM shown in Figure B.1. In this example, most MFrags are instantiated once. The system loss L_{sys} and pointing loss L_{pt}, however, are instantiated twice; once each for the transmitter and receiver. Boltzmanns constant, which was used in the Interference Noise Temperature and Carrier-to-Noise PSD MFrags, is instantiated once but connected to both the C/N_0 and T_{int} nodes. The FCM represented in Figure B.1 can now be used to represent situational

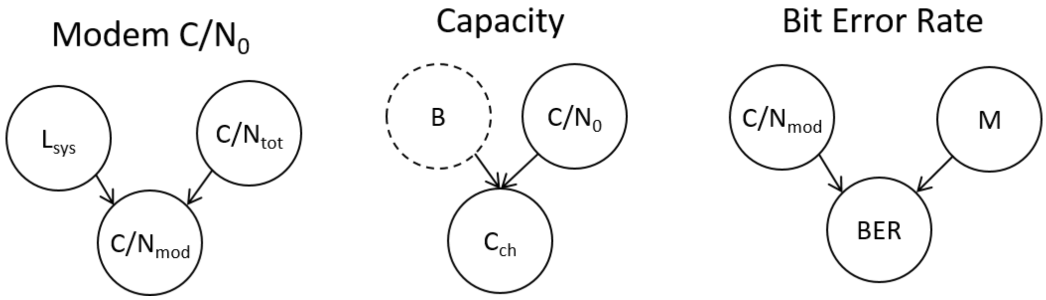

Figure B.5: SATCOM Metric FCMs

awareness of the specified link, evaluate system performance, perform planning, and conduct diagnostic queries in support of a SATCOM resource management capability.

The following sections provide the theoretical formulations associated with the FCM as well as a simulation example.

B.1.1 Theoretical Relationships

The FCM captures the high-level elements associated with a typical link budget [130, 132], including transmitter and receiver losses due to system imperfections as well as path losses due to atmospheric attenuative effects. To begin consider the Equivalent Isotropic Radiated Power (EIRP) in Figure B.2, which is defined functionally here as:

$$EIRP = P_{tx} + G_{tx} - L_{tx,sys}, \tag{B.2}$$

where P_{tx}, G_{tx}, and $L_{tx,sys}$ are the transmitter power, gain, and system losses, respectively. The system losses are further defined by the feed and radome losses:

$$L_{tx,sys} = L_{feed} + L_{rad}. \tag{B.3}$$

The values of those parameters may contain some degree of variation due to physical phenomenology or may only be known/predictable with some degree of uncertainty. The FCM

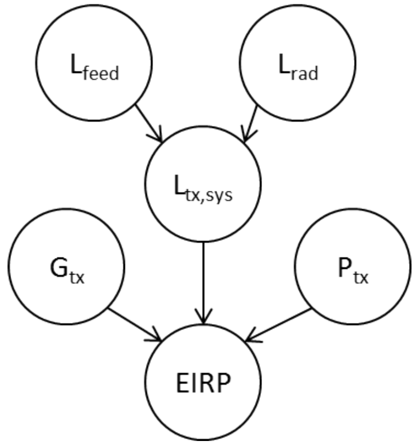

Figure B.6: SATCOM EIRP Functional Causal Model

as represented in Figure B.6 and its associated functional components capture that uncertainty by expressing the probability distribution associated with each parameter. Thus the transmitter system loss probability distribution associated with (B.3) is given by:

$$\phi\left(L_{tx,sys}\right) = \phi\left(L_{tx,sys}|L_{feed}, L_{rad}\right)\phi\left(L_{feed}\right)\phi\left(L_{rad}\right). \tag{B.4}$$

Subsequently, the EIRP probability distribution is then:

$$\phi\left(EIRP\right) = \phi\left(EIRP|L_{tx,sys}, P_{tx}, G_{tx}\right)\phi\left(L_{tx,sys}|L_{feed}, L_{rad}\right) \tag{B.5}$$

$$\phi\left(L_{feed}\right)\phi\left(L_{rad}\right)\phi\left(P_{tx}\right)\phi\left(G_{tx}\right). \tag{B.6}$$

The means and variances associated with the probability distributions can be used to directly assess the expected uncertainty relationships among the various parameters. The transmitter system loss mean μ and variance σ^2 are given simply as:

$$\mu_{L_{tx,sys}} = \mu_{L_{feed}} + \mu_{L_{feed}} \tag{B.7a}$$

$$\sigma^2_{L_{tx,sys}} = \sigma^2_{L_{feed}} + \sigma^2_{L_{feed}}. \tag{B.7b}$$

Similarly, EIRP mean and variance are given as:

$$\begin{aligned}\mu_{EIRP} &= \mu_{P_{tx}} + \mu_{G_{tx}} - \mu_{L_{tx,sys}} \\ &= \mu_{P_{tx}} + \mu_{G_{tx}} - \left(\mu_{L_{feed}} + \mu_{L_{feed}}\right) \end{aligned} \tag{B.8a}$$

$$\begin{aligned}\sigma^2_{EIRP} &= \sigma^2_{P_{tx}} + \sigma^2_{G_{tx}} + \sigma^2_{L_{tx,sys}} \\ &= \sigma^2_{P_{tx}} + \sigma^2_{G_{tx}} + \sigma^2_{L_{feed}} + \sigma^2_{L_{feed}} \end{aligned} \tag{B.8b}$$

The same principles and concepts can be applied to the entire SATCOM link model. In this model, it can be shown that the carrier-to-noise ratio C/N may be used as a proxy for assessing link performance. That is, capacity C and bit error rate (BER) are functions of C/N. C/N is found as a function of the received power P_{rx} and gain-to-temperature ratio G/T:

$$\frac{C}{N} = P_{rx} - 10\log_{10}\left(k_B\right) + \frac{G}{T}. \tag{B.9}$$

Noting that the Boltzmann's constant k_B has no associated variance, the mean and variance are found as:

$$\mu_{C/N} = \mu_{P_{rx}} - 10\log_{10}\left(k_B\right) + \mu_{G/T} \tag{B.10a}$$

$$\sigma^2_{C/N} = \sigma^2_{P_{rx}} + \sigma^2_{G/T} \tag{B.10b}$$

The received power P_{rx} mean and variance is subsequently given as

$$\mu_{P_{rx}} = \mu_{EIRP} - \mu_{L_{link}} \tag{B.11a}$$

$$\sigma^2_{P_{rx}} = \sigma^2_{EIRP} + \sigma^2_{L_{link}} \tag{B.11b}$$

where $EIRP$ is defined in (B.2-B.8), and L_{link} represents the total losses associated with

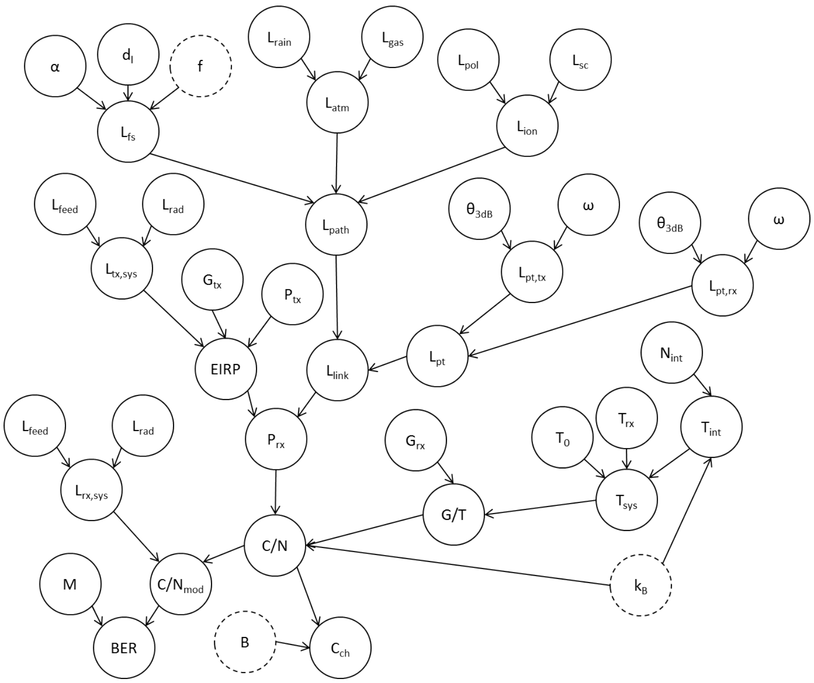

Figure B.7: SATCOM Downlink Functional Causal Model

the SATCOM link.

The mean and variance relationships among the various parameters associated with L_{link} are largely linear, with the exception of free space loss L_{fs} and pointing losses $L_{pt,tx}$ and $L_{pt,rx}$, which contain non-linear functions. While the probability distribution and associated mean and variance can easily be found numerically within the FCM for a particular situation, a closed form functional representation requires an approximation. Using a Taylor Series[1] approximation as defined in (3.24) the free space loss mean and variance are then given as:

$$\mu_{L_{fs}} \approx 20 \log_{10}\left(\frac{c}{4\pi f \mu_{d_l}}\right) \tag{B.12a}$$

$$\sigma^2_{L_{fs}} \approx \left(\frac{20}{\ln(10)\mu_{d_l}}\right)\sigma^2_{d_l}. \tag{B.12b}$$

[1]Note that applying the Taylor Series to non-linear functions assumes that conditions meet convergence criteria [61, 62].

Pointing losses $L_{pt,tx}$ and $L_{pt,rx}$ are similarly approximated using a Taylor Series estimate. Pointing loss in Figure B.7 is the sum of the losses due to off-axis pointing ω of the transmit and receive antennas and imperfections regarding the 3dB contour θ_{3dB}. Each of the pointing losses is given by [130]

$$L_{pt,k} = 12.5 \log_{10} \left(\frac{1 - \cos(0.25\theta_{3dB})}{1 + 0.64\,(1 - \cos(\omega))} \right). \tag{B.13}$$

To account for uncertainties, let (B.13) be given as

$$L_{pt,k} = 12.5 \log_{10} \left(\frac{g_1(\theta_{3dB})}{g_2(\omega)} \right) \tag{B.14}$$

where

$$g_1(\theta_{3dB}) = 1 - \cos(0.25\theta_{3dB}) \tag{B.15a}$$

$$g_2(\omega) = 1 + 0.64\,(1 - \cos(\omega))\,. \tag{B.15b}$$

Applying the Taylor Series approximation (3.24) to (B.15) gives

$$\mu_{g_1} \approx 1 - \cos(0.25\mu_{\theta_{3dB}}) \tag{B.16a}$$

$$\sigma_{g_1}^2 \approx \left(0.25 \sin(0.25\mu_{\theta_{3dB}})\right)^2 \sigma_{\theta_{3dB}}^2 \tag{B.16b}$$

and

$$\mu_{g_2} \approx 1 + 0.64\,(1 - \cos(\mu_\omega)) \tag{B.17a}$$

$$\sigma_{g_2}^2 \approx \left(0.64 \sin(\mu_\omega)\right)^2 \sigma_\omega^2. \tag{B.17b}$$

Substituting back into (B.14) gives the final result

$$\mu_{L_{pt},k} \approx 12.5\log_{10}\left(\frac{1-\cos(0.25\mu_{\theta_{3dB}})}{1+0.64\left(1-\cos(\mu_\omega)\right)}\right) \tag{B.18a}$$

$$\sigma^2_{L_{pt},k} \approx \left(\frac{12.5}{\ln(10)}\right)^2\left[\left(\frac{0.64\sin(\mu_\omega)}{1+0.64\left(1-\cos(\mu_\omega)\right)}\right)^2\sigma^2_\omega\right.$$

$$\left.+\left(\frac{0.25\sin(0.25\mu_{\theta_{3dB}})}{1-\cos(0.25\mu_{\theta_{3dB}})}\right)^2\sigma^2_{\theta_{3dB}}.\right. \tag{B.18b}$$

The receiver gain-to-temperature ratio G/T includes environmental, system, and interference noise sources and similarly requires approximation for a closed form expression of the mean and variance. Given in dB K^{-1} as

$$\frac{G}{T} = G_{rx} - 10\log_{10}\left(T_{sys}\right), \tag{B.19}$$

the mean and variance are approximated by

$$\mu_{G/T} \approx \mu_G - 10\log_{10}\left(\mu_{T_{sys}}\right) \tag{B.20a}$$

$$\sigma^2_{G/T} \approx \sigma^2_{G_{rx}} + \left(\frac{10}{\ln(10)\mu_{T_{sys}}}\right)^2\sigma^2_{T_{sys}}. \tag{B.20b}$$

System noise temperature T_{sys} in Kelvin (K) is the sum of the environmental noise temperature T_0, receiver noise temperature T_{rx}, and interference noise temperature T_{int}, which gives (B.20) as

$$\mu_{G/T} \approx \mu_G - 10\log_{10}\left(\mu_{T_0} + \mu_{T_{rx}} + \mu_{T_{int}}\right) \tag{B.21a}$$

$$\sigma^2_{G/T} \approx \sigma^2_{G_{rx}} + \left(\frac{10}{\ln(10)}\right)^2\frac{\sigma^2_{T_0}+\sigma^2_{T_{rx}}+\sigma^2_{T_{int}}}{\left(\mu_{T_0}+\mu_{T_{rx}}+\mu_{T_{int}}\right)^2}. \tag{B.21b}$$

Noise from intentional and unintentional sources are treated in this example as broadband noise spread across the channel bandwidth B. While T_0 and T_{rx} are inputs to the model, the interference noise temperature T_{int} is calculated from the measured noise power spectral density (PSD) N_{int} in dBW Hz^{-1} (to be calculated in the model) at the aperture as

$$T_{int} = \frac{1}{k_B} 10^{0.1 N_{int}}, \tag{B.22}$$

where k_B is Boltzmann's constant in W/K/Hz. The determination of the interference noise N_{int} depends upon the scenario. If the links between the interference sources and receiver is modeled, then N_{int} will be calculated from the received PSD. The mean and variance are estimated from the Taylor Series (3.24) as

$$\mu_{T_{int}} \approx \frac{1}{k_B} 10^{0.1 \mu_{N_{int}}} \tag{B.23a}$$

$$\sigma^2_{T_{int}} \approx \left(\frac{1}{k_B} 10^{0.1 \mu_{N_{int}}} \ln \left(\frac{1}{k_B} 10^{0.1} \right) \right)^2 \sigma^2_{N_{int}}. \tag{B.23b}$$

Using theoretical mean and variance relationships above, the carrier-to-noise ratio uncertainty $\sigma^2_{C/N}$ is found as

$$\begin{aligned} \sigma^2_{C/N} \approx \sigma^2_{EIRP} + \sigma^2_{L_{fs}} + \sigma^2_{L_{atm}} + \sigma^2_{L_{ion}} + \sigma^2_{L_{pt,tx}} + \sigma^2_{L_{pt,rx}} \\ + \sigma^2_{G_{rx}} + \left(\frac{10}{\ln(10) \mu_{T_{sys}}} \right)^2 \frac{\sigma^2_{T_0} + \sigma^2_{T_{rx}} + \sigma^2_{T_{int}}}{\left(\mu_{T_0} + \mu_{T_{rx}} + \mu_{T_{int}}\right)^2}. \end{aligned} \tag{B.24}$$

Similarly, the carrier-to-noise ratio mean $\mu_{C/N}$ is given as:

$$\begin{aligned} \mu_{C/N} \approx \mu_{P_{tx}} + \mu_{G_{tx}} - \left(\mu_{L_{tx,feed}} + \mu_{L_{tx,rad}} + \mu_{L_{fs}} + \mu_{L_{atm}} + \mu_{L_{ion}} + \mu_{L_{pt,tx}} + \mu_{L_{pt,rx}} \right) \\ + \mu_{G_{rx}} - 10 \log_{10} \left(\mu_{T_0} + \mu_{T_{rx}} + \frac{1}{k_B} 10^{0.1 \mu_{N_{int}}} \right). \end{aligned} \tag{B.25}$$

Many (if not most) of the input parameters to the model in Figure B.7 are not precisely known during the planning process and therefore contain various degrees of uncertainty [130, 132]. Predictions of link loss factors stemming from weather, signal depolarization, pointing errors, and other effects such as foliage may be characterized statistically but not known with high certainty until the time of operation. Similarly noise from potential interference sources may vary, especially with mobile SATCOM ground terminals operating in dense RF environments. The FCM representation presented here inherently incorporates uncertainties into the model and enables analyses of their impacts.

B.1.2 SATCOM Functional Causal Model Example

To illustrate the FCM concept, suppose that the data from Table B.1 is used to assess expected system performance of the model in Figure B.7. Input parameters are modeled as random variables having the specified distribution types (e.g., Gaussian or Beta) and associated parameters. Uncertainty is represented by the standard deviation, with higher standard deviations (relative to the mean) indicating higher degrees of uncertainty.[2]

In this example, a SATCOM downlink is modeled which has uncertainties in path loss, transmitter, and receiver elements. As a result, the received SNR is found to have significant uncertainty as shown in Figure B.8, with a mean value of 20.9 dB and standard deviation of 4.5 dB for this Baseline Case. The uncertainty places the 95% confidence level for SNR at 12 dB, as shown in Figure B.9. The Baseline Case has a mean of $\mu_{SNR} = 20.9$ dB and variance of $\sigma^2_{SNR} = 20.25$. The Reduced Uncertainty case has the same mean but a smaller variance of $\sigma^2_{SNR} = 4.84$, resulting in a 5 dB relative SNR gain associated with the 95% confidence level. If information quality can be improved to reduce the uncertainties in half, then the result is a 2.2 dB SNR standard deviation. The magnitude of SNR uncertainty reduction relative to the baseline case increases the 95% confidence level to 17 dB SNR as shown in Figure B.9. The uncertainty reduction in this example translates to a 5 dB SNR gain. Thus the FCM model can translate information or awareness uncertainty regarding

[2]Note that probability distribution types specified in the Consultative Committee for Space and Data Systems standard 401.0 [132] could also be used.

Table B.1: Scenario input parameters for the SATCOM FCM example.

Parameter	Value	Parameter	Value
Link Parameters			
Channel Freq. (f)	12 GHz	Channel BW (B)	250 kHz
Modulation (M)	8-PSK	Link Distance (d)	40,000 km
Rain Loss (L_{rain})	Beta(4.9,8.16), [0,8] dB	Gasseous Loss (L_{gas})	N(1,0.01) dB
Pol. Loss (L_{pol})	Beta(2.14,2.27), [0,3] dB	Scint. Loss (L_{sc})	Beta (3.37,6.74), [0,6] dB
Transmitter Parameters			
Feed Loss ($L_{tx,feed}$)	N(1,0.01) dB	Radome Loss (L_{rad})	0 dB
Aperture Gain (G_{tx})	N(38,0.1) dBi	3dB Beamwidth (θ_{3dB})	N(2°,0.01°)
Pointing Error (ω_{tx})	N(1°,0.5°)	Tx Power (P_{tx})	N(10,0.01) dBW
Receiver Parameters			
Feed Loss ($L_{rx,feed}$)	N(1,0.01) dB	Radome Loss (L_{rad})	N(0.5,0.05) dB
Aperture Gain (G_{rx})	N(48,0.1) dBi	3dB Beamwidth (θ_{3dB})	N(2.5°,0.01°)
Pointing Error (ω_{rx})	N(1°,0.5°)	Sys. Noise Temp (T_{sys})	N(290,0.25) K
Sky Noise Temp (T_0)	N(45,0.25) K	Int. Noise (N_{int})	N(-240,12) dB/Hz

the SATCOM operating conditions into performance gains and losses.

A FCM-based model inherently enables SATCOM configuration planning using the same model that is used for the predictive analysis discussed in the previous section. While predictive assessments infer expected SATCOM performance from system settings and operating conditions, planning assessments infer required SATCOM system settings from operating conditions and desired performance thresholds. Bayesian Network algorithms are able to do this reverse inference using the same model that is used for the predictive cases. The following section presents an approach that enables planners to manage SATCOM resources in accordance with risk thresholds and situational uncertainty.

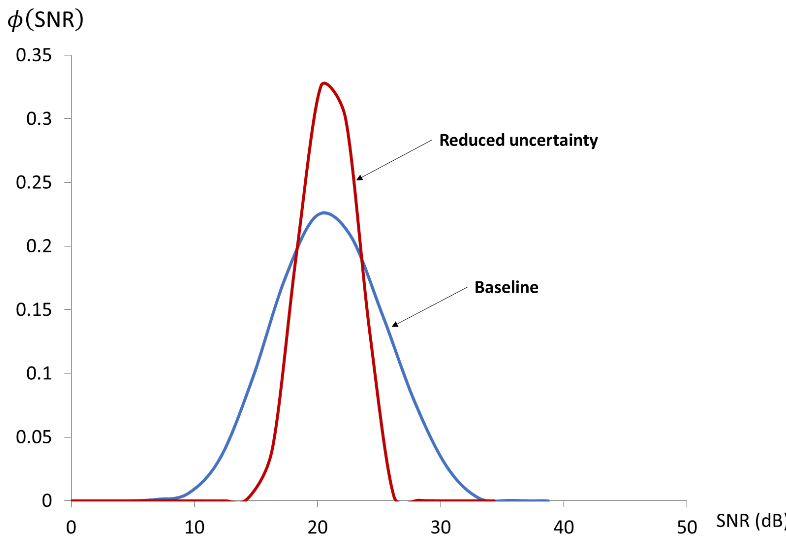

Figure B.8: Modem SNR probability distribution function for the baseline and reduced uncertainty cases.

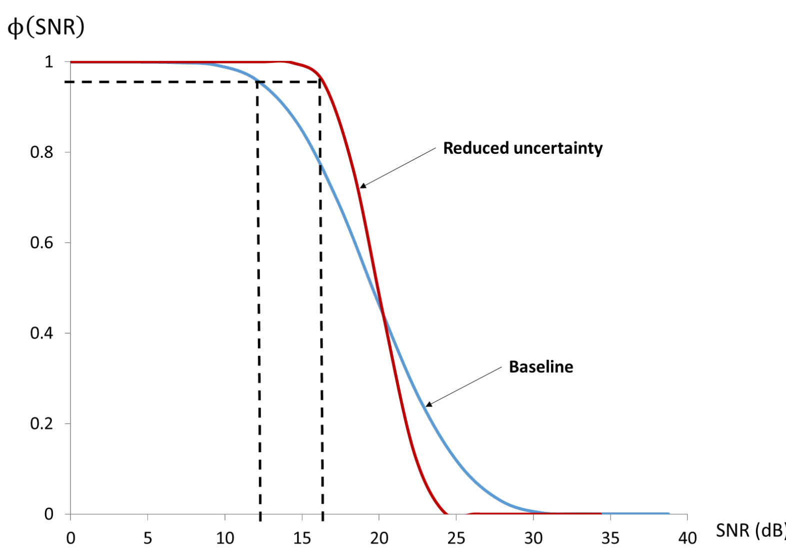

Figure B.9: Modem SNR exceedance probability for the baseline and reduced uncertainty cases.

B.2 Risk-Constrained SATCOM Resource Management

Various techniques have been studied for managing SATCOM resources (see e.g. [133–136]). Allocation assessment and optimization methods explore resource dimensions including frequency reuse, channel bandwidth (e.g., time slot and traffic) allocation, and satellite transmitter power. The optimality of each technique relies on some assessment of expected user demand and achievable link performance. Such predictions, however, have varying degrees of uncertainty as described above. SATCOM resource allocation processes therefore need to incorporate risk factors into the selected technique.

The probabilistic nature of FCM can be used to plan SATCOM resources subject to desired risk thresholds. With this approach, SATCOM planners identify the performance goals and associated risk levels for each link or user. The resulting resource allocation (e.g., transmitted power P_{tx}) and link parameters (e.g., modulation type) needed to achieve the performance goals at the specified risk (or confidence) levels will vary with the level of uncertainty.

Consider a desired performance parameter X that has some degree of uncertainty σ_X^2 associated with its achievable value in a given scenario. Let the probability distribution be given as $\phi(X)$ with an associated cumulative probability distribution $\Phi(X)$. Further suppose that it is desired to have some value of X that does not fall below some threshold x_q with a probability greater than q. Thus the total probability of attaining $X \leq x_q$ be given by

$$\Phi(X \leq x_q) = \int_{-\infty}^{x_q} \phi(X). \tag{B.26}$$

Referring to the illustration in Figure B.10, the probability $\Phi(X \leq x_q) = q$ can be used to define a risk level. It is also illustrated that the threshold x_q can be defined as a function of the mean value μ_X and a multiple a of the standard deviation σ_X. Thus for a given μ_X and risk q, greater uncertainty leads to lower threshold values x_q. Alternatively, it may be desirable to place an exceedance risk threshold on a parameter. The risk calculation then

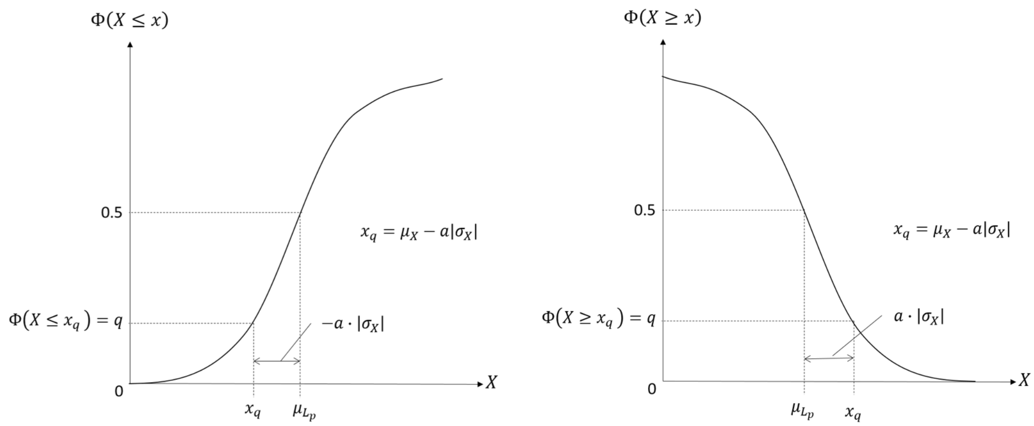

Figure B.10: Illustration of mapping from a value x_q to the associated risk q for shortfall risk $\Phi(X \leq x_q) = q$ (left) and exceedance risk $\Phi(X \geq x_q) = q$.(right).

becomes

$$\Phi(X \geq x_q) = 1 - \Phi(X \leq x_q) = 1 - \int_{-\infty}^{x_q} \phi(X). \tag{B.27}$$

The exceedance risk case is illustrated in right hand plot of Figure B.10.

These concepts can be applied to the SATCOM FCM to establish risk-constrained management of SATCOM resources. In this approach, uncertainty assessments of SATCOM links are made using the FCM and available planning information. Performance and associated risk thresholds for attributes of interest are then applied to each link, allowing planners to determine the corresponding SATCOM resources using inference capabilities of the FCM. The resulting method allows planners to optimize resources allocations subject to the risk constraints (perhaps using techniques such as those in [133–136]). It further allows planners to evaluate performance gains associated with reducing uncertainty levels for each parameter in the FCM.

To illustrate, consider the uncertainty formulations from Section B.1.1. Further, let C/N values be assessed such that its uncertainty is given as a probability distribution $\phi(C/N)$ having a mean $\mu_{C/N}$ and variance $\sigma^2_{C/N}$ given by (B.10) and (B.24). Suppose that a user requires a given C/N level with some degree of confidence q, and the SATCOM resource manager wishes to determine the transmit power P_{tx} required to provide the necessary level of service.

The carrier-to-noise value at the associated risk level is found as:

$$C/N_q = \mu_{C/N} + a\sqrt{\sigma^2_{C/N}}. \tag{B.28}$$

The uncertainty $\sigma^2_{C/N}$ is the cumulative uncertainty of the SATCOM model as given by (B.24). Thus, the requisite transmit power level can be found by (B.25) and (B.28) as:

$$\begin{aligned}\mu_{P_{tx}} \approx C/N_q - a\sqrt{\sigma^2_{C/N}} - \mu_{G_{tx}} + \mu_{L_{tx,feed}} + \mu_{L_{tx,rad}} + \mu_{L_{fs}} + \mu_{L_{atm}} + \mu_{L_{ion}} \\ +\mu_{L_{pt,tx}} + \mu_{L_{pt,rx}} - \mu_{G_{rx}} + 10\log_{10}\left(\mu_{T_0} + \mu_{T_{rx}} + \frac{1}{k_B}10^{0.1\mu_{N_{int}}}\right).\end{aligned} \tag{B.29}$$

The change in transmit level $\Delta\mu_{P_{tx}}$ resulting from a change in $\sigma^2_{C/N}$ (all other factors remaining constant) can be found as:

$$\Delta\mu_{P_{tx}} \approx a\left(\sqrt{\sigma^2_{C/N,1}} - \sqrt{\sigma^2_{C/N,2}}\right) \tag{B.30}$$

Figure B.11 illustrates the power difference given a change in uncertainty for several confidence levels. It can be seen that even small changes in uncertainty have an impact on transmit power requirements. It is therefore important for SATCOM operators to characterize and reduce the amount of uncertainty to attain desired performance and maximize SATCOM resource usage.

A similar analysis can be done for interference noise N_{int}. Its relationship to $\sigma^2_{C/N}$ is given in (B.23), (B.24), and (B.30). The results are plotted in Figure B.12.

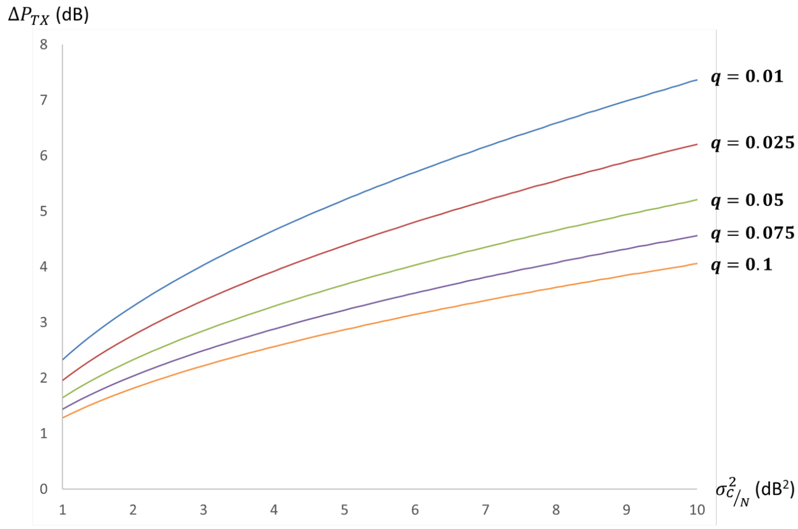

Figure B.11: SATCOM transmit power increase ΔP_{tx} as a function of carrier-to-noise uncertainty $\sigma^2_{\frac{C}{N}}$ and confidence level q.

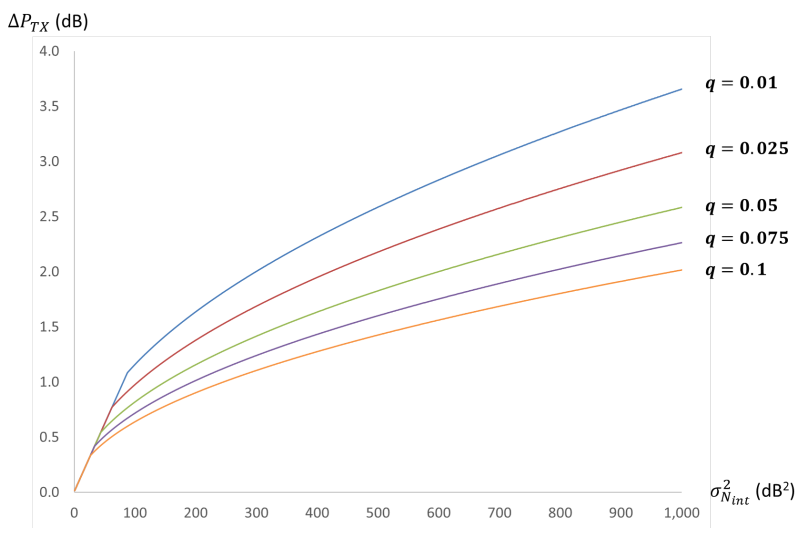

Figure B.12: SATCOM transmit power increase ΔP_{tx} as a function of interference noise uncertainty $\sigma^2_{N_{int}}$ and confidence level q.

B.3 Summary

Advanced SATCOM resource management capabilities are envisioned to provide for dynamic resource adaptation. The advanced capabilities require a SATCOM situational awareness and decision-making approach that represents the cause and effect linkage of relevant phenomenology and operating conditions on link performance. Further, the model must enable the assessment and decision-making under uncertain conditions.

The FCM approach presented here enables predictions of SATCOM link conditions stemming from weather, signal depolarization, pointing errors, and other effects having various degrees of uncertainty. The FCM representation presented here inherently incorporates uncertainties into the model and enables analyses of their impacts.

The probabilistic nature of FCM can be used to plan SATCOM resources subject to desired risk thresholds. With this approach, SATCOM planners identify the performance goals and associated risk levels for each link or user. The resulting resource allocation (e.g., transmitted power P_{tx}) and link parameters (e.g., modulation type) needed to achieve the performance goals at the specified risk (or confidence) levels will vary with the level of uncertainty.

Bibliography

Bibliography

[1] "Report to the president: Realizing the full potential of government-held spectrum to spur economic growth," Executive Office of the President, President's Council of Advisors on Science and Technology, Tech. Rep., Jul. 2012. [Online]. Available: http://www.dtic.mil/docs/citations/ADA565091

[2] "Shared Commercial Operations in the 3550-3650 MHz Band," Federal Information & News Dispatch, Inc., Lanham, United States, Tech. Rep., Jun. 2015. [Online]. Available: http://search.proquest.com/docview/1690460166/abstract

[3] "Dyspan vision," in *2005 First IEEE International Symposium on New Frontiers in Dynamic Spectrum Access Networks, 2005. DySPAN 2005.* IEEE, Nov. 2005, p. v.

[4] "IEEE Standard Definitions and Concepts for Dynamic Spectrum Access: Terminology Relating to Emerging Wireless Networks, System Functionality, and Spectrum Management," *IEEE Std 1900.1-2008*, pp. 1–62, Oct. 2008.

[5] P. Kolodzy, P. Tenhula, L. Van Wazer, M. Marcus, and M. McLaughlin, "Spectrum policy task force final report," Federal Communications Commission, Tech. Rep. ET 02-135, Nov. 2002. [Online]. Available: http://www.fcc.gov/sptf/reports.html

[6] J. S. Seybold, *Introduction to RF Propagation.* Hoboken, N.J: Wiley, 2005.

[7] J. G. Proakis, *Communication Systems Engineering*, 2nd ed. Upper Saddle River, N.J: Prentice Hall, 2002.

[8] M. I. Skolnik, *Introduction to radar systems*, 3rd ed. Boston: McGraw Hill, 2001.

[9] "Spectrum Management: NTIA Planning and Processes Need Strengthening to Promote Efficient Use of Spectrum by Federal Agencies," U.S. Government Accountability Office, Washington, DC, Report to Congressional Commitees GAO-11-352, Apr. 2011. [Online]. Available: http://www.gao.gov/new.items/d11352.pdf

[10] United States, Ed., *Manual of regulations and procedures for federal radio frequency management*, september 2005 ed. Washington, D.C.: U.S. Dept. of Commerce, National Telecommunications and Information Administration, 2005.

[11] M. McHenry, D. McCloskey, D. Roberson, and J. MacDonald, "Spectrum Occupancy Measurements, Chicago Illinois, November 16-18 2005," Shared Spectrum Company, Tech. Rep., Dec. 2005. [Online]. Available: http://www.sharedspectrum.com/papers/spectrum-reports/

[12] M. McHenry and S. Chunduri, "Spectrum occupancy measurements, location 3 of 6: National science foundation building roof, rev 2," Shared Spectrum Company, Tech. Rep., Aug. 2005. [Online]. Available: http://www.sharedspectrum.com/papers/spectrum-reports/

[13] C. Hammerschmidt and H. Ottke, "Spectrum occupancy results from several surveys," in *2013 IEEE International Symposium on Electromagnetic Compatibility (EMC)*, Aug. 2013, pp. 76–81.

[14] C. Hammerschmidt, H. Ottke, and R. Hoffman, "Broadband Spectrum Survey in the Denver and Boulder, Colorado, Metropolitan Areas," Boulder CO, Tech. Rep. NTIA Report TR-13-149, Aug. 2013. [Online]. Available: http://www.its.bldrdoc.gov/publications/2735.aspx

[15] "Cisco visual networking index: Global mobile data traffic forecast update 2014–2019 white paper." [Online]. Available: http://cisco.com/c/en/us/solutions/collateral/service-provider/visual-networking-index-vni/white_paper_c11-520862.html

[16] "Annual Wireless Industry Survey - 2015," 2016. [Online]. Available: http://www.ctia.org/your-wireless-life/how-wireless-works/annual-wireless-industry-survey

[17] G. Fortetsanakis and M. Papadopouli, "How beneficial is the WiFi offloading? A detailed game-theoretical analysis in wireless oligopolies," in *2016 IEEE 17th International Symposium on A World of Wireless, Mobile and Multimedia Networks (WoWMoM)*, Jun. 2016, pp. 1–10.

[18] Q. Zhao and B. Sadler, "A Survey of Dynamic Spectrum Access," *Signal Processing Magazine, IEEE*, vol. 24, no. 3, pp. 79–89, 2007.

[19] J. Peha, "Sharing Spectrum Through Spectrum Policy Reform and Cognitive Radio," *Proceedings of the IEEE*, vol. 97, no. 4, pp. 708–719, Apr. 2009.

[20] M. B. Weiss and M. Altamaimi, "The Cost of Knowing: An economic evaluation of context acquisition in DSA systems," in *Telecommunications Policy Research Conference, 2011*, Sep. 2011. [Online]. Available: http://d-scholarship.pitt.edu/6074/

[21] M. McHenry, E. Livsics, T. Nguyen, and N. Majumdar, "XG dynamic spectrum access field test results [topics in radio communications]," *Communications Magazine, IEEE*, vol. 45, no. 6, pp. 51–57, 2007.

[22] United States Department of Commerce, "Commerce Business Daily PSA #2951," Oct. 2001. [Online]. Available: http://www.fbodaily.com/cbd/archive/2001/10%28October%29/05-Oct-2001/spmsc012.htm

[23] P. Marshall, "DARPA progress towards affordable, dense, and content focused tactical edge networks," in *Military Communications Conference, 2008. MILCOM 2008. IEEE*, 2008, pp. 1–7.

[24] K. Zhang, D. Swain, and M. Lin, "Dynamic Spectrum Access Enabled DoD Net-centric Spectrum Management," in *Military Communications Conference, 2007. MILCOM 2007. IEEE*, 2007, pp. 1–7.

[25] T. Sedmak, "Commerces NTIA Seeks Participants for Spectrum Sharing Innovation Test-Bed," *NTIA Press Release*, Feb. 2008. [Online]. Available: http://www.ntia.doc.gov/ntiahome/press/2008/Testbed_020508.pdf

[26] J. Bernhard, Jeff Reed, and J.-M. Park, "Workshop on Ehancing Access to the Radio Spectrum," National Science Foundation, Arlington VA, Workshop Final Report, Aug. 2010. [Online]. Available: http://www.nsf.gov/mps/ast/nsf_ears_workshop_2010_final_report.pdf

[27] "Presidential Memorandum: Unleashing the Wireless Broadband Revolution," in *Federal Register*, ser. Presidential Documents. Washington, DC: US Government Printing Office, Jul. 2010, vol. 75 No. 126, pp. 38 387–38 389. [Online]. Available: http://www.gpo.gov/fdsys/pkg/FR-2010-07-01/pdf/2010-16271.pdf

[28] "Plan and Timetable to Make Available 500 Megahertz of Spectrum for Wireless Broadband," U.S. Department of Commerce, National Telecommunications and Information Administration, Washington, DC, Tech. Rep., Oct. 2010. [Online]. Available: http://www.ntia.doc.gov/files/ntia/publications/tenyearplan_11152010.pdf

[29] *National Broadband Plan: Analysis and Strategy for Connecting America.* NEW YORK: NOVA SCIENCE, 2011.

[30] "Television band devices," Apr. 2012, 47 CFR, Part 15, Subpart H.

[31] E. F. Drocella, J. Richards, R. Sole, F. Najmy, A. Lundy, and P. McKenna, "3.5 GHz Exclusion Zone Analyses and Methodology," U.S. Department of Commerce, National Telecommunications and Information Administration, Washington, D.C., Tech. Rep. TR-15-517, Jun. 2015. [Online]. Available: http://www.its.bldrdoc.gov/publications/2805.aspx

[32] R. Ramanathan and C. Partridge, "Next generation (XG) architecture and protocol development (XAP)," BBN Technologies Cambridge MA, Tech. Rep., Aug. 2005. [Online]. Available: http://www.dtic.mil/docs/citations/ADA437096

[33] F. Perich, "Policy-Based network management for NeXt generation spectrum access control," in *New Frontiers in Dynamic Spectrum Access Networks, 2007. DySPAN 2007. 2nd IEEE International Symposium on*, 2007, pp. 496–506.

[34] G. Denker, D. Elenius, R. Senanayake, M.-O. Stehr, and D. Wilkins, "A policy engine for spectrum sharing," in *2nd IEEE International Symposium on New Frontiers in Dynamic Spectrum Access Networks, 2007. DySPAN 2007*, Apr. 2007, pp. 55 –65.

[35] "OET Bulletin No. 69: Longley-Rice Methodology for Evaluating TV Coverage and Interference," Federal Communications Commission Office of Engineering and Technology, Bulletin OET Bulletin No. 69, Feb. 2004. [Online]. Available: https://www.fcc.gov/encyclopedia/oet-bulletins-line

[36] G. A. Hufford, Longley, and W. Kissick, "A Guide to the Use of the ITS Irregular Terrain Model in the Area Prediction Mode," US Department of Commerce, Technical Report NTIA 82-100, 1982.

[37] G. Hufford, “The ITS Irregular Terrain Model, version 1.2.2; The Algorithm,” Institute for Telecommunication Sciences, National Telecommunications and Information Administration, Boulder CO, Technical Report, 1985. [Online]. Available: http://www.its.bldrdoc.gov/resources/radio-propagation-software/itm/itm.aspx

[38] A. G. Longley and P. L. Rice, “Prediction of tropospheric radio transmission loss over irregular terrain. a computer method-1968,” DTIC Document, Tech. Rep., 1968.

[39] T. Erpek, M. Mchenry, and A. Stirling, “Dynamic spectrum access operational parameters with wireless microphones,” *IEEE Communications Magazine*, vol. 49, no. 3, pp. 38 –45, Mar. 2011.

[40] H. Mauwa, A. Bagula, M. Zennaro, and G.-A. Lusilao-Zodi, “On the impact of propagation models on TV white spaces measurements in Africa,” in *2015 International Conference on Emerging Trends in Networks and Computer Communications (ETNCC)*, May 2015, pp. 148–154.

[41] J. R. Hampton, N. Merheb, W. Lain, D. Paunil, R. Shuford, and W. Kasch, “Urban propagation measurements for ground based communication in the military UHF band,” *IEEE Transactions on Antennas and Propagation*, vol. 54, no. 2, pp. 644–654, Feb. 2006.

[42] P. C. Roosa, “Basic Elements of Spectrum Management | NTIA,” National Telecommunications and Information Administration, United States Department of Commerce, Washington, D.C., Tech. Rep. NTIA Special Publication 91-25, Aug. 1992. [Online]. Available: http://www.ntia.doc.gov/book-page/basic-elements-spectrum-management

[43] C. v. E. James V. Zidek, “Uncertainty, Entropy, Variance and the Effect of Partial Information,” *Lecture Notes-Monograph Series*, vol. 42, pp. 155–167, 2003. [Online]. Available: http://www.jstor.org/stable/4356236

[44] J. Chen, C. van Eeden, and J. Zidek, “Uncertainty and the conditional variance,” *Statistics & Probability Letters*, vol. 80, no. 2324, pp. 1764–1770, Dec. 2010.

[45] C. Shannon, “A mathematical theory of communication,” *Bell System Technical Journal, The*, vol. 27, no. 3, pp. 379–423, Jul. 1948.

[46] T. M. Mitchell, *Machine Learning.* New York: McGraw-Hill, 1997.

[47] J. Hull, *Options, futures, and other derivatives*, ninth edition.. ed., 2015.

[48] J. Chen, “A Partial Order on Uncertainty and Information,” *Journal of Theoretical Probability*, vol. 26, no. 2, pp. 349–359, Aug. 2011.

[49] M. B. Ted Bergstrom, “Log-Concave Probability and its Applications,,” *Ted C Bergstrom*, vol. 26, no. 2, 2005.

[50] P. E. Smaldino, “Does Learning Imply a Decrease in the Entropy of Behavior?” *arXiv:1501.04358 [cs]*, Jan. 2015, arXiv: 1501.04358.

[51] S. Kay, *Fundamentals of Statistical Signal Processing, Volume I: Estimation Theory*, 1st ed. Englewood Cliffs, N.J: Prentice Hall, Apr. 1993.

[52] Y. Bar-Shalom, X. R. Li, and T. Kirubarajan, *Estimation with Applications to Tracking and Navigation*, 1st ed. Wiley-Interscience, Jun. 2001.

[53] J. Pearl, *Causality: models, reasoning, and inference*, 2nd ed. Cambridge ; New York: Cambridge University Press, 2009.

[54] ——, "An introduction to causal inference," *The International Journal of Biostatistics*, vol. 6, no. 2, Jan. 2010.

[55] ——, "Causal inference in statistics: An overview," *Statistics Surveys*, vol. 3, pp. 96–146, 2009, mathematical Reviews number (MathSciNet): MR2545291; Zentralblatt MATH identifier: 05719273.

[56] D. Koller and N. Friedman, *Probabilistic Graphical Models: Principles and Techniques*. The MIT Press, Aug. 2009.

[57] T. R. Krynski and J. B. Tenenbaum, "The role of causality in judgment under uncertainty," *Journal of Experimental Psychology: General*, vol. 136, no. 3, pp. 430–450, 2007.

[58] K. B. Laskey, "MEBN: a language for first-order bayesian knowledge bases," *Artificial Intelligence*, vol. 172, no. 2-3, pp. 140–178, Feb. 2008.

[59] "CRC standard mathematical tables." *Chemical Rubber Company standard mathematical tables*, 1987.

[60] George. Casella, *Statistical inference*, ser. The Wadsworth & Brooks/Cole Statistics/Probability series. Pacific Grove, Calif: Brooks/Cole PubCo, 1990.

[61] Maurice G. Kendall (Maurice George), *Kendall's advanced theory of statistics.*, 6th ed. London: Edward Arnold ; New York, 1994.

[62] R. C. Elandt-Johnson, *Survival models and data analysis*, wiley classics library ed.. ed., ser. Wiley classics library. New York: Wiley, 1999.

[63] J. M. Wozencraft, *Principles of Communication Engineering*. Prospect, IL: Waveland Press, Inc, 1990.

[64] D. Tse and P. Viswanath, *Fundamentals of wireless communication*. Cambridge University Press, 2005.

[65] H. L. V. Trees, *Nonlinear Modulation Theory*, 1st ed. New York: Wiley-Interscience, Dec. 2002.

[66] J. J. Egli, "Radio Propagation above 40 MC over Irregular Terrain," *Proceedings of the IRE*, vol. 45, no. 10, pp. 1383–1391, Oct. 1957.

[67] J. D. Parsons, *The Mobile Radio Propagation Channel*. Chichester: John Wiley and Sons, Inc, 2000, vol. 2nd ed.

[68] N. Blaunstein, *Radio Propagation in Cellular Networks*, ser. Artech House Mobile Communications Library. Boston: Artech House, Inc, 1999.

[69] W. R. Young, "Comparison of mobile radio transmission at 150, 450, 900, and 3700 mc," *The Bell System Technical Journal*, vol. 31, no. 6, pp. 1068–1085, Nov. 1952.

[70] ——, "Comparison of mobile radio transmission at 150, 450, 900, and 3700 mc," *Transactions of the IRE Professional Group on Vehicular Communications*, vol. 3, no. 1, pp. 71–84, Jun. 1953.

[71] S. Sesia, I. Toufik, and M. Baker, Eds., *LTE, The UMTS Long Term Evolution: From Theory to Practice*, 1st ed. Chichester, U.K.: Wiley, Apr. 2009.

[72] M. Schwartz, *Mobile Wireless Communications.* Cambridge University Press, Dec. 2004.

[73] B. L. Mark and A. O. Nasif, "Estimation of Interference-Free Transmit Power for Opportunistic Spectrum Access," in *2008 IEEE Wireless Communications and Networking Conference*, Mar. 2008, pp. 1679–1684.

[74] ——, "Estimation of maximum interference-free power level for opportunistic spectrum access," *IEEE Transactions on Wireless Communications*, vol. 8, no. 5, pp. 2505–2513, May 2009.

[75] "Netica-J Reference Manual, Version 4.18," Oct. 2010. [Online]. Available: http://www.norsys.com/netica-j/docs/NeticaJ_Man.pdf

[76] P. C. G. Costa and K. B. Laskey, "PR-OWL: A Framework for Probabilistic Ontologies," in *Proceedings of the 2006 conference on Formal Ontology in Information Systems: Proceedings of the Fourth International Conference (FOIS 2006).* Amsterdam, The Netherlands, The Netherlands: IOS Press, 2006, pp. 237–249.

[77] P. C. G. Costa, M. Ladeira, R. Carvalho, K. B. Laskey, L. L. Santos, and S. Matsumoto, "A First-Order Bayesian Tool for Probabilistic Ontologies," in *Proceedings of the 21st International Florida Artificial Intelligence Research Society Conference (FLAIRS-21).* AAAI, 2008.

[78] Z. Quan, S. Cui, and A. Sayed, "An Optimal Strategy for Cooperative Spectrum Sensing in Cognitive Radio Networks," in *Global Telecommunications Conference, 2007. GLOBECOM '07. IEEE*, 2007, pp. 2947–2951.

[79] T. Yucek and H. Arslan, "A survey of spectrum sensing algorithms for cognitive radio applications," *Communications Surveys & Tutorials, IEEE*, vol. 11, no. 1, pp. 116–130, 2009.

[80] S. Zarrin and T. J. Lim, "Belief Propagation on Factor Graphs for Cooperative Spectrum Sensing in Cognitive Radio," in *New Frontiers in Dynamic Spectrum Access Networks, 2008. DySPAN 2008. 3rd IEEE Symposium on*, 2008, pp. 1–9.

[81] D. Davis and F. Hasan, "Collaborative spectrum sensing for cognitive networks - Factors for optimal decision points," in *Wireless Information Technology and Systems (ICWITS), 2010 IEEE International Conference on*, 2010, pp. 1–4.

[82] J. Zhu, B. Zheng, and Y. Zou, "Detection time analysis for the multiple-user cooperative spectrum sensing scheme in cognitive radio networks," *Science in China Series F: Information Sciences*, vol. 52, no. 10, pp. 1915–1925, Oct. 2009.

[83] S. Gao, L. Qian, D. R. Vaman, and Z. Han, "Distributed Cognitive Sensing for Time Varying Channels: Exploration and Exploitation," in *2010 IEEE Wireless Communications and Networking Conference (WCNC)*. IEEE, Apr. 2010, pp. 1–6.

[84] F. Zeng, C. Li, and Z. Tian, "Distributed Compressive Spectrum Sensing in Cooperative Multihop Cognitive Networks," *IEEE Journal of Selected Topics in Signal Processing*, vol. 5, no. 1, pp. 37–48, Feb. 2011.

[85] W. Han, J. Li, Z. Tian, and Y. Zhang, "Dynamic Sensing Strategies for Efficient Spectrum Utilization in Cognitive Radio Networks," *IEEE Transactions on Wireless Communications*, vol. PP, no. 99, pp. 1–12, 2011.

[86] ——, "Efficient Cooperative Spectrum Sensing with Minimum Overhead in Cognitive Radio," *IEEE Transactions on Wireless Communications*, vol. 9, no. 10, pp. 3006–3011, Oct. 2010.

[87] M. Wellens, J. Riihijarvi, M. Gordziel, and P. Mahonen, "Evaluation of Cooperative Spectrum Sensing Based on Large Scale Measurements," in *New Frontiers in Dynamic Spectrum Access Networks, 2008. DySPAN 2008. 3rd IEEE Symposium on*, 2008, pp. 1–12.

[88] D. Cabric, S. Mishra, and R. Brodersen, "Implementation issues in spectrum sensing for cognitive radios," in *Signals, Systems and Computers, 2004. Conference Record of the Thirty-Eighth Asilomar Conference on*, vol. 1, 2004, pp. 772–776 Vol.1.

[89] T. Do and B. L., "Improving Spectrum Sensing Performance by Exploiting Multiuser Diversity," in *Foundation of Cognitive Radio Systems*, S. Cheng, Ed. InTech, Mar. 2012.

[90] S. Tang and B. L. Mark, "Modeling and analysis of opportunistic spectrum sharing with unreliable spectrum sensing," *IEEE Transactions on Wireless Communications*, vol. 8, no. 4, pp. 1934–1943, Apr. 2009.

[91] Z. Quan, S. Cui, and A. Sayed, "Optimal Linear Cooperation for Spectrum Sensing in Cognitive Radio Networks," *Selected Topics in Signal Processing, IEEE Journal of*, vol. 2, no. 1, pp. 28–40, 2008.

[92] Z. Quan, S. Cui, A. Sayed, and H. Poor, "Optimal Multiband Joint Detection for Spectrum Sensing in Cognitive Radio Networks," *Signal Processing, IEEE Transactions on*, vol. 57, no. 3, pp. 1128–1140, 2009.

[93] W.-Y. Lee and I. Akyildiz, "Optimal spectrum sensing framework for cognitive radio networks," *Wireless Communications, IEEE Transactions on*, vol. 7, no. 10, pp. 3845–3857, 2008.

[94] M. Barrie, S. Delaere, and P. Ballon, "Potential viability of third party mobile service platforms for spectrum sensing," in *2010 14th International Conference on Intelligence in Next Generation Networks (ICIN)*, Oct. 2010, pp. 1 –10.

[95] H.-f. Chen, X. Jin, and L. Xie, "Reputation-based linear cooperation for spectrum sensing in cognitive radio networks," *Journal of Zhejiang University SCIENCE A*, vol. 10, no. 12, pp. 1688–1695, Dec. 2009.

[96] M. Weiss, S. Delaere, and W. Lehr, "Sensing as a Service: An Exploration into Practical Implementations of DSA," in *2010 IEEE Symposium on New Frontiers in Dynamic Spectrum*, Apr. 2010, pp. 1 –8.

[97] S. Huang, X. Liu, and Z. Ding, "Short Paper: On Optimal Sensing and Transmission Strategies for Dynamic Spectrum Access," in *3rd IEEE Symposium on New Frontiers in Dynamic Spectrum Access Networks, 2008. DySPAN 2008*, Oct. 2008, pp. 1 –5.

[98] A. P. Iyer, K. Chintalapudi, V. Navda, R. Ramjee, V. Padmanabhan, and C. R. Murthy, "SpecNet: Spectrum Sensing Sans Fronti'eres," in *Proceedings of NSDI 11: 8th USENIX Symposium on Networked Systems Design and Implementation*, Boston MA, Apr. 2011.

[99] T. Erpek, A. Leu, and B. Mark, "Spectrum Sensing Performance in TV Bands using the Multitaper Method," in *Signal Processing and Communications Applications, 2007. SIU 2007. IEEE 15th*, 2007, pp. 1–4.

[100] K. Lee and A. Yener, "Throughput Enhancing Cooperative Spectrum Sensing Strategies for Cognitive Radios," in *Signals, Systems and Computers, 2007. ACSSC 2007. Conference Record of the Forty-First Asilomar Conference on*, 2007, pp. 2045–2049.

[101] H. L. van Trees, *Detection, Estimation, and Modulation Theory*, part i ed. New York: Wiley-Interscience, Oct. 2001.

[102] S. Kay, *Fundamentals of Statistical Signal Processing, Volume II: Detection Theory*, 1st ed. Englewood Cliffs, N.J: Prentice Hall, Feb. 1998.

[103] H. Stark, *Probability and random processes with applications to signal processing*, 3rd ed. Upper Saddle River, NJ: Prentice Hall, 2002.

[104] A. E. Leu, M. McHenry, and B. L. Mark, "Modeling and analysis of interference in listen-before-talk spectrum access schemes," *International Journal of Network Management*, vol. 16, pp. 131–147, Mar. 2006, aCM ID: 1124504.

[105] Y. Li, Y. n. Dong, H. Zhang, H. t. Zhao, H. x. Shi, and X. x. Zhao, "Spectrum Usage Prediction Based on High-order Markov Model for Cognitive Radio Networks," in *2010 IEEE 10th International Conference on Computer and Information Technology (CIT)*, Jun. 2010, pp. 2784–2788.

[106] G. Ning and P. Nintanavongsa, "Time prediction based spectrum usage detection in centralized cognitive radio networks," in *2012 IEEE Wireless Communications and Networking Conference (WCNC)*, Apr. 2012, pp. 300–305.

[107] M. Huk and J. Mizera-Pietraszko, "Contextual neural-network based spectrum prediction for cognitive radio," in *2015 Fourth International Conference on Future Generation Communication Technology (FGCT)*, Jul. 2015, pp. 1–5.

[108] C. Song and Q. Zhang, "Intelligent Dynamic Spectrum Access Assisted by Channel Usage Prediction," in *INFOCOM IEEE Conference on Computer Communications Workshops , 2010*, Mar. 2010, pp. 1–6.

[109] A. K. Sadek, W. Zhang, and S. J. Shellhammer, "Listen-Before-Talk versus treating interference as noise for spectrum sharing," in *3rd IEEE Symposium on New Frontiers in Dynamic Spectrum Access Networks, 2008. DySPAN 2008.* IEEE, Oct. 2008, pp. 1–6.

[110] R. L. Keeney and H. Raiffa, *Decisions with Multiple Objectives: Preferences and Value Tradeoffs*, ser. Wiley series in probability and mathematical statistics. New York: Wiley, 1976.

[111] P. Marshall, "Dynamic spectrum access as a mechanism for transition to interference tolerant systems," in *New Frontiers in Dynamic Spectrum, 2010 IEEE Symposium on*, 2010, pp. 1–12.

[112] K. Larson, L. Cacciatore, S. Crawfor, T. Eng, E. Jacobs, J. Jackson, J. Levin, B. Luther, M. Marcus, T. Maguire, B. Nelson, S. Persaud, R. Repasi, B. Romano, T. Stanley, J. Williams, and J. Wong, "Spectrum policy task force report of the interference protection working group," Federal Communications Commission, Tech. Rep., Nov. 2002. [Online]. Available: http://fcc.gov/sptf/reports.html

[113] M. Z. Win, P. C. Pinto, and L. A. Shepp, "A mathematical theory of network interference and its applications," *Proceedings of the IEEE*, vol. 97, no. 2, pp. 205–230, Feb. 2009.

[114] J. M. Chapin and W. H. Lehr, "COGNITIVE RADIOS FOR DYNAMIC SPECTRUM ACCESS - the path to market success for dynamic spectrum access technology," *IEEE Communications Magazine*, vol. 45, no. 5, pp. 96–103, May 2007.

[115] J. M. Peha and S. Panichpapiboon, "Real-time secondary markets for spectrum," *Telecommunications Policy*, vol. 28, no. 7-8, pp. 603–618, Aug. 2004.

[116] S. Sengupta and M. Chatterjee, "An economic framework for dynamic spectrum access and service pricing," *IEEE/ACM Transactions on Networking*, vol. 17, no. 4, pp. 1200–1213, Aug. 2009.

[117] S. Dixit, S. Periyalwar, and H. Yanikomeroglu, "A competitive and dynamic pricing model for secondary users in infrastructure based networks," in *Vehicular Technology Conference Fall (VTC 2010-Fall), 2010 IEEE 72nd.* IEEE, Sep. 2010, pp. 1–5.

[118] P. C. Fishburn and R. L. Keeney, "Generalized utility independence and some implications," *Operations Research*, vol. 23, no. 5, pp. 928–940, 1975, ArticleType: research-article / Full publication date: Sep. - Oct., 1975 / Copyright 1975 INFORMS.

[119] D. P. Bertsekas, *Introduction to Probability*, 2nd ed. Belmont, Mass: Athena Scientific, 2008.

[120] P. Fishburn, *The Foundations of Expected Utility*, 1st ed. D. Reidel, Sep. 1982.

[121] K. J. Arrow, *Aspects of the theory of risk-bearing.* Helsinki: Yrj Jahnssonin Sti, 1965.

[122] J. W. Pratt, "Risk Aversion in the Small and in the Large," *Econometrica*, vol. 32, no. 1/2, pp. 122–136, 1964.

[123] H. Levy and M. Levy, "Arrow-Pratt Risk Aversion, Risk Premium and Decision Weights," *Journal of Risk and Uncertainty*, vol. 25, no. 3, pp. 265–290, Nov. 2002.

[124] L. Eeckhoudt, *Economic and financial decisions under risk*, C. Gollier and H. Schlesinger, Eds. Princeton, N.J.: Princeton, N.J. : Princeton University Press, 2005.

[125] H. Levy, *Stochastic dominance : investment decision making under uncertainty*, 2nd ed. New York, NY: New York, NY : Springer, 2006.

[126] G. Totsline and R. Gopal, "On managing intelligent satellite networks - an evolutionary in policy based distributed management," in *IEEE Military Communications Conference, 2005. MILCOM 2005*, Oct. 2005, pp. 518–524 Vol. 1.

[127] D. Whitefield and R. Gopal, "Capacity enhancement with dynamic resource management for next generation satellite systems," in *IEEE Military Communications Conference, 2005. MILCOM 2005*, Oct. 2005, pp. 761–767 Vol. 2.

[128] T. Allison, R. Gopal, and S. Arnold, "Analysis and demonstration of policy-based satellite communications resource management," in *MILITARY COMMUNICATIONS CONFERENCE, 2010 - MILCOM 2010*, Oct. 2010, pp. 1533–1540.

[129] X. Tian, Z. Tian, K. Pham, E. Blasch, and D. Shen, "Jamming/anti-jamming game with a cognitive jammer in space communication." International Society for Optics and Photonics, May 2012, pp. 83 850Q–83 850Q–10.

[130] T. M. Braun, 1949, *Satellite communications payload and system*, I. ebrary, Ed. Hoboken, N.J.: Hoboken, N.J. : Wiley, 2012.

[131] J. E. J. E. Allnutt, *Satellite-to-ground radiowave propagation*, 2nd ed., Faculty Author Collection, Ed. London: London : Institution of Engineering and Technology, 2011.

[132] "Radio Frequency and Modulation Systems–Part 1: Earth Stations and Spacecraft," Consultative Committee for Space Data Systems, Tech. Rep. CCSDS 401.0-B, Dec. 2013. [Online]. Available: http://public.ccsds.org/publications/BlueBooks.aspx

[133] A. Jahn, "Resource management model and performance evaluation for satellite communications," *International Journal of Satellite Communications*, vol. 19, no. 2, pp. 169–203, Mar. 2001.

[134] C.-Y. Yang, "Spectrum management and analysis in the nongeostationary (nonGEO) satellite communication system," in *2004 IEEE International Conference on Communications*, vol. 6, Jun. 2004, pp. 3316–3320 Vol.6.

[135] S. I. Wayer and A. Reichman, "Resource management in satellite communication systems – Heuristic algorithms," in *2010 IEEE 26th Convention of Electrical and Electronics Engineers in Israel (IEEEI)*, Nov. 2010, pp. 000 342–000 346.

[136] J. M. Park, U. R. Savagaonkar, E. K. P. Chong, H. J. Siegel, and S. D. Jones, "Efficient resource allocation for QoS channels in MF-TDMA satellite systems," in *MILCOM 2000. 21st Century Military Communications Conference Proceedings*, vol. 2, 2000, pp. 645–649 vol.2.

Curriculum Vitae

Todd W Martin is an engineer with over 25 years of professional engineering experience in aerospace, defense, and wireless communications systems research and development. He has participated in numerous programs at NASA, FAA, OSD, DISA, and DARPA; he has similarly led research efforts sponsored by NSF and AFOSR. He has applied his expertise in complex system dynamics and behavior to a broad range of subjects and technologies spanning manned and unmanned spacecraft, adaptive wireless communications and networking, information fusion, and probabilistic reasoning and computing.

Mr. Martin graduated from Wilmington Area High School in New Wilmington, Pennsylvania in 1987 and received his Bachelor of Science in Aerospace Engineering from The Pennsylvania State University in 1991. He was awarded a Master of Science in Systems Engineering from George Mason University in 2006 with a Graduate Certificate in Command, Control, Communications and Intelligence (C4I) Systems. His Masters Thesis titled "Distributed Information Fusion in Communications Networks with Ad Hoc Connectivity and Non-Deterministic Link Characteristics" established algorithms and analytical methods for implementing and evaluating decentralized information fusion in networks having intermittent communications connectivity.